The role of IKKε, TBK1, and alpha-Synuclein in the pathogenesis of melanoma and pain

Dissertation

zur Erlangung des Doktorgrades

der Naturwissenschaften

vorgelegt beim Fachbereich Biowissenschaften

der Johann Wolfgang von Goethe-Universität

in Frankfurt am Main

von

Moritz Möller

aus Marburg

Frankfurt am Main 2020

(D 30)

Vom Fachbereich Biowissenschaften der

Johann Wolfgang von Goethe-Universität als Dissertation angenommen.

Dekan: Prof. Dr. Sven Klimpel

Gutachter: Prof. Dr. Stefan Eimer

Prof. Dr. Ellen Niederberger

Diese Thesis widme ich meinem Großvater, Freund und Unterstützer Professor Dr. Ernst Lammel.

Contents

1. Introduction

Due to the nature of this work, it is loosely structured into two major parts. Part I focuses on the effects of the protein kinase inhibitor of nuclear factor kappa-B kinase subunit epsilon (IKKε) and the TANK-binding kinase 1 (TBK1) on human malignant melanoma. Part II discusses the localization and characterization of murine alpha Synuclein (α-Syn) in the nociceptive system and its role in different types of pain, including tumor-associated pain.

1.1 The role of IKKε and TBK1 in the pathogenesis of malignant melanoma

1.1.1 Malignant melanoma

1.1.1.1 Definition, epidemiology

Malignant melanoma is an aggressive and early metastatic type of tumor of the skin. In most cases the coloring is black, due to the origin of this tumor, which is often a mutation of melanin-producing cells, the melanocytes. Malignant melanoma is the most common fatal skin disease in the world[1,2]. As of now, every 20th diagnosed cancer is a cutaneous melanoma[3].

Although the number of cases in Germany almost quadrupled between 1980 and 2006, the death rate has remained constant[4]. This is due to the earlier detection and therapy of the disease. Nevertheless, these figures make it clear that the number of people suffering from the disease is increasing rapidly. Currently, the yearly incidence is ~ 35 cases per 100,000 people in Australia and New Zealand, ~ 20 cases per 100,000 people in the USA, and 10-20 cases per 100,000 people in Central Europe[2,5–7]. In the USA, malignant melanoma ranks 5th among the most common tumor diseases in men and 7th in women[8,9].

The increase in incidence is highest in the Caucasian population. Simulations of the incidence trend calculate a doubling of cases every 10-20 years[8]. People with African-American, Asian, and Hispanic backgrounds are significantly less likely to develop malignant melanoma[1,10].

In the USA, malignant melanoma ranks third among the most common skin tumors, but first in the mortality rate, which is 75 %. The mean age of diagnosis of malignant melanoma is 55 years. The mean age at death is 67 years[1,5,11]. In recent years the median survival rate for patients with metastatic melanoma increased from 5.3 months to over 2 years. This is due to new approaches like targeted- and immunotherapy[12,13].

1.1.1.2 Clinical aspects of melanoma

The extremely high lethality of malignant melanoma is based on its very high potential to metastasize and penetrate foreign tissue, if not diagnosed early enough[14]. During development, melanocytes migrate from the neural crest into a variety of tissues. Possible progenitor cells of the malignant melanoma are therefore scattered throughout the body[1]. This is the reason why not only the skin can be affected by the development of malignant melanoma. Possible sites of origin are also found in non-cutaneous tissue, such as the vulva, the vagina, the anus, the central nervous system (CNS), the eye, the paranasal sinus, and the oral mucosa[15,16]. Identifying malignant melanoma in these tissues can be extremely difficult. Late diagnosis, if there is one at all, is usually too late and the tumor has already metastasized. It is therefore of utmost importance to classify and characterize the tumor as early as possible to start the treatment. This is done based on the localization and depth of the affected tissue. The different classification levels of malignant melanoma are the superficial spreading melanoma, lentigo maligna melanoma, nodular melanoma, and acral lentiginous melanoma (Fig. 1.1.1.2.1)[2,11,14].

Interestingly, a large difference is seen between men and women in the formation of malignant melanoma. Overall, men are more susceptible to melanoma than women. Even though in younger years up to the age of 40 years this rate is reversed and women are more susceptible to form a malignant melanoma[17]. Melanoma is reported to form most

often on the shoulders and back of men and the lower limbs of women[18]. This trend is not seen in areas with high UV exposure, though. In areas like Australia and New Zealand, the strongest melanoma formation is on body areas which exhibit a strong UV exposure. Mostly the face, neck, and arms[19].

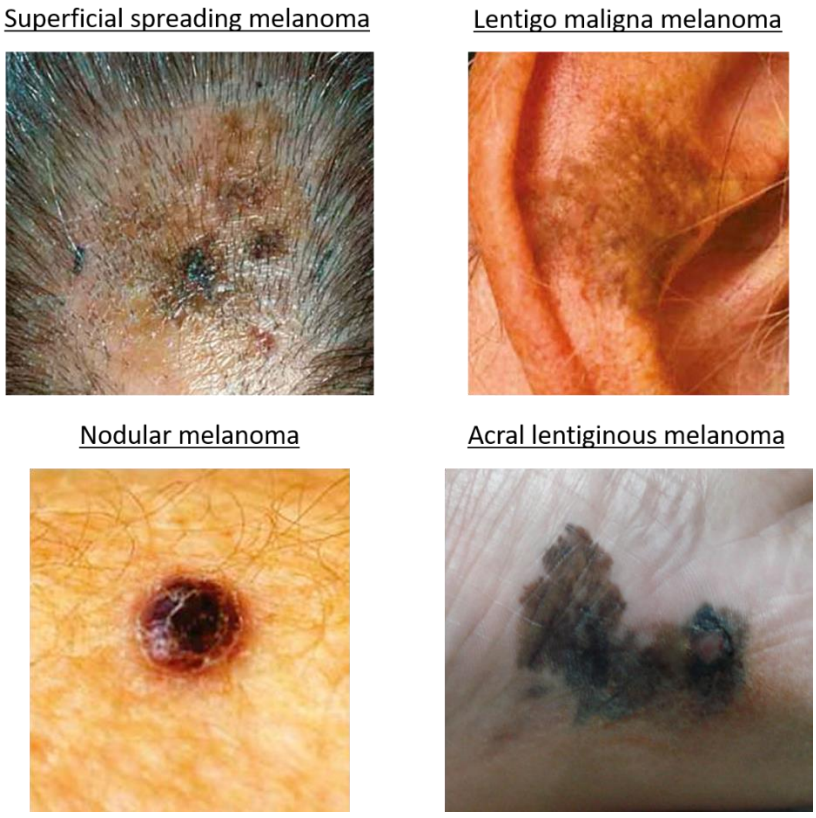

Fig. 1.1.1.2.1: Malignant melanoma subtypes. Representations of the superficial spreading, lentigo maligna, nodular, and acral lentiginous melanoma subtypes.

The early detection of malignant melanoma is based on the "ABCDE" criteria[11]. It is examined whether the affected area is asymmetric, has an irregular border, if the color is not uniform, if the diameter is larger than 6 mm, and whether it changes over time. Conspicuous areas then can be further characterized through tumor measurement according to Breslow[20]. This type of measurement is still the most important prognostic factor for the possible diagnosis of malignant melanoma. The Breslow characterization measures tumor thickness and tumor invasion depth. Measurement starts from the upper

layer of the epidermis to the deepest layer of tumor invasion (Fig. 1.1.1.2.2 A). In parallel a classification system according to Clark has developed[14]. This also looks at the depth to which the tumor penetrates. This depth of penetration is classified from the epidermis to the subcutaneous fat with levels I-V (Fig. 1.1.1.2.2 B).

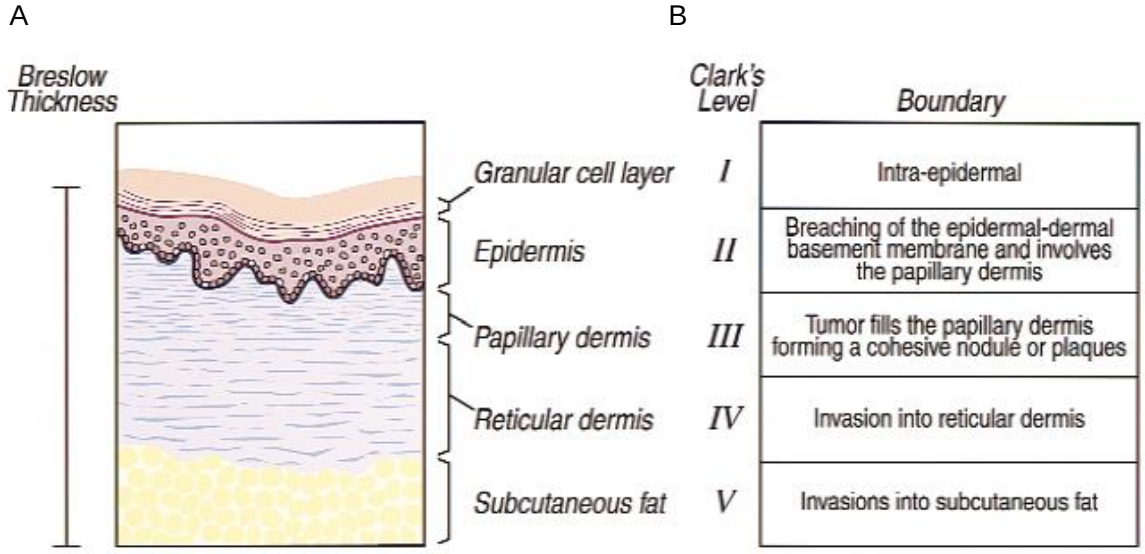

Fig. 1.1.1.2.2: Pathophysiological classification systems for the characterization of melanocytes. The tumor size after Breslow measures the total thickness and depth of invasion of the tumor (A). The level as done by Clark measures the anatomical structures invaded by the tumor (Chin et al. 1998[14]).

1.1.1.3 Formation and progression of malignant melanoma

Malignant melanoma originates from melanocytes, which are responsible for the pigmentation of the skin. It is assumed that melanoma cells, after their development, escape the control of keratinocytes. This happens through very precise regulation of specific keratinocyte and melanoma cell-cell receptors. The lack of control ultimately causes melanoma cells to detach from the basal cell layer and to metastasize[21].

There are many possibilities how a melanocyte becomes a melanoma cell. However, it is assumed that this happens because of an interplay of genetic, phenotypic, and environmental factors. The combination of these factors influences the incidence and the

molecular signaling pathways involved in malignant melanoma formation and progression[1,6,8]. It is now generally agreed on that UV radiation is the biggest risk factor for the development of malignant melanoma[22,23]. As already described, countries such as Australia and New Zealand have a much higher incidence than any other country. The increased UV exposure not only leads to DNA damage and mutations but also oxidative stress in the form of increased ROS production. Recent studies are beginning to show an increasing correlation between oxidative stress and melanoma formation[24].

Phenotypic risk factors for the development of malignant melanoma are the number and localization of naevi, and skin, hair and eye color[25]. The incidence in the African American population is only a fraction compared to the Caucasian population. A possible reason for this is the increased pigmentation, and thus better protection against UV radiation, of this part of the population[3].

The genetic risk factors are manifold and some of them have not yet been very well investigated. The gene most frequently associated with malignant melanoma, which is also mutated in at least 50 % of all cases, is the rapidly accelerated fibrosarcoma (BRAF) gene. BRAF encodes the serine/threonine kinase b-Raf of the mitogen-activated protein kinase (MAPK) pathway. Mutations of the BRAF gene are not only the main genetic cause of malignant melanoma but also of non-Hodgkin lymphoma, colorectal cancer, papillary thyroid carcinoma, non-small cell lung cancer, and many other tumor types[26,27]. The most common mutation is the BRAF V600E mutation, which is often found in patients with advanced malignant melanoma[28].

Directly following BRAF, p53 is an extremely important target for genetic approaches in melanoma research and therapy. p53 is a strong activator of apoptosis and cell cycle arrest. It is regularly activated by cellular stress, such as UV radiation or increased ROS levels, but also by the activation of oncogenes. In about 90 % of all melanoma cells, a mutation in the p53 gene is present. Of these, 10 % have an inactivating point mutation. This high mutation rate of the tumor suppressor p53 suggests a decisive role in the development and progression of malignant melanoma. Recent studies used p53 gene therapy and showed that melanoma growth, migration, and invasion were significantly inhibited, and the survival rate in patients was increased[29,30].

A variety of other genes was found to be mutated in different forms of malignant melanoma. The most important ones were CDKN2A, CDK4, NRAS, NF1, and SF3B1[31,32].

Cyclin-dependent kinase inhibitor 2A (CDKN2A) and cyclin-dependent kinase 4 (CDK4) are involved in the cell cycle progression and regulation. The NRAS gene is involved in the control of cell growth. Neurofibromin 1 (NF1) inhibits the RAS/MAPK pathway and can, therefore, alter cell growth. SF3B1 encodes a splicing factor. It has a wide variety of functions, but was found to be mutated in melanoma, leukemia, and breast cancer[33–38].

In addition to the risk factors already mentioned, there are several others. A weakened immune system, either through previous illness or the intake of immunosuppressants, promotes the development of malignant melanoma. Also, a familial or personal history of melanoma diseases[39]. People with the rare autosomal recessive disease Xeroderma Pigmentosum also have an increased risk of developing malignant melanoma due to the genetic background of this disease. Furthermore, there is an unexpected risk factor for melanoma development: Parkinson's disease (PD). First studies suspected a connection between L-DOPA intake and the increased risk of melanoma. However, subsequent studies could not confirm this assumption. Still, a strong correlation between PD and melanoma formation is seen[1,6,25,40–42].

1.1.1.4 Autophagy in malignant melanoma

Autophagy is a strongly regulated and natural process in cells. The function of this process is the removal of unnecessary or dysfunctional components by lysosomal degradation without activation of the immune system as seen in necrosis. The damaged particles are enclosed within a double-membraned vesicle. This so-called autophagosome fuses with available lysosomes, which leads to the process of degradation and recycling of the components[43].

Autophagy emerged as an important regulatory pathway in a wide variety of tumors. Many cancer cells hijack the autophagic process to create chemo- and radiotherapy immunity[44]. The correct regulation of this process is necessary for tumor survival and progression.

While the induction of autophagy resulted in tumor survival and progression in some tumors, it acted as a tumor suppressor in other tumors[45,46].

The current hypothesis for the role of autophagy in cancer, which is also true for malignant melanoma, is that the process acts tumor suppressive in the early stages of tumor development and tumor protective in the advanced stages (reviewed in [47]). A study by Lazova et al. describes autophagy in malignant melanoma cells as “a constitutive metabolic state for invasive and metastatic melanoma cells”[48]. With the facts as they are discovered as of this time, it can be hypothesized that the inhibition of autophagy has inhibitory effects on melanoma development and increases the effect of other therapeutic options.

1.1.1.5 Therapy strategies

Currently, the most important and effective treatment option for malignant melanoma is removal. If the melanoma is detected early enough and removed, the prognosis for complete recovery is very good, despite the high mortality rate. In recent decades, the early detection of melanoma has become much better with the ABCDE criteria and the subsequent measurement according to Breslow, and Clark. As a result, the lethality of malignant melanoma relative to the diagnosed cases has decreased significantly[9]. If the melanoma is not removed early on, only more aggressive therapies remain.

These include the usual radiotherapy or chemotherapy with interferon-α. However, these therapies are not effective to a satisfactory degree. This may be because melanomas are able to induce an anti-apoptotic phenotype that protects them from this type of therapy. In the meantime, however, new approaches for the therapy of malignant melanoma are being developed.

One possible therapy is the targeted gene therapy of p53. In initial studies, this therapy has shown great success. Confirmation by further studies remains to be seen[29].

Another therapy option that has developed between 2011 and 2015 is a combination therapy of BRAF and MEK inhibitors. Studies have shown a significant improvement in

the patients' survival rate after using this method. This therapy eventually became the worldwide standard for BRAF mutant and non-removable melanoma. Some successes were also seen with NRAS/MEK inhibitors.

After the discovery of the PD-1 receptor, more and more studies on anti-PD1 therapies were conducted. These showed a positive effect on the 1-year survival rate of patients. The PD-1 therapies showed strong side effects, though. This made the search for other PD1 inhibitors mandatory (reviewed in [49]).

Since all these therapies, except for surgical removal, have strong side effects, lead to resistance development in the tumor, or don't have any effect on the specific melanoma subtype, research is needed to find more effective therapies with fewer side effects.

1.1.2 The NF-κB signaling pathway and associated proteins

1.1.2.1 The NF-κB signaling pathway and Iκ-B proteins

The modulation of the nuclear factor kappa-light-chain-enhancer of activated B-cells (NF-κB) signaling pathway is one of the most effective ways to influence cell growth, proliferation, survival, and apoptosis. This signaling pathway also plays an important role in the immune response to pathogens and inflammatory processes[50,51].

The classical canonical signaling pathway starts with the activation of different pro-inflammatory receptors, e.g. T-/B-cell receptors, Toll-like receptors, or TNF receptors. Possible ligands are cytokines, TNFα, and lipopolysaccharides (LPS). Other activation factors are free radicals, heavy metals, and UV radiation, which is particularly important in the context of melanoma development. This activation of TNF-, toll-like-, or T-cell receptors starts the following cascade[52,53]:

The different receptor subtypes activate a variety of enzymes, e.g. TRAF6 via ZAP-70 or SYK. TRAF6 activates TAB1/2/3, which can also be activated via TRAF2 activation by the TNF receptor. TAB1/2/3 forms a complex with TAK1 and activates the NEMO/IKK complex. Another way to activate this complex is the activation of growth factor receptors,

which activate Ras. Ras leads to PI3K phosphorylation. One end of this cascade is the activation of the NEMO/IKK complex. The indirect activation of the kinases IKKα and IKKβ, and of the complex partner NF-κB-essential modulator (NEMO) by proteins such as TRAF6 or Ras leads to phosphorylation of Iκ-Bα, followed by the proteasomal degradation of Iκ-Bα. The nuclear localization sequence of the NF-κB heterodimer is now available in an open form. A very common heterodimer is p50/p65. p50 is processed constitutively from p105 and serves mainly for binding to Iκ-Bα. p65, also known as RelA, has the transcription factor properties[54,55]. An additional way of p50/p65 activation is via p38 or JNK activation of the MAPK pathway. This pathway can be activated via cellular stress or UV radiation amongst other factors. The p50/p65 heterodimer translocates into the nucleus, where it acts as a transcription factor for a variety of genes, most of which regulate the immune response or cell growth (Fig. 1.1.2.1)[51].

In normal cells, this signaling pathway is activated as required. However, mutations in the signaling cascade can lead to permanent activation. The permanent activation of this signaling pathway has carcinogenic effects and has been linked to the development and progression of various tumors. These include breast, colon, prostate, ovarian and pancreatic cancer (reviewed in [56]).

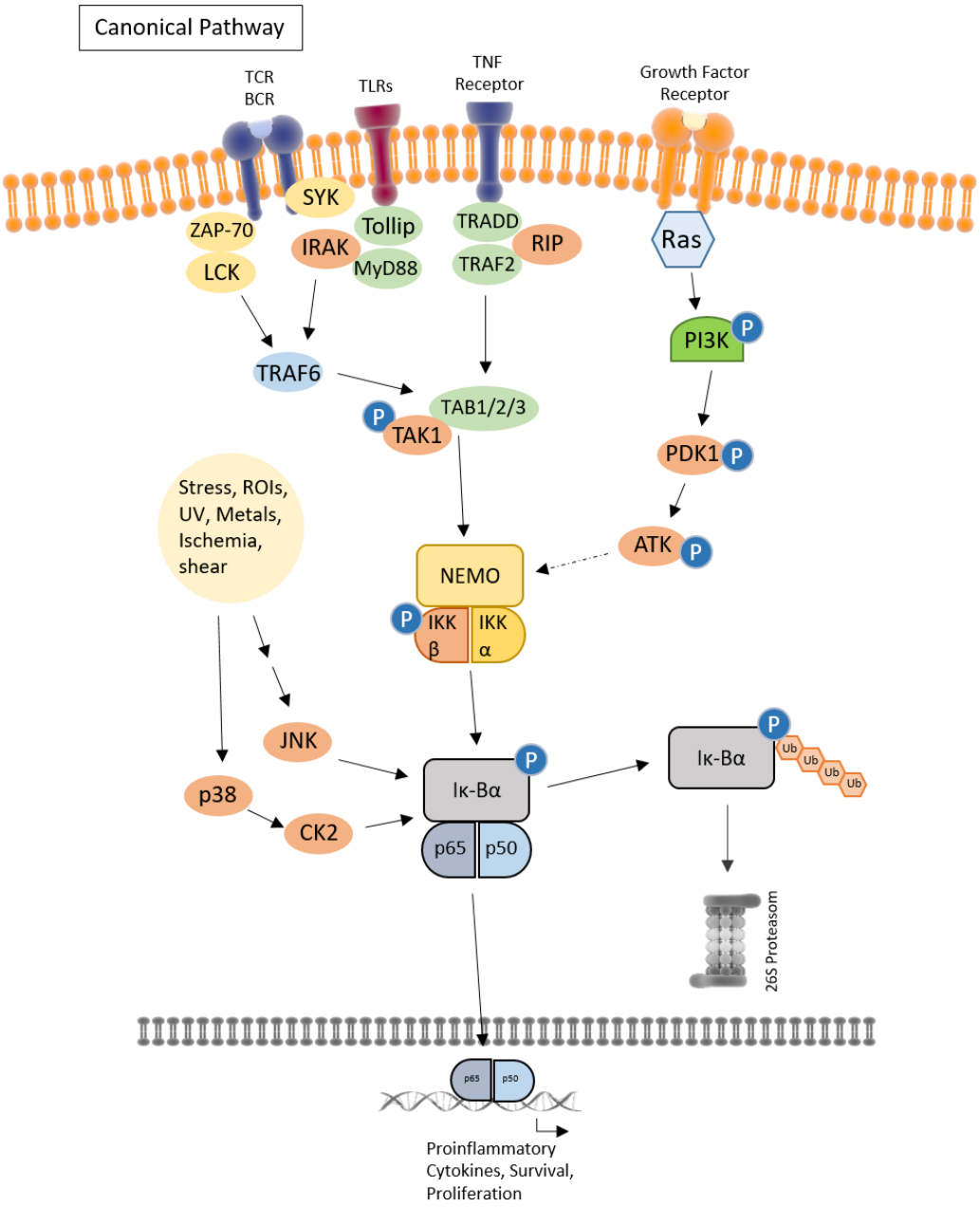

Fig. 1.1.2.1: Canonical NF-κB activation pathway. The classical canonical NF-κB signaling pathway leads to an activation of the NF-κB transcription factor. **TCR/BCR** T-cell receptor/B-cell receptor, **TLR** Toll-like receptor, **TNF** Tumor-necrosis factor, **SYK** Tyrosine kinase**, ZAP-70** Zeta-chain-associated protein kinase 70**, LCK** Lymphocyte-specific tyrosine kinase**, TRAF** TNF receptor-associated factor**, IRAK** Interleukin-1 receptor-associated kinase**, Tollip** Toll interacting protein**, MyD88** Myeloid differentiation primary response 88**, TRADD** TNF receptor type 1-associated DEATH domain protein**, RIP** receptor-interacting protein kinase**, TAB** TGF-beta-activated kinase**, TAK1** Mitogen-activated protein kinase kinase kinase**, Ras** Rat sarcoma GTPase**, PI3K** Phosphoinositide 3-kinase**, PDK1** Pyruvate dehydrogenase lipoamide kinase isoenzyme 1**, ATK** Artichoke**, JNK** c-Jun N-terminal kinases**, p38** Mitogen-activated protein kinase**, CK2**

Casein kinase 2, **NEMO** NF-κB essential modulator, **IKK** Iκ-B kinase, **IK-Bα** Inhibitor of NF-κB subunit alpha, **P** Phosphate group, **Ub** Ubiquitin, **ROI** Radical oxygen species, **UV** Ultraviolet light.

1.1.2.2 The alternative IKKε and TBK1 NF-κB signaling pathway

Alternative activation of the NF-κB signal pathway is achieved via the IKKε/TBK1 complex. The stimulation of LPS-, PMA-, or cytokine-sensing receptors activates the IKKε/TBK1 kinase complex, which is involved in interferon 1 and NF-κB signaling. The IKKε/TBK1 complex is able to directly phosphorylate IKKβ, Iκ-Bα, and p65. While the classical IKK subunits phosphorylate Iκ-Bα at serine 32 and 36, IKKε phosphorylates the inhibitory Iκ-Bα only at serine 36[57–59]. The different phosphorylation targets lead to direct and indirect activation of the p50/p65 heterodimer and thus to its translocation into the nucleus.

Another possibility for the IKKε/TBK1 complex to influence cellular processes is the activation of the interferon signaling pathway. IKKε/TBK1 form complexes with the TRAF-associated NF-κB activator (TANK), the NAK-associated protein 1 (NAP1), and the similar to NAP1 and TBK1 adaptor (SINTBAD) protein[60,61]. This complex formation leads to the phosphorylation and activation of interferon regulatory factors 3 and 7 (IRF3/7). IRF3 and IRF7 homo- or heterodimerize and translocate into the nucleus, where they act as a transcription factor for type 1 interferon (Fig. 1.1.2.2)[60,62–64].

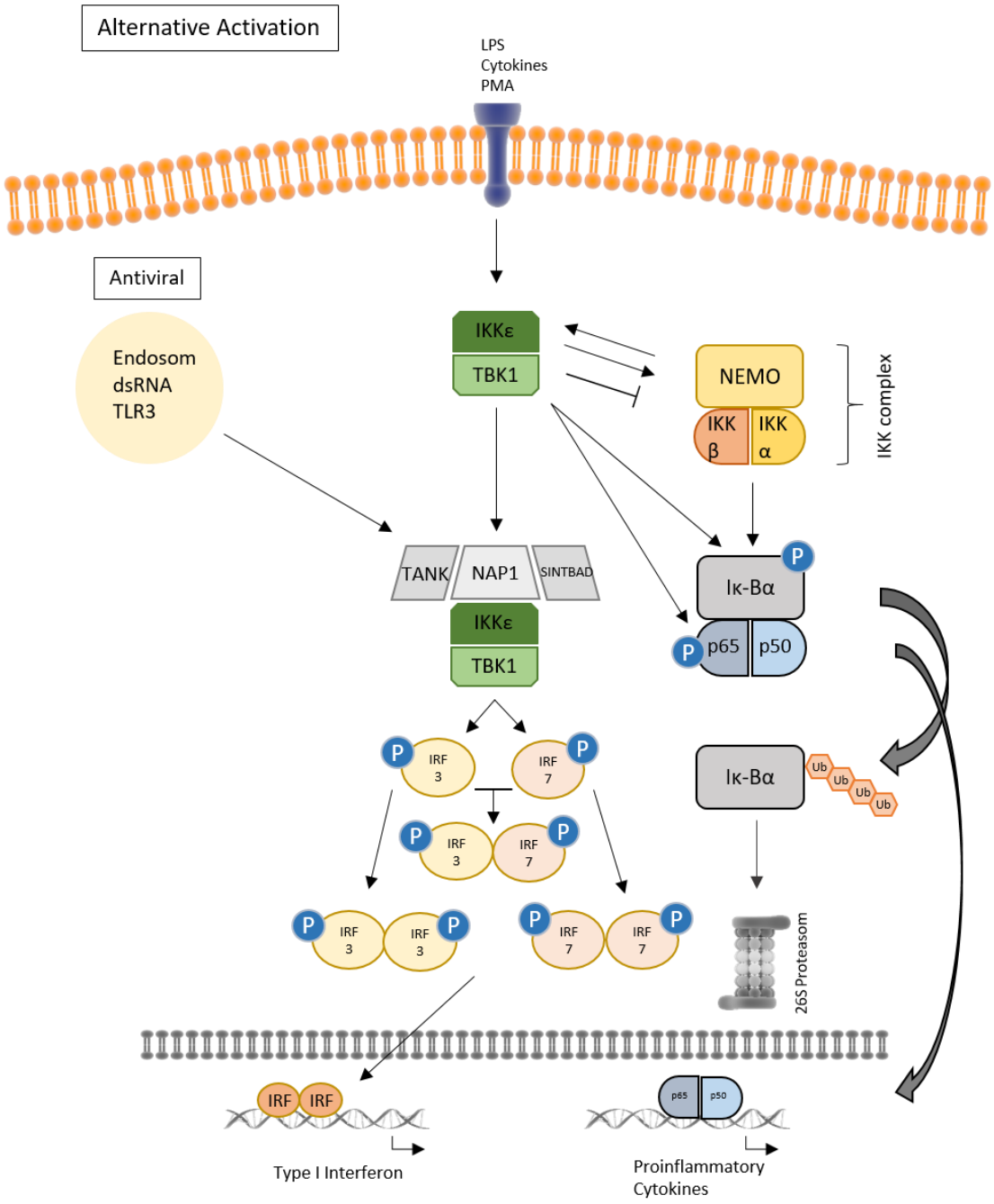

Fig. 1.1.2.2: The alternative NF-κB signaling pathway. In addition to the classical canonical NF-κB signaling pathway, alternative activation pathways of NF-κB exist. The alternative NF-κB activation pathway is closely related to the interferon type 1 signaling cascade and leads to the expression of type 1 interferons, additionally to NF-κB related genes. **Iκ-Bα** Inhibitor of NF-κB subunit alpha, **IKK** Iκ-B kinase, **IRF** interferon regulating factor, **LPS** lipopolysaccharide, **NAP1** NAK associated protein, **NEMO** NF-kappa-B essential modulator, **PMA** Phorbol-12-myristate-13-acetate, **SINTBAD** similar to NAP1 and TBK1 adaptor, **TANK** TRAF family member-associated NF-kappa-B activator, **TBK1** TANK binding kinase 1, **TCR** T cell receptor, **TLR** Toll-like receptor.

1.1.2.2 The pathophysiological role of the NF-κB pathway in malignant melanoma

Permanent activation of the NF-κB signaling pathway is observed in many different types of tumors (reviewed in [56]). As described above, activation of this pathway leads to the expression of proteins that promote proliferation, growth, migration, and other oncogenic factors[65].

Ongoing activation of the NF-κB signaling pathway can occur through a wide range of events. These include mutations of components in the signaling pathway, chronic inflammation, and the activation of oncogenic factors. *In vitro*, NF-κB is permanently active in malignant melanoma cells and not activated as necessary[57,63]. In human melanoma cells, increased expression of p65, and p105/50 was found as well as increased expression and nuclear localization of the p50/65 heterodimer. The reason for this was described to be overactivity of the IKKs[58]. Interestingly, the upregulation of NF-κB monomers was also found in samples of uveal melanoma, but the inflammatory status of the samples differed between pro- and anti-inflammatory. This shows that not only the NF-κB pathway induced activation of the immune system, but a wide variety of factors influence the interplay between melanoma development and the immune system. But the effect of NF-κB on melanoma development is still confirmed with this study[66].

The activation of the NF-κB signaling pathway in melanoma cells also results in the secretion of CXCL1, CXCL8, and CCL5. These chemokines further contribute to cellular growth, apoptosis, the ability to metastasize and form a feedback loop to keep the NF-κB signaling pathway running[59].

The permanent activation of the NF-κB pathway has clear oncogenic effects and promotes the development and growth of melanomas. This signaling pathway can be activated directly, as described above, but also indirectly through the influence of other signaling pathways.

1.1.2.3 Associated pathways and key regulators

The NF-κB pathway is integrated into a network of other signaling cascades. The influence of a single factor in this network has the potential to affect the entire network (Fig. 1.1.2.3). The deregulation of this complex network in tumor cells has several effects that ultimately ensure the survival of the tumor cell. The most important signaling pathways to be mentioned in this context are the MAPK signaling pathway and the PI3K/Akt signaling pathways (reviewed in [67]).

According to different studies, the invasion of melanoma cells into the surrounding tissue may result in the deregulation of the MAPK pathway[68,69], which subsequently modulates expression and activation of Ras, b-Raf, MEK1, 2, and ERK1/2 in tumor cells. ERK1/2 acts as an oncogenic transcription factor. Over 200 substrates of ERK1/2 are already described. The most famous of them are probably the transcription factors Elk1, c-Fos, and c-Jun. The phosphorylation of these factors by ERK1/2 leads to proliferative and migrative effects[70]. Also, ERK1/2 affects NF-κB and activates this transcription factor[59,69]. The MAPK pathway can be activated by the binding of EGF to EGF receptors or by the binding of LPS to TLR4. This leads to the phosphorylation of GTPase rat sarcoma (Ras), which phosphorylates b-Raf. b-Raf in turn activates, among others, MEK1, 2, which phosphorylate the extracellular signal-regulating kinase (ERK1/2), also known as p44-42. ERK1/2 regulates the transcription of genes important for proliferation and apoptosis[61,71]. According to the important role of MAPKs in melanoma pathophysiology, inhibitors of the pathway are used as antitumor therapy (reviewed in [72]).

The PI3K/Akt/mTOR pathway can be initiated by TLR4, EGFR, or Ras. PI3K modulates Akt, which has a very broad target spectrum. As an example, Akt has the ability to disinhibit CyclinD1, a very important factor in cell cycle progression[73]. Also, Akt can influence the IKKε/TBK1 complex activity and thus the alternative NF-κB signaling pathway[74]. Further targets of Akt are the p53 inhibitor mouse double minute 2 (MDM2), and the mammalian target of rapamycin (mTOR). p53 is the best-known tumor suppressor, and activation of its inhibitor leads to pro-oncogenic effects. It is also suspected that melanoma resistance against radiotherapy is induced by p53 inhibition. A study from Krayem et al. showed that reactivation of p53 renders melanomas more susceptible to radiotherapy[75]. mTOR is a key activator of various signaling pathways, all

of which are related to cell growth and metabolism[76,77]. Additionally, it was found that melanoma progression is often associated with the activation of Akt, which stabilizes TLR4. This leads to a feedback loop and melanoma progression[78].

Also, there are various cross-links between the PI3K initiated PKC signaling pathway and the canonical NF-κB signaling pathway[58,68,71]. The most important connector is the MAPK p38, which was found to promote vascular invasion and pro-survival autophagy in melanoma. The inhibition of p38 reversed these effects[79,80].

Figure 1.1.2.3 is intended to give an impression of the complexity of this signaling network and which factor has which influence on other factors. In this context, it is important to not only study the NF-κB signaling pathway, but also key proteins of other signaling pathways that have a direct or indirect influence on the NF-κB signaling pathway, or on key tumor characteristics, e.g. cell growth, proliferation, cell cycle, and apoptosis.

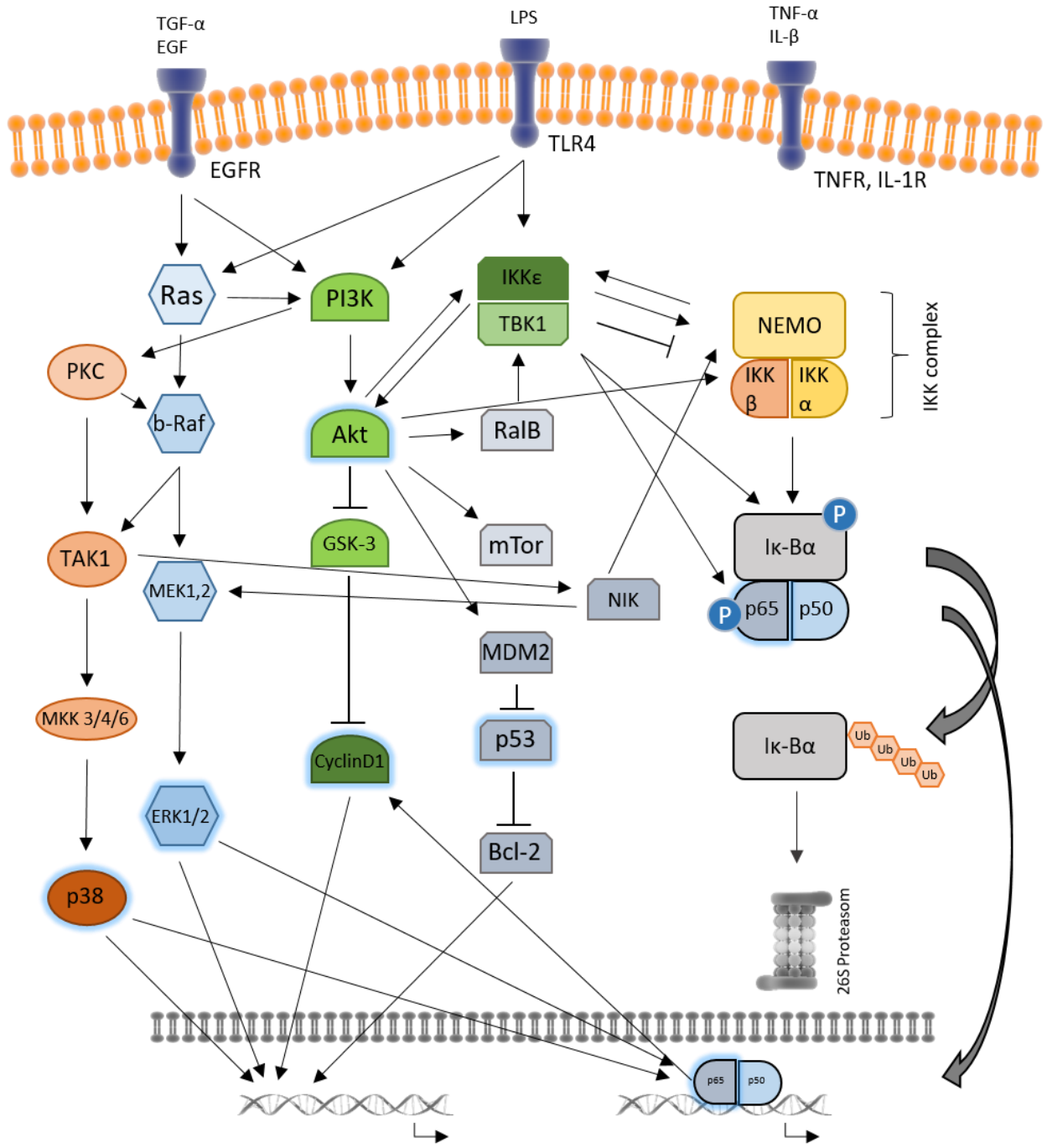

Fig. 1.1.2.3: NF-κB and associated signaling pathways. The signaling cascades of the NF-κB, MAPK, and PI3K/Akt signaling pathways influence each other in a complex intracellular signaling network. Activation/overexpression of the key regulators p38, ERK1/2, Akt, p65, CyclinD1, and p53 leads to cell cycle progression, angiogenesis, inhibition of apoptosis, cell proliferation, migration, adhesion, and invasion as well as the transcription of pro-inflammatory genes. Investigated interaction partners are highlighted in blue. **Akt** Protein kinase B, **Bcl-2** B-cell lymphoma-2, **b-Raf** Rapidly accelerated fibrosarcoma, **EGF** Epidermal growth factor, **EGFR** Epidermal growth factor receptor, **ERK1/2** Extracellular regulating kinases, **GSK-3**

Glycogen synthase kinase-3, **Iκ-Bα** Inhibitor of NF-κB subunit alpha, **IKK** Iκ-B kinase, **IL-β** interleukin-β, **IL-1R** interleukin-1 receptor, **LPS** lipopolysaccharide, **MDM2** mouse double minute 2, **MEK1,2** MAP-ERK kinase 1,2, **MKK 3/4/6** Mitogen-activated kinase kinase 3/4/6, **mTOR** mammalian target of rapamycin, **NEMO** NF-κB essential modulator, **NIK** NF-κB inducing kinase, **PI3K** Phosphoinositide-3-kinase, **PKC** Protein kinase C, **TAK1** TGF-β activated kinase-1, **TBK1** TANK binding kinase 1, **TGF-α** Tumor growth factor-α, **TLR4** Toll-like receptor 4, **TNF-α** Tumor necrosis factor-α, **TNFR** Tumor necrosis factor receptor, **RalB** Ras-like GTPase B, **Ras** Rat sarcoma.

1.1.3 IKKε and TBK1

1.1.3.1 Characterization of IKKε and TBK1

Iκ-B Kinase subunit epsilon (IKKε) and TANK-binding Kinase 1 (TBK1) both belong to the IKK family. IKKε is 80 kDa in size, its gene IKBKE is located on chromosome 1 q32.1. TBK1 is 83.6 kDa in size and the gene is encoded on chromosome 12 q14.2. The sequence of the kinase domain of these two kinases shows a similarity of 33 % to IKKα and 31 % to IKKβ. Due to this similarity, they were assigned to the IKK-affiliated kinases[59,63,81]. IKKε and TBK1 each consist of an N-terminal catalytic kinase domain, a helix-loop-helix motif, and a C-terminal leucine zipper. This motif enables homo- and heterodimerization of these proteins. The difference between IKKα and IKKβ is that IKKε and TBK1 do not have a NEMO-binding domain[69].

IKKε, often called inducible IKK, was originally discovered as an LPS-inducible protein in mouse macrophages. Sequence analysis showed a high similarity to the already known IKKs, so the term IKKε was chosen for this kinase[81,82]. The expression of IKKε can be induced via LPS, TNFα, IL-1, IL-6, PMA, viral pathogens, and IFN-γ[57,65,68,82,83].

TBK1, also known as NAK, was originally identified as a TNF receptor-associated factor 2 (TRAF2)-associated kinase (T2K) in a yeast screening system for protein interactions[65]. Due to the high similarity, TBK1 was assigned to the IKKs and further experiments showed that TBK1 can activate NF-κB. Later experiments showed that the complexation of IKKε and TBK1 was necessary for NF-κB activation[63]. However, while IKKε is an inducible kinase, TBK1 is permanently expressed.

These two IKK-associated kinases share a 67 % identical sequence[84].

A major difference between these two kinases is their expression pattern. TBK1 is permanently expressed in almost all cells. Exceptions are, however, cells of the retina and blood. IKKε expression is mainly induced and the expression is more limited. High protein expression was found in the brain, endocrine tissue, lung, gastrointestinal tract, liver, kidney, male and female tissue, and lymphoid tissue.

The IKKε/TBK1 complex is involved in inflammatory diseases, metabolic disorders, pain, and cancer[65,69,85]. Both kinases have been increasingly investigated and confirmed as oncogenes in recent years[86,87] (reviewed in [88]).

1.1.3.3 The pathophysiological role of IKKε and TBK1 in cancer

It has already been mentioned that mutations that activate the NF-κB pathway have oncogenic effects. IKKε as an activator of NF-κB forms a basis for exactly such mutations. Overexpression of IKKε is associated with viability, proliferation, and progression of tumor cells. Studies have already shown that overexpression of IKKε is additionally correlated with nuclear accumulation of p65[69,76]. This happens both via the direct activation of NF-κB, and via activation of Akt. This kinase activates, among other signaling pathways, also NF-κB[89].

In 2007, IKKε was described as oncogenic for the development of breast cancer. IKKε is overexpressed in over 30 % of all breast cancers, due to an amplification of the IKKε gene locus 1q32[90]. According to this finding, it was shown that knockdown of IKKε leads to an inhibition of proliferation, migration, and invasion of breast and pancreatic cancer cells *in vitro*. Reduced activity of NF-κB was postulated as the reason for this[91–93].

Another important pathway for tumor development is the activation of the mTOR pathway via phosphorylation and thereby inhibition of TSC1 by IKKε. This deregulated activity of mTOR can contribute to tumor development[94].

Another example of the oncogenic effect of IKKε was found in connection with the deubiquitinating enzyme CYLD which acts as a tumor suppressor. IKKε can

phosphorylate CYLD, which inhibits its ability to deubiquitinate and leads to reduced tumor suppression[97].

IKKε is also overexpressed in esophageal squamous cell carcinoma. Its upregulation correlated negatively with the three-year survival rate of patients and positively with the tumor progression. Therefore, it was postulated that IKKε acts as an important marker in this type of cancer[95]. The same correlation between disease prognosis and IKKε expression was seen in stage I non-small cell lung cancer. TBK1 expression was also increased in this cancer type. Patients that showed an increased expression of both proteins had a worse disease progression than patients, which just showed an increase in either IKKε or TBK1[96].

TBK1 acts in complex with RalB and Sec5. These proteins form the exocyst complex, which is involved in cellular growth and migration. Another TBK1 complex, together with Ras, RalGEF, and RalB, is known to act as an oncogenic complex which is closely related to the NF-κB signaling pathway[71,98].

In KRAS-dependent tumor cells, TBK1 promotes the degradation of Iκ-Bα, which leads to the activation of NF-κB. Also, TBK1 induces the expression of the anti-apoptotic factor Bcl-X_L[99]. Additionally, TBK1 was found to control autophagy initiation in cancer cells via phosphorylation of Syntaxin 17[100]. Especially in fibroblast and non-small cell lung cancer cells a tumorigenic potential of TBK1 on KRAS was observed[84,101].

In addition to the direct tumor-promoting properties of TBK1, it was discovered that it induces angiogenesis, which is essential for tumor growth. This is achieved by phosphorylation of proangiogenic factors, such as IFN-β[102].

In this paragraph, only some important examples and findings are listed. Due to the strongly cross-linked effects of IKKε and TBK1, these enzymes can intervene in many different signaling pathways. Deregulation of these enzymes leads to a variety of diseases. One of these diseases is certainly cancer, which can manifest itself in many different types.

1.1.3.4 Relevance of IKKε and TBK1 for the development and progression of malignant melanoma

The role of IKKε in breast cancer, pancreatic cancer, and non-small cell lung cancer has already been studied in more detail. Initial studies have also shown an effect of IKKε in glioblastoma models[103,104]. However, the role of IKKε and TBK1 in melanoma has not yet been investigated in detail.

A study from 2014 showed that TBK1 promotes the motility of melanoma cells by activating the Ras signaling pathway. Also, the activation of TBK1 by Ras was discovered in two melanoma cell lines. This feedback loop increased tumor cell invasion. According to these findings, it could also be shown that inhibition of TBK1 suppresses the ability of these cells to migrate and invade[105].

Our group investigated the influence of IKKε on murine B16 melanoma cells. Both the inhibition by the IKKε/TBK1 inhibitor amlexanox, and a specific knockdown of IKKε led to reduced proliferation and progression of these melanoma cells. One reason for this result was a blockade of the cell cycle in the G1 phase. The analysis of important key proteins of associated pathways led to the conclusion that the observed effect is not only due to an effect on NF-κB but also due to a regulation of Akt and MAPK signaling[106].

In the meantime, two other interesting studies on this topic have been published. In 2016 it was postulated that IKKε inhibits the T-cell immune response by regulating NFATc1. This inhibition led to a worse disease progression in a murine *in vivo* melanoma model. The study concluded that IKKε would be an interesting target for immunotherapy in cancer[107].

In 2017, Eskiocak et al. discovered that IKKε/TBK1 inhibitors had a good outcome in the treatment of BRAF/MEK inhibitor-resistant melanomas. Since most therapies are based on a modulation of either BRAF or MEK this result is promising. It indicates, that IKKε/TBK1 inhibitors target other pathways than BRAF or MEK inhibitors[108].

The current study situation shows that IKKε alone, and in complex with TBK1, is a promising target for the therapy of malignant melanoma. The present study will further pursue this hypothesis.

1.1.3.5 Amlexanox as a specific IKKε/TBK1 inhibitor

Amlexanox is a specific inhibitor of the IKKε/TBK1 complex. This substance is used in many studies, including this one, for the inhibition of IKKε and TBK1. Amlexanox is a small-molecule inhibitor with an IC_{50} = 1-2 µM for IKKε and TBK1 inhibition *in vitro*. The kinase activity is competitively inhibited by the binding of amlexanox at the ATP binding site. Since the ATP binding site of IKKε and TBK1 share a 72 % homology, amlexanox acts identically on both kinases. Despite the high structural similarity between IKKε, TBK1, and the other IKKs, the classical IKKs are not inhibited by amlexanox[109]. Only one other kinase is known to be inhibited by amlexanox in this concentration.

In the USA amlexanox was used primarily for the treatment of oral aphthae. In Japan, on the other hand, the range of applications was wider, as it was also used for the treatment of bronchial asthma and allergic rhinitis. Amlexanox inhibits the histamine and leukotriene release of leukocytes and mast cells and has a corresponding inhibitory effect on the immune system[110,111]. This effect is used in cases of immune system hyperactivity, for example in aphthae or allergic reactions. Medical trials have shown a very good tolerance of amlexanox. In the meantime, the molecular mechanisms have been clarified and the good tolerability has led to attempts to repurpose amlexanox for the treatment of other diseases[112–115].

In 2013, Reilly et al. discovered that amlexanox inhibits the IKKε/TBK1 complex and thus the activation of NF-κB and related signaling pathways. In their study the authors investigated obesity in a mouse model. Since obesity is always associated with chronic inflammation of the liver and fatty tissue, amlexanox was a good therapeutic option. The inflammatory reactions in obese mice were shown to be due to an upregulation of IKKε and TBK1. After the administration of amlexanox, the mice lost weight, showed increased insulin sensitivity, and the inflammation decreased[109].

Another study in 2015 investigated molecular processes in joint disease. Amlexanox was able to inhibit osteoclast formation. As causes, the authors name multiple effects in the NF-κB, MAPK, MEK, and PKC signaling pathways[116]. The complex interplay between these pathways makes an IKKε/TBK1-mediated effect plausible.

Studies from our group investigated the effect of amlexanox on the neural system and pain perception. It was found that IKKε contributes to nociceptive sensitization during neuroinflammatory processes. Amlexanox inhibited neuroinflammation by reducing the phosphorylation of p65, thereby reducing the nociceptive response in models of inflammatory pain[117].

In a first approach to the melanoma topic, our group showed that knockout of IKKε inhibits pain sensation in a murine melanoma model. Additionally, IKKε$^{-/-}$ melanoma cells barely showed any tumor growth at all after inoculation, while normal melanoma cells grew regularly in IKBKE$^{-/-}$ animals[106].

A few years ago another target of amlexanox was found. The competitive inhibition of the ATP binding site of enzymes seems to be effective not only in IKKε/TBK1 but also in some G-protein coupled receptor kinases (GRK). The investigated GRK 5 plays a role in arteriosclerosis and diabetes. Since these diseases are also characterized by inflammation, amlexanox can attack two sites, the GRKs and the NF-κB signaling pathway[118,119].

Amlexanox has proven to be a safe and specific drug. Probably the biggest advantage is that it can influence several signaling pathways that play a major role in inflammatory diseases without having strong side effects itself. The effect on IKKε and TBK1, which play a major role in many tumors, makes amlexanox an interesting therapeutic option for a wide range of tumors[62,120,121].

1.1.4 Objectives of part I

The following hypotheses underlie this work:

Compared to human melanocytes, IKKε and TBK1 are overexpressed in human malignant melanoma cells. The same goes for the expression in melanoma metastases compared to healthy naevi.

IKKε and TBK1 contribute to the proliferation and migration of human malignant melanoma cells via NF-κB, and associated pathways, and are therefore relevant for tumor growth.

Inhibition of IKKε and TBK1 leads to reduced cell proliferation and migration of malignant melanoma cells.

The expression of IKKε and TBK1 affects NF-κB activation as well as MAPKs, which are key factors in carcinogenesis.

IKKε and TBK1 are colocalized with tumor markers, and additionally affect the immune system.

The present study is aimed to further clarify the relevance of IKKε and TBK1 in the initiation, progression, and metastasis of human malignant melanoma. To test the hypothesis the expression of IKKε and TBK1 in melanocytes compared with melanoma cells, and samples of healthy naevi compared with melanoma metastases should be investigated. These results will clarify if IKKε or TBK1 are regulated during the melanoma tumor progression. Then, the effect of IKKε/TBK1 on different tumor characteristics, like proliferation, migration, and invasion, will be investigated via *in vitro* experiments of melanoma cells with and without IKKε/TBK1 inhibition. The *in vitro* experiments are completed with functional analysis of different relevant pathways by specific inhibition of these pathways, as well as molecular experiments concerning the expression and phosphorylation of key proteins. It is planned that the results obtained at this point are transferred into an *in vivo* model. Immune-deficient nude mice are inoculated with melanoma cells and treated with the IKKε/TBK1 inhibitor amlexanox, which was already used for the *in vitro* experiments. Finally, primary melanoma samples will be stained for IKKε, TBK1, structural, immune, and tumor markers.

After finishing all these experiments a clearer picture of the involvement of IKKε and TBK1 in the formation and progression of malignant melanoma should be obtained.

1.2 The role of alpha-Synuclein in the nociceptive system

1.2.1 Characterization and physiological functions of alpha-Synuclein

Alpha-Synuclein (α-Syn) is a 14 kDa protein with major implications in the neurological field. It is best known as the main component of Lewy bodies in Parkinson's disease (PD). Its physiological functions have not yet been fully understood and there are still many open questions about this protein. It was discovered that a possible causal connection between malignant melanoma and PD exists, though. Additionally, PD patients often experience pain as a symptom of the disease. Therefore, the investigation of the role of α-Syn in the nociceptive system is an important part of this work to find out about the physiological role of the protein and what implications it might have in malignant melanoma.

α-Syn is encoded by the SNCA gene, which is located on chromosome 4q22.1. The protein consists of three domains (Fig. 1.2.1.1):

The amphipathic region of α-Syn is encoded by amino acids 1-60. This region contains seven imperfect KTKEGV repeats, which are very similar to those of apolipoproteins. The proposed function is the binding of the protein to the lipid membrane[122,123]. A recent study found that the ubiquitination of this domain can lead to proteasomal degradation of α-Syn monomers and aggregates[124].

From amino acid 61-95 the non-amyloid-β component (NAC) domain is encoded. This domain regulates the conformational change from a random coil to a β-sheet structure. Previous research assumes that the NAC domain is responsible for the aggregation and toxicity of α-Syn[125–127]. Binding of this region by a synthesized compound inhibits α-Syn aggregration[128]. Additionally, this domain can bind and activate the protein phosphatase 2A, which is often associated with neurodegenerative disorders[129].

The acidic tail domain is encoded by amino acids 96-140. On the one hand this domain acts against the aggregation of the protein[130,131], on the other hand it enables interaction with other proteins[132]. Truncation of this domain is often found in α-Syn deposits in PD patients. Artificial truncation of α-Syn leads to monomers

that easily oligomerize[133]. This domain is also believed to be important for the ability of α-Syn to bind calcium ions[134,135]. Additionally, α-Syn's chaperone-like function is assigned to this domain[136].

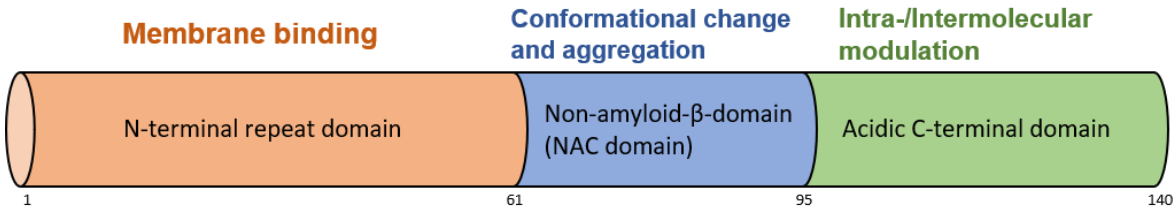

Fig 1.2.1.1: Schematic structure of α-Syn. The amphipathic region is marked in orange, the NAC domain in blue, and the acidic tail in green. The main task of the corresponding region is mentioned above.

α-Syn is mainly expressed in nervous tissue where it is accumulated in presynaptic nerve terminals[137]. Also, its expression has been found in kidney, skin, fatty, and lymphoid tissue.

α-Syn is part of a protein family called "intrinsically-disordered". Proteins from this family do not have a stable 3-dimensional structure and are described as hubs in protein interaction networks. Due to this property and the variable tissue expression, a broad spectrum of α-Syn functions is likely[138,139].

Originally, it was assumed that α-Syn physiologically occurs as a monomer and oligomerizes in pathophysiological states. However, recent studies found an equilibrium between monomers, membrane-bound oligomers, and helically folded tetramers as the most likely physiological α-Syn forms. It has been suggested that the misinterpretation of the monomeric form is due to the experimental setups. Recombinant bacterial expression protocols and overexpression studies have been used regularly for *in vitro* studies. Furthermore, the usual procedure in protein analysis is denaturation of the protein, which can lead to misleading results in a protein that exists as a physiological tetramer[140]. Currently, it is assumed that α-Syn oligomerizes in both the physiological and pathophysiological states. In its physiological form it is in equilibrium with monomeric and

oligomeric forms, as well as in soluble- and membrane-bound states (Fig. 1.2.1.2). However, if various factors, which will be discussed later, cause a pathophysiological oligomerization, α-Syn starts to fibrillate. The fibrils are then able to deposit and disturb physiological cell processes[141].

Several different physiological functions of α-Syn have been found. It is believed to have implications in exocytosis[142], interactions with tubulin[143], inhibition of the proapoptotic proteins caspase 3 and p53[144], recycling of synaptic vesicles[145], and support of synaptic transmission and plasticity[146]. α-Syn is also able to dilate the exocytic fusion pore[147]. This effect primarily affects the liberation of slowly-released cargo, like neuropeptides (reviewed in [148]). Additionally, α-Syn is able to bind and activate the protein phosphatase 2A, which is often associated with neurodegenerative diseases[129]. This finding opens the possibility of α-Syn binding and modulating a variety of similar enzymes and regulation of signaling pathways. Interestingly, α-Syn is able to bind to the insulin-degrading enzyme, which increases the proteolytic activity of the enzyme and arrests α-Syn in an oligomeric form[149]. Since the oligomeric form of α-Syn is discussed as a physiological form the binding and modulation of other proteins might very well be one of α-Syn's main functions.

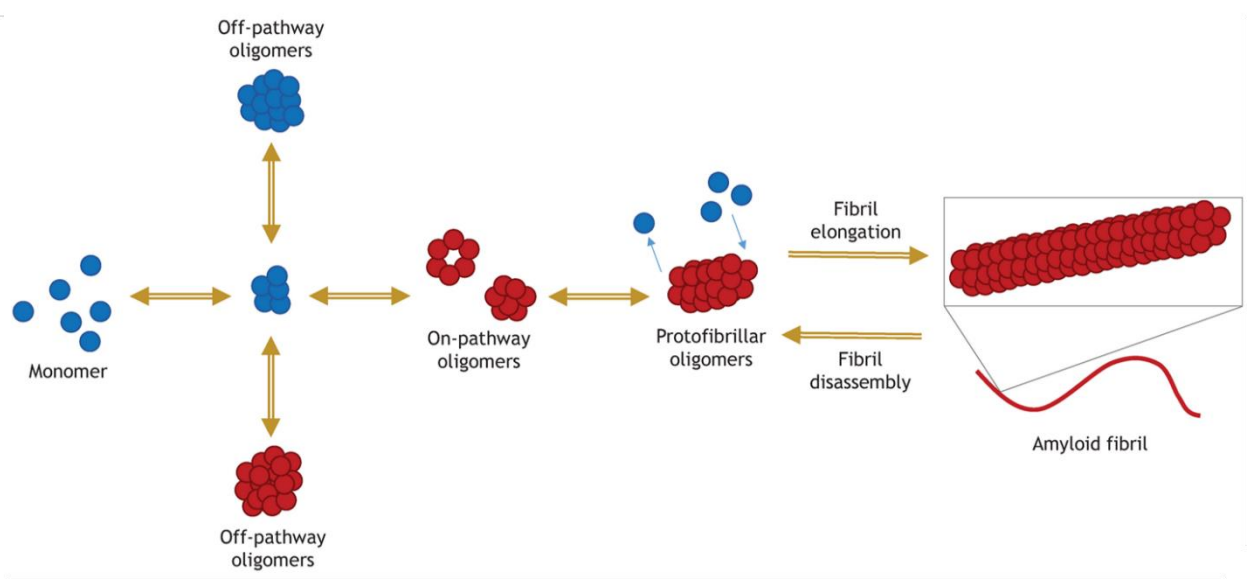

Fig. 1.2.1.2: Hypothesized procedure of α-Syn oligomerization. Monomers gather to form oligomers, which in turn oligomerize to fibrils. There is an equilibrium between all these states (adapted from Roberts and Brown 2015[150]).

SNCA$^{-/-}$ mice were created to investigate the physiological functions of α-Syn. In these animals, which were also used for this project, the SNCA gene is disrupted by replacing exons 4 and 5 with a neomycin resistance gene. SNCA$^{-/-}$ animals are viable, fertile, and have a normal life span. They do not show any obvious abnormalities whatsoever[151]. The only difference to wildtype (WT) animals found so far is a slight anxiety-like phenotype. In an open field test, SNCA$^{-/-}$ animals spent less time in the middle of the setup. Molecular investigations showed that their synaptic transmission is influenced. These animals have fewer synaptic vesicles in hippocampal neurons and the vesicle reserve pool is reduced by 50 %[152]. Also, microglia from SNCA$^{-/-}$ animals reacted more strongly to pro-inflammatory cytokines, such as TNF-α and IL-6[153]. This leads to the conclusion that α-Syn acts as an anti-inflammatory agent, most likely via modulation of different molecular pathways.

1.2.2 Pathophysiological functions of alpha-Synuclein

Although the physiological properties of α-Syn are still quite unclear, its pathophysiological functions are already well understood. The reason for this is that α-Syn has been identified as a major hallmark of three neurodegenerative diseases, which are summarized as synucleinopathies. These are Parkinson's disease, dementia with Lewy bodies (DLB)[154,155], and Multiple System Atrophy (MSA)[156]. The large involvement of α-Syn in these diseases, especially in PD, has led to very intensive research in this area.

PD is the second most common neurodegenerative disease. It comes right after Alzheimer's disease. Statistically, 1-2/1,000 individuals suffer from PD at all times. The prevalence of PD increases with age. From 0.6 % at the age of 65-69 to 2.6 % at the age of 85-89. This results in a general prevalence of 1 % for people aged 60 and older[157]. The average age at disease onset is 65-70 years. About 5 % of cases are classified as young-onset since patients are 40 years of age or younger[158]. Annually ~ 15/100,000 people are diagnosed with PD (reviewed in [159]).

PD is a progressive disease and affects the central nervous system. In 1817 it was first described by James Parkinson as "shaking palsy". As the name already indicates one of

the main symptoms of the disease is tremor. Other symptoms are rigidity, bradykinesia, akinesia, dystonia, dysphagia, and hypomimia. Furthermore, one of the main non-motor symptoms is pain. This symptom is often diagnosed before PD itself[160]. There are also psychiatric symptoms such as dementia depression, apathy, anxiety, and executive dysfunctions[161–163]. In 1912 the scientist Fritz H. Lewy discovered protein inclusions in neurons of PD patients. These inclusions consist to a very large extent of α-Syn and were named Lewy bodies according to the discoverer[154,164]. A little later the same kind of inclusions was found in neurites, which were accordingly termed Lewy neurites[165]. Interestingly, these types of protein inclusions are not only found in synucleinopathies, but also the hippocampus of Alzheimer's disease patients[166]. This finding strongly suggests that the role of α-Syn in neurodegenerative diseases is greater than originally thought.

In α-Syn inclusions the protein is present in a fibrillary confirmation. The reason for this seems to be mutations of the SNCA gene or incorrect posttranslational modifications of the native protein[167]. This defective α-Syn is no longer regulated according to its physiological functions, oligomerizes, and finally forms pathophysiological fibrils. The deposition of these fibrils causes oxidative stress, and synaptic and mitochondrial dysfunctions[168,169] (Fig. 1.2.2). These dysfunctions damage the cell and can finally lead to cell death. It is important to know, that even though α-Syn is found in these intraneuronal inclusions, a variety of additional factors influence the emergence and progression of PD (reviewed in [170]).

In the past few years, results also emerged that α-Syn may be involved in the formation and progression of malignant melanoma. A high correlation between PD and melanoma formation is seen. Different studies found a high expression of α-Syn in melanoma cells and an involvement of α-Syn in melanin production in melanoma cells[171,172]. There a no definitive results yet, but it seems that α-Syn can be associated with diseases apart from neurodegenerative ones.

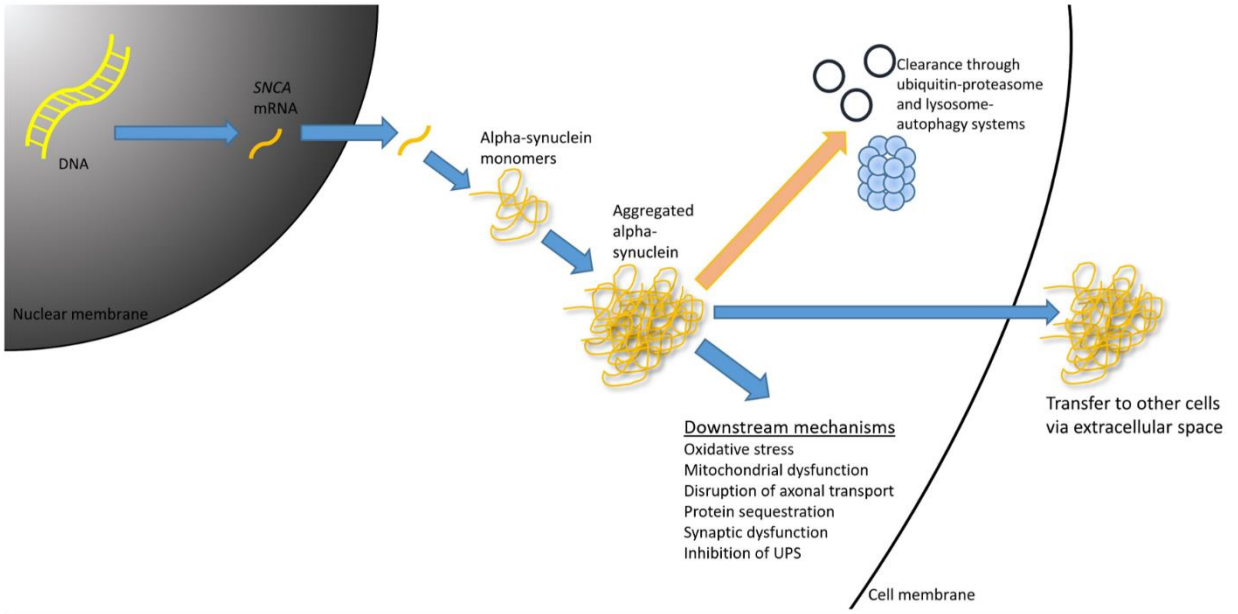

Fig. 1.2.2: Pathological changes of the α-Syn protein. The protein misfolds due to a variety of reasons. The misfolded protein aggregates to pathological oligomers and fibrils. Finally, they form the so-called Lewy bodies and Lewy neurites, which damage the cell via different mechanisms (adapted from Stoker et al. 2018[173]).

1.2.3 The nociceptive system

The term "Pain" has been defined as "an unpleasant, subjective, sensory, and emotional experience associated with actual or potential tissue damage" (International Association for the Study of Pain). Although it is often considered disturbing or annoying, acute pain is an extremely important physical function. The feeling of pain warns us of a potential or acute injury. Thus, the sensation of pain is one of the most important body defense mechanisms. This effect can be seen particularly well in diseases that impair pain sensation. These pain-insensitive patients tend to hurt themselves regularly because the body does not warn them of the potential or acute damage[174]. In addition to the term “pain” there is the term “nociception”, which is significantly different, even though they are often used as synonyms. "Pain" refers to the subjective sensation of the individual, while "nociception" refers to the objective, measurable neurobiological origin, transmission, and coding of the noxious stimulus and pain reaction[175].

The sensation of pain usually leads to a withdrawal reaction to protect the body. It is a complex sensory and emotional process, which is influenced by various biological and psychological factors, such as the density of nociceptors in the skin, but also past experiences, fear, or anxiety[176]. Pain can be classified into many different types. In this thesis, I focused on physiological, inflammatory, neuropathic, and tumor-associated pain.

1.2.3.1 Physiological pain

Physiological pain describes an appropriate response to an acute noxious stimulus, which can be roughly divided into thermal, chemical, or mechanical stimuli. These stimuli must be strong enough to evoke a painful sensation usually leading to the withdrawal of the affected part of the body from the stimulus. The physiological sensation of pain is easily localized and rapidly fades away after the stimulus has gone[177,178].

Physiological pain is usually initiated by the activation of nociceptors. Nociceptors are free nerve endings that act as sensory receptors of the peripheral somatosensory nervous system. They have a high activation threshold and react to various thermal, chemical, and mechanical stimuli. The activation of nociceptors leads to the development of an action potential in the Aδ and C fibers involved (Fig. 1.2.3.1.1)[177]. One of the biggest receptor type families in the nociceptive system are the transient receptor potential (TRP) channels. TRP channels are non-selective cation channels that depolarize the membrane after activation and generate an action potential. The best-known subtypes are the TRPV1 channels, which react to heat and capsaicin, and the TRPM8 channels, which react to cold and menthol[179].

Aδ fibers are myelinated neurons that generate a fast (conduction velocity 3-30 m/s) signal. The resulting pain is sharp and well localized. The activation of non-myelinated C fibers results in a slow (conduction velocity 0.5-2 m/s) signal. This creates a diffuse and dull pain. Additionally, a recent study indicated that some mechanical nociception of the skin is transmitted via “ultra-fast” Aβ fibers (conduction velocity 33-75 m/s)[180]. This is a pretty interesting result since until now it was believed that nociceptive fibers are exclusive of the Aδ and C fiber type. The cell bodies of the Aδ and C fiber neurons gather in the dorsal root ganglia (DRG). These have nociceptive extensions into the dorsal horn of the

spinal cord. The synapses of the primary nociceptive neurons are in laminae I and II, which project on secondary afferent neurons[181]. These fibers transmit the signal into the thalamus, from where it is projected via third-order neurons into various areas, such as the cortex or the amygdala. A very important area in the processing of pain is the periaqueductal grey matter (PAG). This area processes the nociceptive signals and sends modulating signals back to the spinal cord, which can either increase (sensitize) or decrease (desensitize) the nociception (Fig. 1.2.3.1.2)[182]. This feedback mechanism provides a very fine-tuned and appropriate continued response to the noxious stimulus and the potential tissue damage[183].

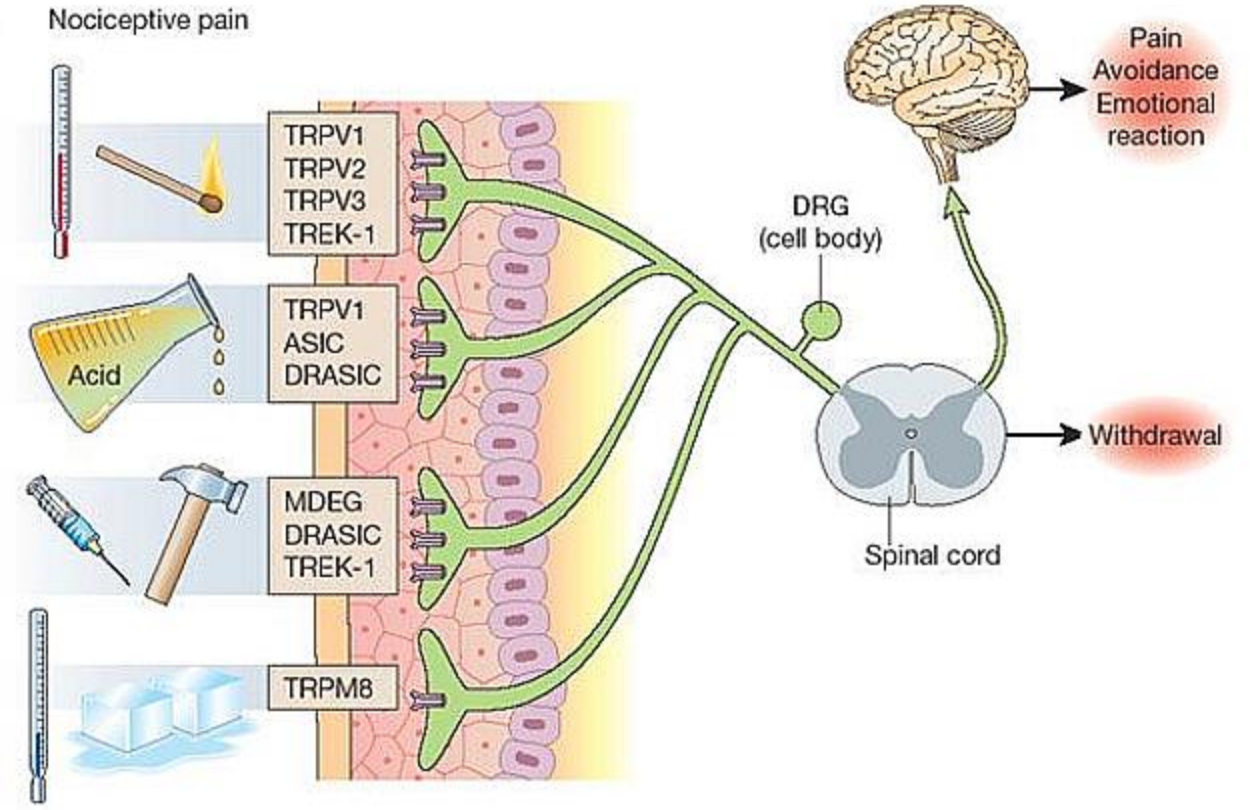

Fig. 1.2.3.1.1: Nociceptive pain. Noxious stimuli, evoked by the activation of different receptors through thermal, chemical, or mechanical stimuli, are transduced into electrical activity. The signal is transmitted through the spinal cord into the brain, where it is processed. **TRP** Transient receptor potential, **TREK** Potassium channel subfamily K member 2, **ASIC** Acid-sensing ion channel**, DRASIC** Dorsal root acid-sensing ion channel, **MDEG** Mammalian degenerin (Scholz and Woolf 2002[142]).

The most important excitatory neurotransmitter in the spinal cord is the amino acid glutamate. Glutamate is released from central terminals of primary afferent neurons. It acts on postsynaptic α-amino-3-hydroxy-5-methyl-4-isoxazolepropionic acid (AMPA)-, N-methyl-D-aspartate (NMDA)-, and metabotropic glutamate (mGlu) receptors. Weak and short-lasting signals activate only AMPA receptors. NMDA and mGlu receptors require an already pre-depolarized postsynaptic membrane and high glutamate levels to be activated. The activation of these receptors leads to modulations of protein expression in the affected neuron, which makes reactivation more likely (reviewed in [184]).

Injury or cell damage, followed by the release of neuropeptides, can lead to peripheral sensitization. This results in an increased sensitivity to different stimuli. A pathological long-term activation of the nociceptive signaling pathway followed by corresponding molecular adaptations leads to the central sensitization of the signaling pathway. This manifests itself in the form of hyperalgesia and allodynia[177,185]. Hyperalgesia is an enhanced response to a noxious stimulus, while allodynia is a nociceptive response to a non-noxious stimulus.

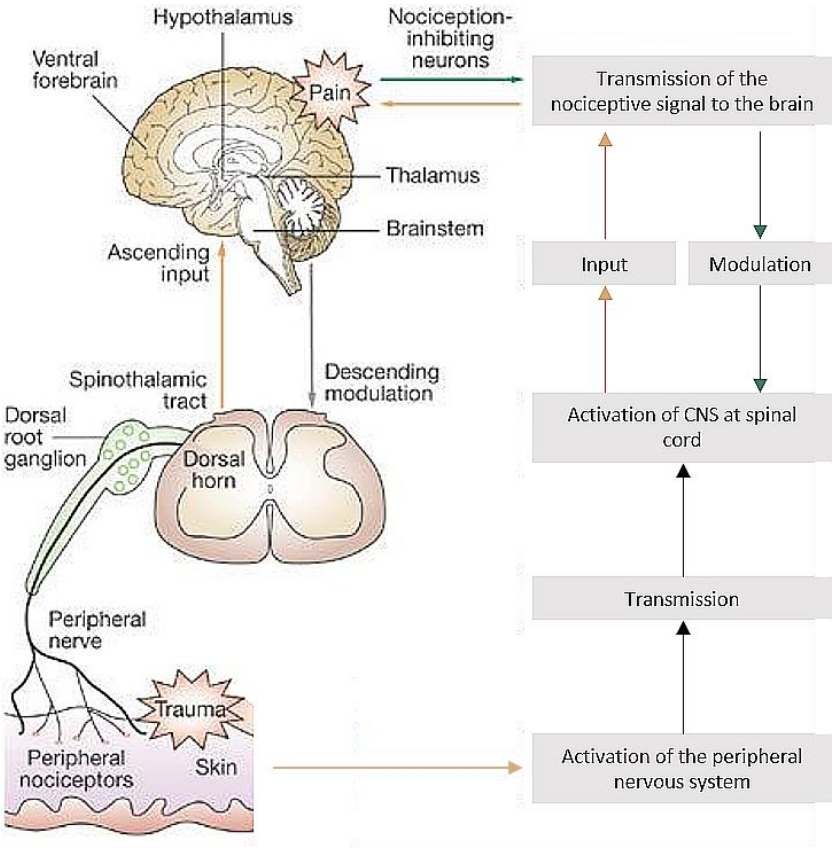

Fig. 1.2.3.1.2: The nociceptive pathway. After the activation of peripheral nociceptors, the action potential is transmitted into the dorsal horn of the spinal cord. From there, the signal is transmitted onto second-order neurons, which project into the brain. The signal is processed, and a descending pathway is able to modulate the nociceptive transmission (adapted from Bingham et al. 2009[186]).

1.2.3.2 Tumor-associated pain

Tumor-associated pain can occur at any point in a tumor disease. Either as a symptom of the disease, or as a result of treatment by chemotherapy, radiation therapy, or surgery[187,188]. As of this point 64 % of patients with advanced cancer report pain[189]. Depending on the cause of the tumor-associated pain, the pain quality is described as either localized and dull, or as diffuse, crampy, and deep[190]. Uncontrollable pain is a common problem in cancer and effective treatment is currently still a major challenge.

The neurobiological and neurochemical mechanisms are multimodal and have characteristics of physiological, inflammatory, and neuropathic nociception[191]. The tumor, surrounding stroma, and immune cells release neuroimmune mediators, which interact with a variety of receptors and induce amplified signals and hyperstimulation of primary nociceptive afferences[192,193]. Some of these factors are endothelin, bradykinin, IL-6, granulocyte macrophage colony-stimulating factor, TNF-α, and NGF[194]. Another mechanism of tumor-associated pain that has already been investigated is the pathophysiological acidification of the tumor environment. The anaerobic conditions in the tumor microenvironment increase the metabolism in the tumor cells, which leads to a release of protons. Protons sensitize the primary sensory afferents. Another mechanism triggered by protons is the direct activation of the TRPV1 channel. Furthermore, the acidification of the tumor environment affects the expression of pain-relevant ion channels in the corresponding afferences[195,196].

The greatly increased metabolism of tumors also increases the proteolytic activity in this tissue. The cleavage products of this proteolytic activity bind to protease-activated receptors (PAR)[195,197,198]. PAR1-4 are able to initiate the release of the neurotransmitters CGRP and substance P from nociceptive afferents, which consequently activate other

nociceptors in the surrounding tissue. CGRP and substance P are considered as a cause of tumor-associated mechanical allodynia[195,199].

In addition to the molecular cascades induced by the release of various transmitters, tumor growth, migration, and invasion also play a decisive role in tumor-associated pain. Tumor growth into surrounding tissue mechanically damages nociceptive neurons and hypersensitizes them. This process is known as the neuropathic component of tumor pain[200,201]. Another phenomenon that can trigger tumor-associated neuropathy is the active proliferation of skeletal-inherent, primary sensory, and sympathetic afferents. The new formation of distal nerve endings leads to neuroma-like structures and appears to be NGF-dependent[202,203]. The increase in sensory afferents can lead to increased stimulation of the nociceptive system.

The standard therapy for tumor-associated pain is the administration of opioid and non-opioid analgesics. The therapy is adjusted according to pathophysiology and pain intensity. For mild pain, non-opioid analgesics, especially NSAIDs, are administered. Some countries also allow the use of cannabinoids, as it proved effective in some types of cancer[189]. For moderate to severe pain, different opioids are administered as required. Often a combination therapy is used to increase the effectiveness of the treatment[190]. Still, the effectiveness is not sufficient and approx. 30 % of cancer patients continue to experience tumor-associated pain[189]. Interestingly, a recent study showed that pain also affects tumor growth. They found that animals experiencing neuropathic pain had larger and heavier tumors in a xenograft model compared to animals without a neuropathic pain model. Additionally, they reported that animals who were treated for the pain had smaller and lighter tumors compared to untreated animals[204]. This finding makes the investigation of effective analgesics even more important. It seems like the correct analgesic treatment does not only help the patients deal with the disease but also affects tumor growth.

1.2.3.3 Inflammatory pain

Inflammatory pain is triggered or promoted by inflammatory processes. Stimulation of immune cells, for example by tissue damage or infections, plays an important role in this process. The immune cells secrete pro-inflammatory markers, such as interleukins, bradykinin, but also protons (Fig. 1.2.3.3)[205] which lower the activation threshold of nociceptors. The consequences are a facilitated activation, or spontaneous activity, of these nociceptors leading to hyperalgesia and allodynia.

Other important mediators of inflammatory pain are prostaglandins (PG). PGs are produced from arachidonic acid by cyclooxygenase (COX)-1 and COX-2. While COX-1 produces the basal level of PGs, COX-2 is induced by pro-inflammatory cytokines or growth factors. Different PGs can trigger a variety of effects by binding to GPCRs. In the nociceptive pathway, PG E_2 (PGE_2) plays the most important role as it is responsible for the prostaglandin-mediated effects, including hyperalgesia[206,207].

The pain qualities of inflammatory pain can be very different reaching from a local dull or stabbing pain to an unspecific discomfort. In general, inflammatory pain has a longer duration than physiological pain and can last from days to weeks. Some diseases, such as rheumatoid arthritis, trigger inflammation that can last for many years[208]. This unusually long duration of inflammation is a major problem since it is a chronic pain disease.

Chronic inflammatory diseases are considered to be the greatest threat to human health. Currently, about 60 % of all people die from chronic inflammatory diseases, such as chronic respiratory diseases, and diabetes. It is assumed that the number of patients suffering from chronic inflammatory diseases will continue to rise steadily for at least the next 30 years. New therapy approaches may act against this prognosis. These inflammatory diseases cause a long-lasting sensitization of the CNS and the pain processing system (reviewed in [209]). For the health and well-being of the patients, it is necessary to intervene as early as possible and decrease or stop inflammation[210]. Standard therapeutics are non-steroidal anti-inflammatory drugs (NSAIDs) such as Ibuprofen and Diclofenac. Drugs from this group reversibly inhibit COX-1 and COX-2, thereby inhibiting the production of PGs[211]. The different PGs can sensitize nociceptive nerve endings by decreasing the threshold of sodium channels, they induce vasodilation and an increase in body temperature, and they modulate the immune system. By blocking

these effects inflammatory nociception is reduced. Typical side effects of NSAIDs are nausea, diarrhea, constipation, gastrointestinal ulceration, and headache. The chronic intake of NSAIDs can also increase the risk of hypertension. Since PGs have a broad physiological spectrum the side effects can be just as variable.

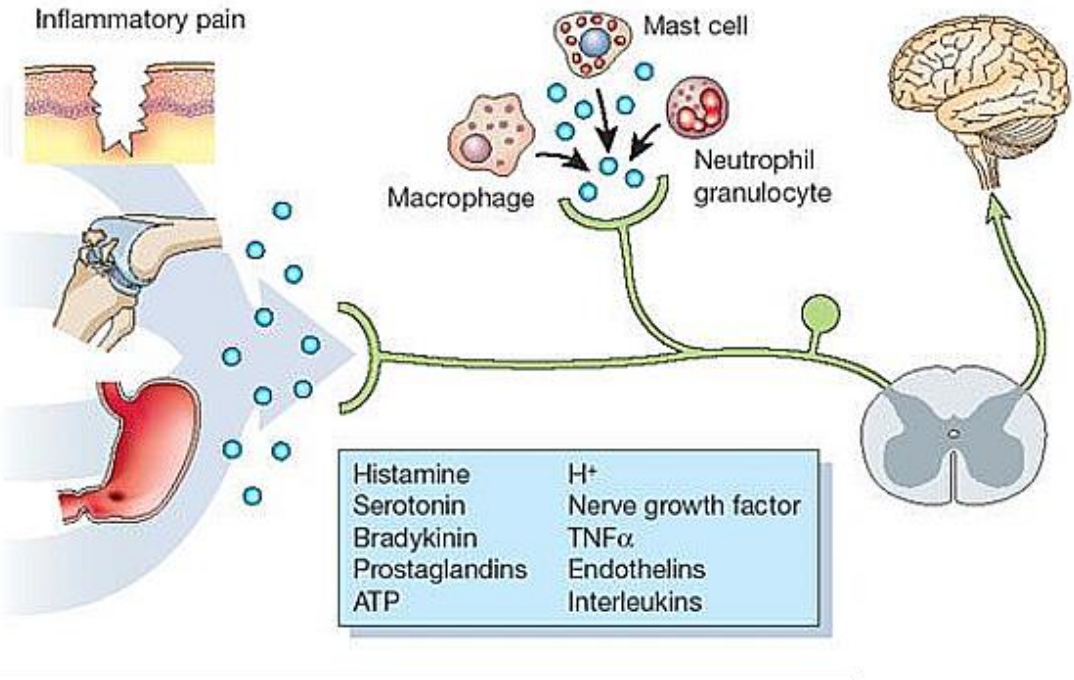

Fig. 1.2.3.3 Initiation of inflammatory pain. Pro-inflammatory activation of immune cells leads to the secretion of inflammatory mediators. These mediators decrease the activation threshold of nociceptors, which leads to allodynia and hyperalgesia (Scholz and Woolf 2002[177]).

1.2.3.4 Neuropathic pain

Neuropathic pain is an abnormal type of pain that arises after the damage of neurons due to various reasons. The most common causes of nerve damage are traumatic injuries affecting the PNS or CNS. In addition, metabolic diseases, e.g. diabetes mellitus[212], neurological diseases, e.g. multiple sclerosis, or viral diseases, e.g. herpes zoster[213–215] induce modifications in the neuronal and immune system that lead to this pathological type of pain. Another way to develop neuropathic pain is by intake of neurotoxic drugs, e.g. chemotherapeutics, such as Oxaliplatin or Cisplatin[216].

Neuropathic pain is described as shooting, burning, prickling, or electrical. In addition to the spontaneous occurrence of this pain, dysesthesia, allodynia, and hyperalgesia may also occur[217]. About 3-4.5 % of the world population and 7-8 % of the European population suffer from neuropathic pain[218]. Due to the almost permanent pain and the very poor therapeutic possibilities, this type of pain results in a reduced quality of life, reduced mobility, and often in an incapacity to work. Patients suffering from neuropathic pain often develop depression as an accompanying symptom[219].

The exact mechanism of neuropathic pain is still not precisely researched but many mechanisms are already discovered. Studies found long-lasting alterations at the molecular level of pain processing cells, e.g. upregulation of calcitonin gene-related peptide (CGRP), brain-derived neurotrophic factor (BDNF), c-Fos, TRPV1, and TRPA1, and hypersensitivity to TNF-α[220] (reviewed in [221]). These changes are triggered by nerve damage via metabolic, neurological, or traumatic damage. Many hypotheses of how these changes are initiated, and which mechanisms and pathways are involved exist. Most often, neuropathic pain is initiated by traumatic nerve injury. A faulty regeneration leads to a sensitization of the system. The neurons become hyperactive and develop spontaneous activity and abnormal excitability[222]. A faulty regeneration that is often found involves the deregulated expression and functionality of Nav channel types[223–225], hyperpolarization-activated cyclic nucleotide-gated (HCN) cation channels[226–228], as well as a decrease in the resting-potential generating potassium equilibrium current. These effects lead to an easier excitation and signal transmission in the affected neuronal systems. Mechanisms in the CNS include functional changes in dorsal horn neurons, reduced activity of inhibitory interneurons, and hypoactivity associated with the

descending antinociceptive pathway[229]. Glial cells have also been shown to influence the central sensitization. After a nerve injury, glial cells release pro-inflammatory cytokines and the excitatory neurotransmitter glutamate, which sensitizes the surrounding neuronal tissue[230]. One study also found a strong connection between lysophosphatidic acid (LPA) signaling and the development and maintenance of neuropathic pain. LPA released by spinal neurons acts on microglia and astrocytes, which release BDNF and cytokines. These molecules sensitize the spinal neurons in a pathophysiological loop mechanism. Accordingly, the inhibition of this pathway by the usage of LPA receptor antagonists was able to inhibit the neuropathic pain in the mouse model used (reviewed in [231]).

Even today, the treatment of neuropathic pain is still very difficult and incomplete. The painkillers available, such as the NSAIDs Ibuprofen and Diclofenac, or Paracetamol, are generally ineffective. The treatment strategy usually includes a combination of antidepressants, anticonvulsants, sodium channel blockers, NMDAR antagonists, and opioids. Individual therapy has to be found out for every patient. However, even with this combination therapy, about 30 % of patients still suffer from pain[232,233]. Also, this mass of drugs is associated with several partially severe side effects. Paracetamol intake can lead to liver damage, kidney failure, and depression. Opioids induce respiratory depression and have an addiction risk. Alternative therapeutic approaches such as neurostimulation techniques have been developed, but the long-term effect remains to be seen[234]. Capsaicin patches or the injection of botulinum neurotoxin A are also used[235,236]. In the meantime, the therapeutic benefit of cannabinoids is also being evaluated. Cannabinoids act on the endocannabinoid system by binding to CB1 and CB2 receptors where they exert analgesic and anti-inflammatory effects[237,238] (reviewed in [239]). However, all these treatment strategies do not provide complete relief for the patients. Therefore, it is imperative to understand the mechanisms of neuropathic pain more precisely to open up new therapeutic options.

1.2.4 Objectives of part II

Not much is known about the function of α-Syn in physiological, inflammatory, neuropathic, and tumor-associated nociception *in vivo*. The pain symptom of PD implies at least a correlation between α-Syn expression and pain. Since α-Syn acts as a molecular hub, a causal connection between it and the nociceptive system is plausible. Furthermore, α-Syn plays a role in tumor development and progression, which makes a role in tumor-associated pain likely. Therefore, part II of the present study aims to investigate the impact of α-Syn in models of acute, inflammatory, neuropathic, and tumor-associated pain by analyzing behavioral and molecular differences between WT and $SNCA^{-/-}$ mice.

For a start, it should be investigated where, and if at all, α-Syn is expressed in the spinal cord and if a co-expression with different neuronal markers is seen. Then it will be checked for motor function and behavioral differences in models of acute pain using wild type and α-Syn knock-out mice. After that, the behavior and molecular changes during and after models of inflammatory, neuropathic, and tumor-associated pain will be investigated. At the end of this work, I intend to gain more insight into the role of α-Syn in the nociceptive pathway.

2. Material

2.1 Chemicals and assays

2.1.1 Chemicals

Tab. 2.1.1: List of chemicals.

Substance	Manufacturer
4-[3-(4-Iodophenyl)-2-(4-nitrophenyl)-2H-5-tetrazolio]-1,3-benzene disulfonate (WST-1)	Sigma-Aldrich, St. Louis, USA
4’,6-diamidino-2-phenylindole (DAPI)	AppliChem GmbH, Darmstadt, Ger
Acetic acid 99 – 100 %	Thermo Fisher Scientific, Waltham, USA
Acetone	Carl Roth GmbH & Co, Karlsruhe, Ger
Acrylamide	Carl Roth GmbH & Co, Karlsruhe, Ger
Agarose	Sigma-Aldrich, St. Louis, USA
Amlexanox	Cayman Chemical, Hamburg, Ger
Ammonium persulfate (APS)	Carl Roth GmbH & Co, Karlsruhe, Ger
Aqua-Poly/Mount	Polysciences, Warrington, USA
B-27 supplement	Invitrogen GmbH, Karlsruhe, Ger
Bafilomycin A1 (BafA)	Cell Signaling Technology, Cambridge, UK
Bovine serum albumin (BSA)	AppliChem GmbH, Darmstadt, Ger
Bradford reagent	Sigma-Aldrich, St. Louis, USA

Bromphenol blue	Serva Electrophoresis GmbH, Heidelberg, Ger
Chloroform ($CHCl_3$)	Merck KGaA, Darmstadt, Ger
Cholera toxin	Sigma-Aldrich, St. Louis, USA
Collagenase I	Sigma-Aldrich, St. Louis, USA
Dimethyl sulfoxide (DMSO)	Thermo Fisher Scientific, Waltham, USA
Dispase I	Roche Diagnostics GmbH, Mannheim, Ger
DNA Ladder Mix 100-10.000 bp	Carl Roth GmbH & Co, Karlsruhe, Ger
DNAse I	Promega GmbH, Mannheim, Ger
Endothelin1	Sigma-Aldrich, St. Louis, USA
Ethanol 70 %	Carl Roth GmbH & Co, Karlsruhe, Ger
Ethanol absolute	Sigma-Aldrich, St. Louis, USA
Fetal calf serum (FCS), hormone-free	Biochrom GmbH, Berlin, Ger
Glutamine	Life technologies GmbH, Darmstadt, Ger
Glycerol	Carl Roth GmbH & Co, Karlsruhe, Ger
Glycine	Sigma-Aldrich, St. Louis, USA
Human stem cell factor	Sigma-Aldrich, St. Louis, USA
Isoflurane	Abbott GmbH & Co KG, Wiesbaden, Ger
Isopropanol (2-Propanol) 100 %	Carl Roth GmbH & Co, Karlsruhe, Ger
KH_2PO_4	Carl Roth GmbH & Co, Karlsruhe, Ger
Laminin	BD GmbH, Heidelberg, Ger
LB-Medium (Lennox)	Carl Roth GmbH & Co, Karlsruhe, Ger

Matrigel Basement Membrane HC	Corning Inc., NY, USA
Methanol	Sigma-Aldrich, St. Louis, USA
Na_2HPO_4 x H_2O	VWR International, Radnor, USA
Nerve growth factor (NGF)	Merck KGaA, Darmstadt, Ger
Normal goat serum (NGS)	Sigma-Aldrich, St. Louis, USA
Odyssey blocking buffer	Li-COR GmbH, Bad Homburg, Ger
PD98059 (PD)	Cell Signaling Technology, Cambridge, UK
Pefabloc SC-protease-inhibitor	Carl Roth GmbH & Co, Karlsruhe, Ger
Penicillin/Streptomycin	Sigma-Aldrich, St. Louis, USA
Phosphate-buffered saline (PBS)	Thermo Fisher Scientific, Waltham, USA
Phosphosafe™ reagent	Life technologies GmbH, Darmstadt, Ger
Poly-L-lysine	Sigma-Aldrich, St. Louis, USA
Ponceau S	Carl Roth GmbH & Co, Karlsruhe, Ger
Potassium chloride (KCl)	AppliChem, Darmstadt, Ger
Propidium Iodide	Sigma-Aldrich, St. Louis, USA
Pyrrolidinedithiocarbamate ammonium (PDTC)	Bio-Techne GmbH, Minneapolis, USA
RNAse A	VWR International, Radnor, USA
RNAse free water	Qiagen GmbH, Hilden, Ger
RNAse ZAP	Sigma-Aldrich, St. Louis, USA
Roti®-Histofix 4.5 %	Carl Roth GmbH & Co, Karlsruhe, Ger
Rotiphorese Gel30 (37.5:1) [Acrylamid]	Carl Roth GmbH & Co, Karlsruhe, Ger

Roti-Safe Gel stain	Carl Roth GmbH & Co, Karlsruhe, Ger
Sodium chloride (NaCl)	Sigma-Aldrich, St. Louis, USA
Sodium dodecyl sulfate (SDS)	AppliChem GmbH, Darmstadt, Ger
Sucrose	Sigma-Aldrich, St. Louis, USA
Sulforhodamine B (SRB)	MP Biomedicals, Santa Ana, USA
Tetradecanoyl phorbol acetate	Sigma-Aldrich, St. Louis, USA
Tetramethylethylendiamine (TEMED)	Carl Roth GmbH & Co, Karlsruhe, Ger
Tissue-Tek O.C.T. compound	Sakura GmbH, Staufen, Ger
Transfer buffer	Bio-Rad Laboratories Inc, Munich, Ger
Trichloroacetic acid 99 %	Carl Roth GmbH & Co, Karlsruhe, Ger
Tris base	AppliChem GmbH, Darmstadt, Ger
Tris-HCl	Carl Roth GmbH & Co, Karlsruhe, Ger
Triton X-100	Merck KGaA, Darmstadt, Ger
Tween 20	Sigma-Aldrich, St. Louis, USA
Zymosan A	Sigma-Aldrich, St. Louis, USA
β-Mercaptoethanol	Sigma-Aldrich, St. Louis, USA

2.1.2 Assays

Tab. 2.1.2: List of assays.

Assay	**Manufacturer**
Glutamate-Glo Assay	Promega GmbH, Mannheim, Ger
REDExtract-N-Amp PCR ReadyMix	Sigma-Aldrich, St. Louis, USA

Verso cDNA Synthesis Kit	Thermo Fisher Scientific, Waltham, USA

2.2 Antibodies

2.2.1 Primary Antibodies

Tab. 2.2.1: List of primary antibodies.

Antibody	Host	Manufacturer
Akt1	Rabbit	Cell Signaling Technology, Cambridge, UK
alpha-Synuclein	Mouse	Becton, Dickinson and Company, Franklin Lakes, USA
beta Actin	Rabbit	Thermo Fisher Scientific, Waltham, USA
beta Actin	Mouse	Thermo Fisher Scientific, Waltham, USA
CD3	Rabbit	Ventana Medical Systems, Inc., Oro Valley, USA
CD45	Rabbit	Abcam, Cambridge, UK
CGRP	Mouse	Santa Cruz Biotechnology, Dallas, USA
CGRP-647	Mouse	Santa Cruz Biotechnology, Dallas, USA

CyclinD1	Rabbit	Cell Signaling Technology, Cambridge, UK
GABA-A	Guinea Pig	Synaptic Systems GmbH, Göttingen, Ger
GAD67	Mouse	Abcam, Cambridge, UK
HSP90	Rabbit	Becton, Dickinson and Company, Franklin Lakes, USA
IB4 – 488	Griffonia simplicifolia	Thermo Fisher Scientific, Waltham, USA
IKK epsilon	Rabbit	Cell Signaling Technology, Cambridge, UK
IKK epsilon	Mouse	Active Motif, La Hulpe, Bel
IKK epsilon	Mouse	Bio-Techne GmbH, Wiesbaden, Ger
LC3b	Rabbit	Cell Signaling Technology, Cambridge, UK
p38	Rabbit	Cell Signaling Technology, Cambridge, UK
p44-42	Rabbit	Cell Signaling Technology, Cambridge, UK
p53	Mouse	Dako Deutschland GmbH, Hamburg, Ger
p62	Mouse	Abcam, Cambridge, UK
p65	Rabbit	Cell Signaling Technology, Cambridge, UK

P-Akt1	Rabbit	Cell Signaling Technology, Cambridge, UK
Pan-Cytokeratin	Mouse	Abcam, Cambridge, UK
PD1	Rabbit	Abcam, Cambridge, UK
P-p38	Rabbit	Cell Signaling Technology, Cambridge, UK
P-p44-42	Rabbit	Cell Signaling Technology, Cambridge, UK
P-p65	Rabbit	Cell Signaling Technology, Cambridge, UK
TBK1/NAK	Rabbit	Cell Signaling Technology, Cambridge, UK
Tyrosine Hydroxylase	Rabbit	Thermo Fisher Scientific, Waltham, USA
V-Glut1	Rabbit	Abcam, Cambridge, UK

2.2.2 Secondary Antibodies

Tab. 2.2.2: List of secondary antibodies.

Target species – dye	**Host**	**Manufacturer**
Guinea Pig – AF594	Goat	Thermo Fisher Scientific, Waltham, USA
Mouse – 680	Goat	Li-COR GmbH, Bad Homburg, Ger

Mouse – 800	Goat	Li-COR GmbH, Bad Homburg, Ger
Mouse – AF488	Goat	Thermo Fisher Scientific, Waltham, USA
Mouse – AF647	Goat	Thermo Fisher Scientific, Waltham, USA
Mouse – Cy3	Sheep	Sigma-Aldrich, St. Louis, USA
Rabbit – 680	Goat	Li-COR GmbH, Bad Homburg, Ger
Rabbit – 800	Goat	Li-COR GmbH, Bad Homburg, Ger
Rabbit – AF488	Goat	Thermo Fisher Scientific, Waltham, USA
Rabbit – AF647	Goat	Thermo Fisher Scientific, Waltham, USA
Rabbit – Cy3	Sheep	Sigma-Aldrich, St. Louis, USA
Ms + Rb - HRP	Goat	PerkinElmer, Waltham, USA

2.3 Cell culture media and buffer

2.3.1 Cell culture media

Tab. 2.3.1: List of cell culture media.

Medium	Manufacturer
Dulbecco’s Phosphate Buffered Saline (DPBS) (1x)	Thermo Fisher Scientific, Waltham, USA
Dulbecco's Modified Eagle's Medium (DMEM)	ATCC, Wesel, Ger
Dulbecco's Modified Eagle's Medium (DMEM) + GlutaMAX-I	Thermo Fisher Scientific, Waltham, USA
Eagle's Minimum Essential Medium (EMEM)	ATCC, Wesel, Ger
Neurobasal Medium (1x)	Thermo Fisher Scientific, Waltham, USA
RPMI Medium 1640 (1x) + GlutaMAX-I	Thermo Fisher Scientific, Waltham, USA

2.3.2 Buffers and solutions

Tab. 2.3.2: List of buffers and solutions, their composition, and manufacturer, if bought.

Buffer	Composition	Manufacturer
0.1 % PBST	1 L PBS 1 mL Tween 20	-
0.1 % PBSTx	1 L PBS 1 mL TritonX 100	-

0.5 M Tris	6.06 g Tris base 100 mL H2O	-
1.5 M Tris	18.18 g Tris base 100 mL H2O	-
10x SDS buffer	30 g Tris Base 150 g Glycine 10 g SDS 1 L H2O	-
10x TBE buffer	108 g Tris 55 g boric acid 40 mL 0.5 M EDTA, pH 8.0 Ad 1 L H2O	-
4x Lämmli buffer	277.8 mM Tris-HCL, pH6.8 44.4 % (v/v) Glycerol 4.4 % LDS 0.02 % Bromphenol blue	Bio-Rad Laboratories Inc, Munich, Ger
Antibody buffer (IHC)	10 % NGS 3 % BSA PBSTx	-
Antibody buffer (Phenoptics)	TBS 1 % BSA	-

Antibody buffer (WB)	50 % Odyssey Blocking buffer 50 % PBST	-
AR6 Buffer	-	PerkinElmer, Waltham, USA
AR9 Buffer	-	PerkinElmer, Waltham, USA
Blocking buffer (IHC)	3 % BSA PBS	-
Blocking Buffer (Phenoptics)	10 % FCS 0.5 % TritonX-100 PBS	-
LB-Medium	20 g LB-Medium 1 L H2O	-
Odyssey Blocking buffer	-	Li-COR GmbH, Bad Homburg, Ger
PBS	10 g NaCl 0.25 g KCl 1.77 g Na2HPO4 x H2O 0.25 g KH2PO4 1 L H2O	-
Propidium iodide staining solution (PI-solution)	200 µg PI 2 mg RNAse A 10 mg PBS	-

TBS	0.1 M Tris-HCl 0.15 M NaCl 0.05 % Tween20	-
TBST	0.1 M Tris-HCl 0.15 M NaCl 0.05 % Tween20 H_2O	-
TRI reagent	0.4 M Ammonium-thiocyanate 0.8 M Guanidinium-thiocyanate 0.1 M Sodium acetate 5 % Glycerin 1 kg Phenol Acetic acid 2.6 L H2O	Sigma-Aldrich, St. Louis, USA
Wet Blot buffer (WB)	15.5 g Tris base 72 g Glycine 1 L Methanol 4 L H2O	-

2.4 Consumables and equipment

2.4.1 Consumables

Tab. 2.4.1: List of consumables.

Consumable	Manufacturer
µ-Plate, 24 Well, Black	ibidi, Martinsried, Ger
0.45 µM Filter	Sarstedt, Nürnbrecht, Ger
1.2 mL syringes	B.Braun Melsungen AG, Melsungen, Ger
1.5 and 2 mL reaction vessels	Eppendorf, Hamburg, Ger
15 and 50 mL Falcon tubes	Greiner Bio-one CELLSTAR, Kremsmünster, Aus
20, 200 and 1000 µL pipette tips	Sarstedt, Nürnbrecht, Ger
23 G and 27 G microlance	Becton, Dickinson and Company, Franklin Lakes, USA
5, 10, and 25 mL serological pipettes	Greiner Bio-one CELLSTAR, Kremsmünster, Aus
6, 12, 24 and 96-well plates	Greiner Bio-one CELLSTAR, Kremsmünster, Aus
Disposable scalpel	FEATHER Safety Razor Co., Ltd., Osaka, Jap
Ep T.I.P.S Standard/Bulk 100-5000 µL pipette tips	Eppendorf, Hamburg, Ger
Glass coverslip	Thermo Fisher Scientific, Waltham, USA
IncuCyte Image Lock 96-well plates	Essen BioScience, Ltd., Hertfordshire, UK
Ja! Cornflakes	Rewe, Köln, Ger

KwikFil Borosilicate Glass Capillaries	World Precision Instruments, Sarasota, USA
MicroAmp Fast Optical 96-Well Reaction Plate with Barcode (0.1 mL)	Applied Biosystems, Waltham, USA
MicroAmp Optical Adhesive Film	Applied Biosystems, Waltham, USA
Microscope slide Superfrost PLUS	Thermo Fisher Scientific, Waltham, USA
PAP pen	Sigma-Aldrich, St. Louis, USA
Parafilm M	Sigma-Aldrich, St. Louis, USA
Pasteur pipettes	WU Mainz, Mainz, Ger
ThinCerts, 24 Well, 8.0 µM	Greiner Bio-one CELLSTAR, Kremsmünster, Aus
TransBlot Turbo Mini-size nitrocellulose membrane	Bio-Rad Laboratories, Hercules, USA
TransBlot Turbo Mini-size transfer stacks	Bio-Rad Laboratories, Hercules, USA
Vasco nitrile gloves	B.Braun Melsungen AG, Melsungen, Ger

2.4.2 Equipment

Tab. 2.4.2: List of equipment.

Equipment	**Manufacturer**
BeadBug 6 Microtube Homogenizer	Benchmark Scientific, Sayreville, USA
BZ-9000 (BIOREVO)	Keyence, Neu-Isenburg, Ger
Centrifuge 5804R & 5810R	Eppendorf, Hamburg, Ger
Cryostat CM 3050S	Leica Biosystems, Wetzlar, Ger

Dynamic Plantar Aesthesiometer 3745	Ugo Basile, Gemonio, Ita
Eppendorf Thermomixer Compact	Eppendorf, Hamburg, Ger
FACS Canto II	Becton, Dickinson and Company, Franklin Lakes, USA
Fluorescence microscope AXIO Observer Z1, AxioCam MRm, HXP120 Fluoreszenz	Carl Zeiss, Oberkochen, Ger
Gastight syringes	Hamilton Company, Reno, USA
Gel Documentation System	Bio-Rad Laboratories, Hercules, USA
GFL incubator 3031 & 7601	Gesellschaft für Labortechnik, Burgwedel, Ger
Hot/Cold Plate	Stoelting, Wood Dale, USA
Image Xpress Micro XLS Widefield High-Content Imaging System	Molecular Devices, LLC., San Jose, USA
IncuCyte 96-pin wound making tool	Essen BioScience, Ltd., Hertfordshire, UK
Laboratory hood HERA Safe	Heraeus, Hanau, Ger
Laboratory scale	KERN & Sohn GmbH, Balingen, Ger
Mastercycler	Eppendorf, Hamburg, Ger
Microcentrifuge 5415R	Eppendorf, Hamburg, Ger
Microplate reader	Tecan, Männedorf, Swi
Mixer Mill	Retsch Technology GmbH, Haan, Ger
Mouse Rota-Rod	Ugo Basile, Gemonio, Ita
NALGENE Cryo 1 °C Freezing Container	Thermo Fisher Scientific, Waltham, USA
NanoDrop One/One microvolume spectrophotometer	Thermo Fisher Scientific, Waltham, USA

Odyssey Infrared Scanner	Li-COR GmbH, Bad Homburg, Ger
Pipetus	Hirschmann Laborgeräte GmbH & Co. KG, Eberstadt, Ger
Platform shaker Duomax 1030	Heidolph Instruments, Schwabach, Ger
Quant Studio 5	Thermo Fisher Scientific, Waltham, USA
Surgical equipment	World Precision Instruments, Sarasota, USA
Trans-Blot Turbo	Bio-Rad Laboratories, Hercules, USA
Vacuum centrifuge concentrator 5301	Eppendorf, Hamburg, Ger
Vortex-Genie 2	Scientific Industries, Inc., New York, USA
Water bath SW22	Julabo, Seelbach, Ger
Western Blotting equipment	Bio-Rad Laboratories, Hercules, USA

2.5 Primer

Tab. 2.5: List of primers

Target Gene	**Sequence**	**Manufacturer**
TRPM8 (ms)	FW 5’-CGCACTCCTCACCTT TTGTCT-3’ RV 5’-CCTGCTGCTTCTG TCCTCTT-3’	Biomers.net GmbH, Ulm, Ger

GAPDH (ms)	FW 5′-CAATGTGTCCGTC GTGGATCT-3′ RV 5′-GTCCTCAGTGTAGC CCAAGATG-3′	Biomers.net GmbH, Ulm, Ger
COX-2	FW 5’-AGACACTCAGGTAGA CATGATCTACCCT-3’ RV 5’- GGCACCAGACCAAA GACTTCC-3’	Biomers.net GmbH, Ulm, Ger
c-Fos	FW 5’- ACCATGATGTTCTCG GGTTTCAA-3’ RV 5’- GCTGGTGGAGATGG CTGTCAC-3’	Biomers.net GmbH, Ulm, Ger
IKKε	FW 5’- GTACAAGGCCCGAA ACAAGA-3’ RV 5’- TCCTCCACTGCGAA TAGCTT-3’	Biomers.net GmbH, Ulm, Ger
TBK1	FW 5’- TGCTTACCCCAGTT CTTGCA-3’ RV 5’- CCCCAGCACTTCTC CTGATC-3’	Biomers.net GmbH, Ulm, Ger

Akt1	FW 5'- GGCTGGCTGCAC AAACG-3' RV 5'- GACTCTCGCTGAT CCACATCCT-3'	Biomers.net GmbH, Ulm, Ger

2.6 Cell lines and mouse strains

2.6.1 Cell lines

Tab. 2.6.1: List of cell lines.

Cell line	Vendor
A375M	ATCC, Wesel, Ger
B16-F10	Wellcome Trust Functional Genomics Cell Bank, London, UK
HERMES1	Wellcome Trust Functional Genomics Cell Bank, London, UK
SK-Mel-28	CLS, Eppelheim, Ger

2.6.2 Mouse strains

Tab. 2.6.2: List of mouse strains.

Background	Mutation	Breeder
C57Bl/6J x 129	SNCA	The Jackson Laboratory, Bar Harbor, USA

C57Bl/6J	Foxn1	Janvier Labs, Le Genest-Saint-Isle, Fra
C57Bl/6J	-	Charles River Laboratories, Sulzfeld, Ger

2.6.2.1 Animal ethics

All mice were either bought from a commercial vendor or transferred from a commercial breeding facility one to two weeks before the start of an experiment. They were housed under constant conditions, including a 12 h light-dark cycle and a room temperature of 21 ± 1 °C. Food and water were available *ad libitum*. For the experiments, adult mice at the age of 6-12 weeks were used, unless stated otherwise.

The experiments complied with the guidelines of GV-SOLAS for animal welfare in science and were in line with the European and German regulations for animal research. Additionally, all experiments were approved by the local Ethics Committee for Animal Research (Regierungspräsidium Darmstadt, Germany). The approval identifications are FK/1081 and FK/1092. All efforts were made to minimize animal suffering and to reduce the number of animals used.

2.7 Software

Tab. 2.7: List of software.

Software	Version	Manufacturer
Citavi	5	Swiss Academic Software, Wädenswil, Swi

FlowJo	10	Becton, Dickinson and Company, Franklin Lakes, USA
Gel Doc QuantityOne Software	4.6.8	Bio-Rad Laboratories, Hercules, USA
Image Studio Lite	4	Li-COR Biosciences, Lincoln, USA
ImageJ	1.52e	Wayne Rasband (Dev.)
IncuCyte ZOOM Software	2016A	Essen BioScience, Ltd., Hertfordshire, UK
inForm	2.4	PerkinElmer, Waltham, USA
Office	2019	Microsoft Corporation, Redmond, USA
Prism	7	GraphPad Software, Inc., La Jolla, USA
Quant Studio Design and Analysis Software	1.2	Applied Biosystems, Waltham, USA
Windows	10	Microsoft Corporation, Redmond, USA
Zen (blue edition)	3.1	Carl Zeiss, Oberkochen, Ger

3. Methods

3.1 Animal experiments

3.1.1 Behavioral experiments

Before nociceptive behavioral experiments could be performed, the motor coordination of the animals was assessed with the Rotarod and the Hanging wire test. Animals that couldn't perform these tests were excluded from further behavioral experiments. Well-functioning motor control is necessary for the following nociceptive behavioral tests since they are based on motoric reactions of the animals.

The behavioral tests were all done at a similar time of the day (10 am – 3 pm) to make sure the animals were all in the same activity phase. Before each behavioral test, the animals were allowed to habituate to the experimental room and the experimenter for at least 30 min before testing.

The experimenter was blinded for the genotype or treatment of the animals, respectively. A similar number of male and female animals were used for all experiments, except the melanoma xenograft where only males were used.

3.1.1.1 Rotarod test

The animal was placed headfirst on top of the rotating rod (Fig. 3.1.1.1). It was allowed to freely move around. The goal of the animal was to stay on the rod. It didn't matter if the animal walked or clung to it since both behaviors indicate an intact motoric function. The speed was adjusted to 18 rpm and the cut off time for this experiment was 90 s. The animals were allowed to perform three to four training units to become used to the procedure. If the animals stayed on the rod for 90 s during the experiment, they were defined as motoric well-functioning.

Fig. 3.1.1.1: Rotarod test to assess motoric functions. The speed was adjusted to 18 rpm and the cut-off time was 90 s. The animals had to balance on the rotating black rod.

3.1.1.2 Hanging wire test

An animal was placed on top of a metal grid, which was then lifted approx. 40 cm into the air. The grid with the animal was turned upside down above a cage filled with bedding material to cushion a potential fall. The goal of the test for the animal was to hold onto the downside of the grid for 60 s. Animals without motoric deficits accomplished this task easily. If mice failed in this test they were excluded from further behavioral experiments.

3.1.1.2 Hot/Cold Plate test

The device was either heated up to 52 °C or cooled down to 4 °C. Then, the animal was placed on the metal plate of the Hot/Cold Plate test (Fig. 3.1.1.2). The time was stopped until the animal showed some avoidance or painful behavior, e.g. walking up the plastic cage, licking/flinching of the paws, or jumping. The cut off time for the Hot Plate test was 25 s, and for the Cold Plate test 40 s to avoid tissue damage.

Fig. 3.1.1.2: Hot/Cold Plate test for the measurement of thermal nociception. The device was set to either 52 °C or 4 °C and the cut-off time was 25 s or 40 s, respectively.

3.1.1.3 Dynamic Plantar test for mechanical sensitivity

The paw withdrawal latency (PWL) to mechanical stimulation was assessed with an automated testing device (Aesthesiometer). It consisted of a steel rod, which was pushed against the plantar side of the hind paws, and a metal grid (Fig. 3.1.1.3). Before the test started the animals were placed on top of the metal grid, each under an upside-down water glass to restrict movement. The animals were habituated to the environment for 60-90 min. Then, the test was started. The force of the rod increased with 0.5 g/s for 10 s. 5 g was set as maximum force to prevent mechanical tissue damage. After a 10 s ramp, the force was hold for an additional 10 s to enable the animals to react to the stimulus. If the animal reacted and lifted the paw the device stopped the time and the metal rod sank to its starting position. The PWL of both hind paws was measured three to five times and the mean was calculated. The ΔPWL was calculated with the equation:

“((ipsi-contra)/contra*100) * (-1) “.

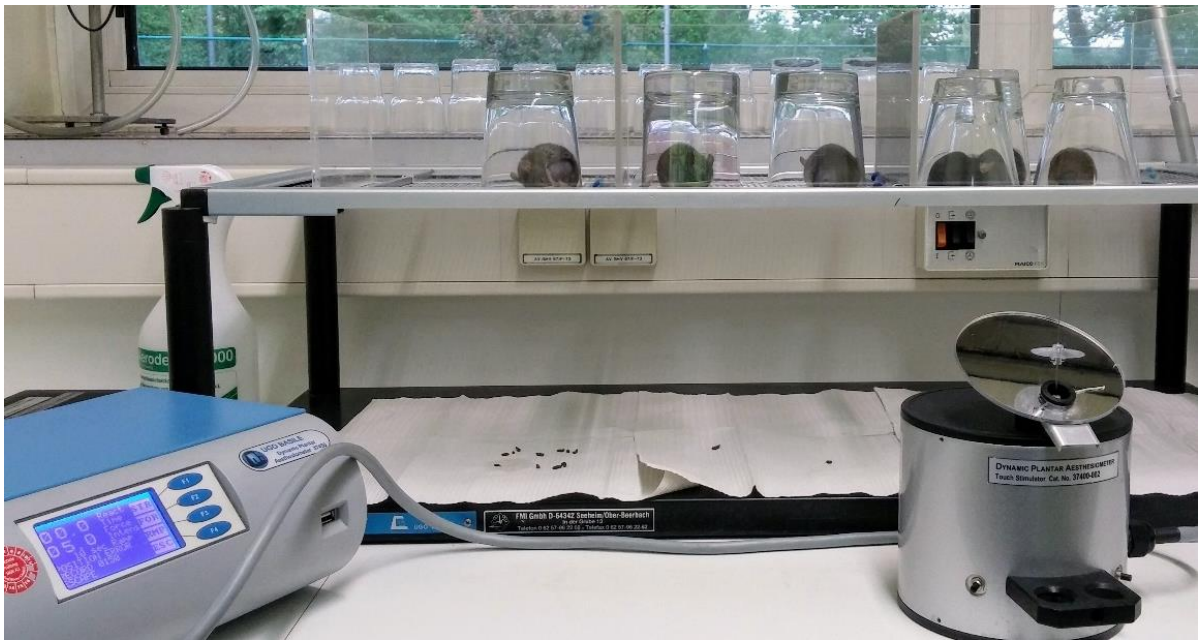

Fig. 3.1.1.3: Aesthesiometer for the Dynamic Plantar test. Mice were habituated for 60-90 min before the test started. Paws were measured 3-5 times.

3.1.1.4 Formalin test for inflammatory nociception

For this model of short-lasting inflammatory pain, a mouse was placed in a clear plastic cylinder for 30 min with the experimenter in front of it to habituate (Fig. 3.1.1.4). After the 30 min were over, an inflammation of the left hind paw was induced by injection of 20 µL of a 5 % formalin/PBS solution subcutaneously into the dorsal side of the left hind paw. The mouse was put back into the cylinder and the time spent licking of the injected paw was recorded in 5 min intervals for 45 min. The licking time correlates to the pain intensity and was plotted against the 5 min intervals. The responses between $SNCA^{-/-}$ and wildtype littermates were compared. The animals were sacrificed at indicated time points after injection (2 h or 8 h) for organ collection.

Fig. 3.1.1.4: Mouse during its 30 min habituation for the formalin test. Rodents don't like to be in an open space without a possibility to hide. Therefore, the habituation was necessary to achieve constant results between different individuals.

3.1.1.5 Zymosan test for inflammatory nociception

The Zymosan test is a model for longer-lasting inflammatory pain. The animals were habituated to the Dynamic Plantar Aesthesiometer. Then, the left hind paw was injected with 20 µL of a 10 mg/mL solution Zymosan A in PBS. Unlike formalin, Zymosan A was injected subcutaneously into the plantar side of the paw. The animals were put back into the test device and the mechanical pain threshold was recorded hourly from two to eight hours. The process of the inflammation could easily be detected with the observation of the paw. It increased in size and reddened. The animals were sacrificed after the last measurement and tissue was collected.

3.1.2 Spared Nerve Injury for neuropathic pain behavior

The SNI model is based on the lesion of two of the three terminal branches of the sciatic nerve (tibial and common peroneal branches) leaving the third branch (sural branch) intact. This model produces neuropathic pain without the regeneration of the damaged nerve[240].

The animal was anesthetized with a 2 % isoflurane-carbogen anesthetic. The left hind leg was shaved, and the animal was placed with the nose in an inhalation mask. The skin caudal to the femur was cut which exposed the thigh muscle. The muscle was opened via blunt dissection to expose the sciatic nerve. The tibial and common peroneal branches of the nerve were tied off with suture thread (5 – 0) and an approx. 2 mm piece of the two branches was transected distal to the knot (Fig. 3.1.2). The two parts of the nerve were put back under the muscle and the skin was stitched with the same type of thread as used before. The mouse was put back in its home cage and observed until it woke up from anesthesia.

A successful operation took between seven and ten minutes and it took the mouse approx. one to two minutes in its home cage to recover.

The dynamic plantar test was performed before the induction of neuropathic pain and 3, 7, 14, 21, and 28 days after the operation. The animals were sacrificed after the last measurement and tissue was collected.

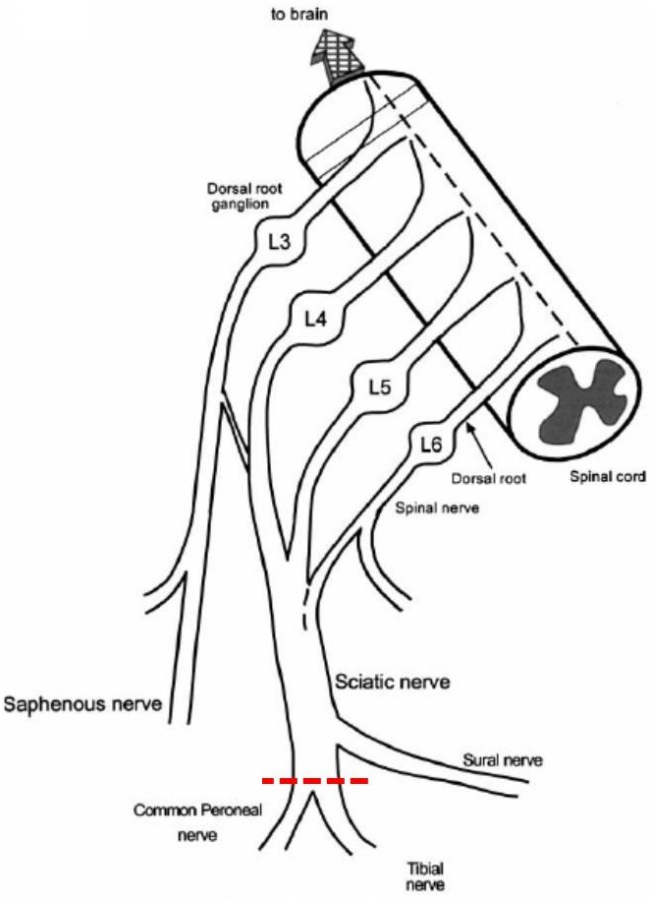

Fig. 3.1.2: Illustration of the SNI. For the SNI, two of the three branches of the sciatic nerve, the tibial and common peroneal branches, are tied off and transected. The sural nerve is left intact. The dotted red line indicates the position where the branches are tied off. This results in neuropathic pain (adapted from Decosterd and Woolf, 2000[240]).

3.1.3 Melanoma model for tumor-associated pain

3.1.3.1 Melanoma cell inoculation

To create a model of tumor pain, mouse melanoma cells were injected into the left hind paw of the animals. 2.5 * 10^5 cells of the cell line B16-F10 were resuspended in 20 µL PBS. The mouse was anesthetized with a 2 % isoflurane-carbogen anesthetic and 20 µL of the cell solution were injected subcutaneously into the plantar side of the left hind paw. Since the cell line originates from a mouse melanoma no immunoreactivity was given and

the tumor growth could be observed under physiological conditions. The animals were put back into the home cage and observed until they regained consciousness.

The Dynamic Plantar test and paw volume measurement were done before the injection as a baseline measurement and on days 3, 7, 14, and 21 after injection to assess mechanical hyperalgesia.

The animals were sacrificed after the last measurement and tissue was collected.

3.1.3.2 Paw volume measurement

To assess the size of the tumor, the paw volume was measured with a plethysmometer. The animal was put in a forced handle and the paw was immersed into the water-filled cylinder of the device up to a constant mark on the ankle. The volume of displaced water was recorded by the plethysmometer and was equal to the volume of the paw. The growth of the tumor led to an increased paw volume.

3.1.4 Melanoma xenograft

A human melanoma was created in Foxn1 mice by injection of human melanoma cells subcutaneously into the flanks of the animal. For this model, the cell line SK-Mel28 was used. 5 x 10^6 cells / 100 µL PBS were resuspended. The mouse was anesthetized with a 2 % isoflurane-carbogen anesthetic and 100 µL of the cell solution were injected subcutaneously into the flank of the mouse. The animals were injected into both flanks. After injection, they were put back into the home cage and observed until they regained consciousness.

3.1.4.1 Treatment

Animals were systemically treated with the IKKε/TBK1 complex inhibitor amlexanox or the vehicle DMSO. The substances were administered via feeding with cornflakes. Two to three days before injection of the melanoma cells, the animals got 2 g cornflakes per

animal put in their cage to habituate the animals to the cornflakes. Starting with the injection of the melanoma cells into the mouse paw, DMSO or amlexanox were added to the cornflakes. Amlexanox was dissolved in DMSO to achieve a 13.3 mg/mL stock solution. 200 µL of a 10 % sucrose/water solution containing amlexanox at a final concentration of 25 mg/kg body weight or the corresponding 0.1875 % DMSO were added per 1 g of cornflakes.

The cornflakes were air dried for about 30 min to prevent them to be soggy. They were put into the cage of the corresponding animal group. Our group already showed that this way of drug administration leads to a stable uptake of the drug[241]. The cornflakes were added on five consecutive days, followed by a pause of two days. The weight of the animals was monitored every 2-3 days.

3.1.4.2 Tumor size measurement

The size of the tumor was measured on days 4, 7, 9, 11, 14, 16, 18, 21, 23, 25, and 28 with a digital caliper. The length (L) and the width (W) were measured while the animal was in a forced grip. The volume of the tumor was calculated with the equation "$V = \pi / 6 * 1.69 * (L * W)^{1.5}$"[242].

The animals were sacrificed on day 28. The tumor was dissected, weighed, and frozen in liquid nitrogen until further use.

3.1.5 Cerebrospinal fluid extraction

The animal was sacrificed by CO_2 inhalation and final blood withdrawal. The head of the animal was placed in a stereotaxic instrument and secured with headpins. The neck was stretched by pushing down the snout. Then, the skin of the neck was cut, and the muscles were opened by blunt dissection. This uncovered the dura mater, which borders the cisterna magna (Fig. 3.1.5). A glass capillary was inserted through the dura mater into the cisterna magna and placed there. It filled up with a clear liquid, the cerebrospinal fluid (CSF). After approx. 20 s, it wouldn't fill up further. The capillary was removed and put into

a sample tube. The tube with the capillary was briefly centrifuged to gather the CSF in the tube. Then, the capillary was removed, and the sample frozen in liquid nitrogen. Normally, a CSF volume of about 5 – 15 µL was extracted.

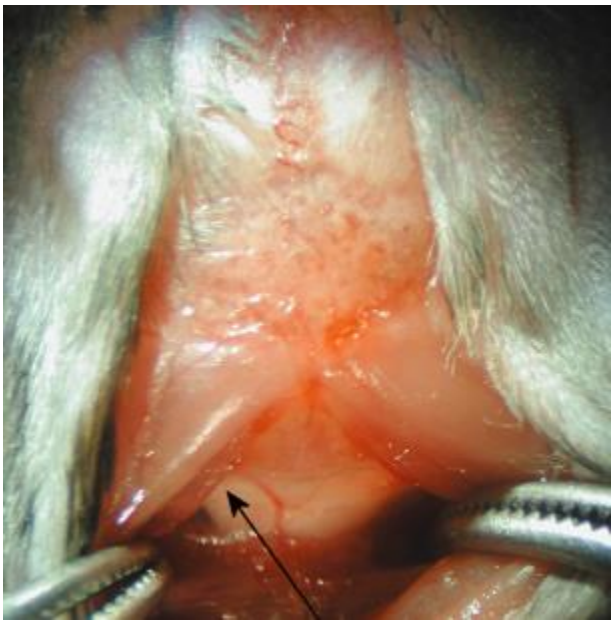

Fig. 3.1.5: The uncovered dura mater, bordering the cisterna magna, of a mouse. The black arrow indicates the point of CSF extraction via a glass capillary (Liu et al. 2008[243]).

3.1.6 Perfusion and fixation of mice for immunohistochemistry

The animal was subjected to CO_2 inhalation until the state of asphyxia was reached. It was then placed in a laboratory hood and the chest cavity was opened. The dissection was very careful and as blunt as possible to ensure that no organ was damaged. Then, a blunt needle, which was attached to a liquid pump, was inserted into the left ventricle of the heart, the right atrium was opened with a scissor and the pump was started. The organism was flushed with an isotonic saline solution for 2 min. The flow rate of the pump was set to 25 mL per minute. Then, the pump was stopped, the solution switched to 2 % PFA in PBS, and started again. The time and flow rate were the same as for the saline

solution. During the perfusion with PFA, the mouse was fixated, and the muscles started to cramp. It was made sure that the spinal cord remained straight.

The perfused animal was dissected, and tissue was taken. It was handled extremely carefully to not damage it. After dissection, the tissue was stored in 2 % PFA for 30-60 min.

3.1.6.1 Tissue embedding

After PFA storage, the tissue was incubated in 20 % sucrose in PBS for 4-6 hours at 4 °C. After that, the 20 % sucrose was replaced with 30 % sucrose in PBS o/n at 4 °C. The next day, the tissue was prepared further by removing residues from other tissues, e.g. connective tissue, with the help of a binocular. The tissue was placed in a cryomold, which in turn was filled with the Tissue-Tek O.C.T. compound. The mold was placed on dry ice for at least 2 min to freeze the Tissue-Tek. The mold was stored at -80 °C until slices were prepared.

3.1.6.2 Object slide preparation

The mold was stored at -20 °C o/n to warm it up. On the next day, the tissue block was pushed out of the mold and fixated on the metal mount of the cryostat with Tissue-Tek. The Tissue-Tek hardened at -20 °C in the cryostat for 60 min. Then, the mount was adjusted in the cryostat and 50 µm thick slices were cut off until the tissue was reached. Slices of 12 to 14 µm were cut with the automatic cutting option of the cryostat. The slice stretcher was tipped to the side and a specimen slide was put on top of the slice. The slice clung onto the relatively warm specimen slide

At the end of a cutting session, the rest of a tissue block, if not used up entirely, was cut off the mount and pushed back into the mold. The exposed tissue was covered with Tissue-Tek and the mold was stored at -80 °C.

3.2 Cell culture experiments

3.2.1 Cell lines and culture

The cells were cultured in a humidified incubator at 37 °C with 5 % CO_2 and the cell culture media contained 10 % FCS if not stated otherwise.

3.2.1.1 B16-F10

The murine melanoma cell line B16-F10 was obtained from the Wellcome Trust Functional Genomics Cell Bank. The cell line originates from the melanoma of a C57Bl/6J mouse. They were cultivated in ATCC's DMEM medium. Since B16-F10 cells tend to differentiate if they grow too sparely or too dense, they were passaged three times a week. Mondays 8 x 10^5 cells were passaged, Wednesdays they were split 1:10, and Fridays 6 x 10^5 cells were passaged. Cells were washed with PBS and treated with Trypsin to dispense them from the cell culture flask. The enzymatic reaction was stopped by the addition of FCS-containing cell culture medium. The cell solution was centrifuged for 3 min at 200 g. The supernatant was discarded, and the cells were resuspended in medium.

3.2.1.2 SK-Mel28

The human SK-Mel28 cell line originates from the melanoma of a 51-year-old male. The cells express mutant BRAF, EGFR and TP53, and wildtype CDKN2A and N-Ras. The cell line was commercially bought from CLS. The cells were cultivated in ATCC's EMEM medium and passaged two to three times a week when they were around 80-90 % confluent. Cells were washed with PBS and treated with Trypsin to dispense them from the cell culture flask. The reaction was stopped, the cells were centrifuged, and resuspended in fresh medium.

3.2.1.3 A375M

The human A375M cell line originates from the melanoma of a 54-year-old female. The cells express mutant BRAF and CDKN2A, and wildtype EGFR, TP53, and N-Ras. The cell line was commercially bought from ATCC. The cells were cultivated in ATCC's DMEM medium and treated the same as SK-Mel28 cells.

3.2.1.4 HERMES1

This human cell line originates from the melanocyte of a 24-year-old male. The cells were cultivated with RPMI 1640 medium. The cell line was obtained from the Wellcome Trust. For the optimization of cell culture conditions 220 nM tetradecanoyl phorbol acetate, 220 pM cholera toxin, 11 nM endothelin1, and 10 ng/mL human stem cell factor were added to the medium. The cells were cultivated at 10 % CO_2, and they were split every two to three days to keep the confluency at max. 70 %.

3.2.2 Proliferation analysis

To analyze the effects of IKKε inhibition on cell proliferation the WST-1 and SRB assays were used as endpoint analysis. The WST-1 assay is based on the number of metabolically active cells, while the SRB assay is based on cellular proteins of fixated cells in the well of a cell culture plate. These assays could be done directly after one another.

3.2.2.1 WST-1 assay

5 x 10^4 cells were disseminated in 500 µL medium into a well of a 24-well plate. Cells were allowed to set for 24 h. Then, the medium was changed to fresh medium with the treatment. As conditions, negative control, vehicle (DMSO), and 10, 20, 30, and 50 µM amlexanox were used, all incubated in duplicate for 48 h.

The medium was discarded and 300 µL fresh medium were added per well. 30 µL WST-1 reagent were added and the cells were incubated for 90 min at 37 °C. During this time, the cells metabolized WST-1 to Formazan. Finally, the absorption of the wells at 450 and

620 nm was measured with a microplate reader. The 620 nm measurement was used as a reference for calculations.

3.2.2.2 SRB assay

After the measurement of the WST-1 assay, the SRB assay was done. 60 µL of 50 % TCA were added to the WST-1 containing medium. The plate was incubated for 1 h at 4 °C. This precipitated proteins and fixated the cells. The supernatant was discarded, and the plate was rinsed five times with H_2O. Then, it was dried for 1-2 h at 60 °C.

300 µL SRB solution (0.4 % in 1 % acetic acid) were added to the wells and incubated for 30 min on a shaker at RT. The SRB solution was discarded and the wells were rinsed five times with 1 % acetic acid. The plate was dried for 1-2 h at 60 °C.

750 µL 10 mM Tris/HCl solution were added to dissolve the dye. The plate was incubated for 10 min on a shaker at RT. The absorption at 540 nm was measured with a microplate reader and used for further calculations.

3.2.3 Migration assays

Migration is one of the most important factors for tumor growth and development. Three different types of migration assays to assess the effect of IKKε inhibition on the migrative abilities of human melanoma cells were used.

3.2.3.1 Transwell assay

This assay is based on the migration of cells through a membrane with a pore size of 8 µM. The inserts with the membranes were positioned into the wells of a 24-well plate. The wells were filled up with 750 µL culture medium. For the negative control, FCS-free medium was used. Then, 5 x 10^4 cells were disseminated in 300 µL FCS-free medium into the inserts. Amlexanox or DMSO were added as treatment into the inserts. The cells

were incubated for 48 h at 37 °C. During this time, the cells were able to migrate towards the FCS-rich medium through the membrane.

The medium was discarded and the wells, as well as the inserts, were washed twice with PBS. 1 mL 4 % PFA was added for 2 min per insert to fixate the migrated cells. The PFA was discarded and the inserts were washed twice with PBS. Then, the cells were permeabilized with 1 mL 100 % methanol for 20 min. The methanol was discarded, and the inserts were washed twice with PBS. The inside of the insert was freed from cells by cleaning it with a cotton bud. 800 µL DAPI solution were added per insert for 2 min to stain the remaining cells. The inserts were washed twice with PBS. Finally, the membrane was cut free from the insert with a scalpel and placed on a specimen slide with the outside up. A drop of Aqua-Poly/Mount was put on top of the membrane and a cover slide was added on top of that.

The number of migrated cells was assessed on a microscope. Pictures of three different areas of the membrane were taken with 10x magnification and the number of cells was counted with the help of ImageJ's automated cell counting tool. The mean of the three areas was taken as cell count.

3.2.3.2 ibidi migration assay

The second migration assay is based on cells growing into a gap and closing it. The assay was performed in cooperation with the group of Dr. S. Schiffmann (Fraunhofer IME-TMP, Frankfurt, Ger).

For this assay, ibidi's 24-well, black µ-plates with two-chamber culture inserts were used. 30,000 (SK-Mel28) or 40,000 (A375M) cells were disseminated in 70 µL medium per chamber. The medium already contained the treatment, if one was used. After 24 h at 37 °C, the inserts were carefully removed with sterile forceps and the wells were washed once and then filled with 500 µL medium containing 2 % FCS and the corresponding treatment. The plate was closed with adhesive film and placed under the Image Xpress microscope at 37 °C. Pictures of the cell-free gap were taken on two positions per gap every 2 h for a total of 36 h.

The width of the cell-free gap was measured in every picture and the change was analyzed over time.

3.2.4 Invasion assay

The invasion assay was used to assess the invasive abilities of the melanoma cells by adding an additional physical barrier to the Transwell assay.

Matrigel was diluted with FCS-free medium to a concentration of 0.3 mg/mL. To do that, the frozen Matrigel was thawed on ice. Matrigel is liquid at approx. 0 °C. At higher and lower temperatures, it becomes more viscous. 100 µL of this Matrigel dilution were added into a Transwell insert and incubated for 24 h at 37 °C.

After that, the protocol was the same as the Transwell assay. The invasive capacity was calculated with “Number of invasive cells / Number of migrated cells * 100”.

3.2.5 Autophagy assay

5 x 10^5 cells were disseminated in 3 mL medium into a 6 cm cell culture dish. The cells were incubated for 24 h at 37 °C. The medium was changed to FCS-free medium containing 20 µM Chloroquine. Chloroquine inhibits autophagosome and lysosome fusion and therefore the dissociation and degradation of LC3b. The relevant treatments were added to the dishes and the cells were incubated for 24 h at 37 °C. The cells were harvested, and proteins were isolated.

The autophagic activity was assessed by Western Blot analysis of LC3b-II and p62 expression.

3.2.6 Cell cycle analysis

A cell cycle analysis was done to assess if the treatment with amlexanox influences cell cycle progression. The cells were all arrested in the same phase of the cell cycle and were then allowed to start proliferating from there. The analysis of the cell cycle was done by staining with propidium iodide (PI) with subsequent FACS analysis.

6 x 10^5 cells were disseminated in 10 mL medium into 10 cm cell culture dishes and incubated for 24 h at 37 °C. Then, the medium was changed to an FCS-free medium and the cells were incubated for another 24 h. This was done to align the cell cycle stage, so all cells start at the G1/G0 phase.

The medium was changed to the normal cell culture medium and the treatment was added. The cells were incubated for 24 h at 37 °C. The cells were harvested, washed once with PBS, and were then resuspended in 500 µL PBS. 4.5 mL 70 % ethanol (4 °C) were added to the cell suspension. This solution was stored for at least 24 h at -20 °C.

On the day of the FACS analysis, the cells were centrifuged for 5 min at 1200 g at 4 °C. The supernatant was discarded, and the pellet was resuspended in 5 mL cold PBS. The cells were centrifuged a second time, the supernatant was discarded, and the cells were resuspended in 500 µL cold PBS. The suspension was transferred into a FACS tube. 500 µL 0.25 % PBSTx were added for 5 min on ice. The cells were centrifuged for 5 min at 1200 g at 4 °C and the supernatant was discarded.

The pellet was resuspended in 200-500 µL PI staining solution and incubated in the dark for 30 min on ice. Meanwhile, the FACS scanner was turned on and the measurement was prepared.

The unstained negative control was measured first. Living single cells were gated. Cells from this gate were analyzed for PI staining. The negative control gave the reference for a negative PI signal. Then, 100,000 events were measured for every stained sample.

For analysis, FlowJo’s cell cycle analysis tool was used. PI-positive single cells were gated. The tool analyzed all positive cells and calculated the number of cells in the G1, S, G2, <G1, and >G2 phase (Fig. 3.2.6). The distribution of cells in these different cell cycle phases was compared between the different treatments.

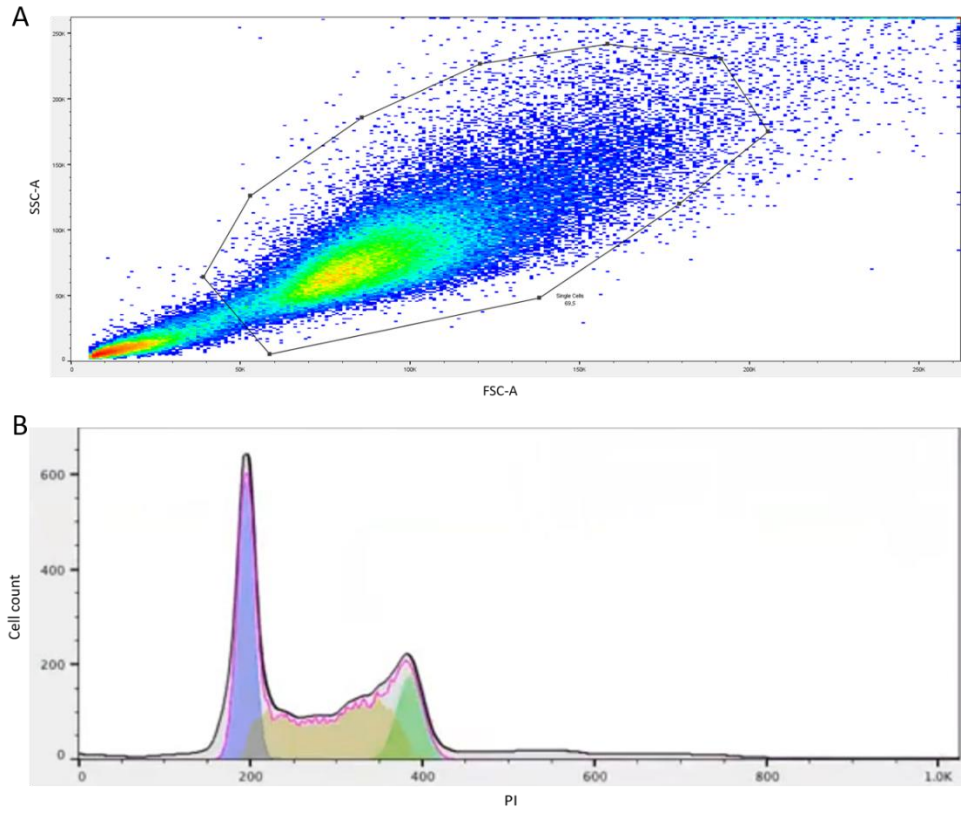

Fig. 3.2.6: Gating schematic for cell cycle analysis. Events were recorded and single cells were gated via SSC-A and FSC-A splitting (A). FlowJo's Cell Cycle Analysis tool was used on this single-cell gate. The tool resulted in an analysis of the different cell cycle phases (B). Blue = G1-, Yellow = S-, and Green = G2-Phase.

3.3 Molecular experiments

3.3.1 Genotyping via polymerase chain reaction

Genotyping of SNCA$^{-/-}$ mice was done with ear punch biopsies. The DNA was isolated with the REDExtract-N-Amp Kit. Briefly, the biopsy was cut with a scissor. Per Sample 12.5 µL of Tissue Preparation Buffer and 50 µL Extraction Solution were added. The samples were incubated for 10 min at RT. Then, the samples were incubated at 95 °C for 3 min. The reaction was stopped by the addition of 50 µL neutralizing buffer. The DNA could be stored at 4 °C or used directly for a PCR.

For the genotyping of every sample, two reactions were done. One for the SNCA wildtype sequence and one for the SNCA knock-out sequence. Each reaction consisted of 2 µL DNA, 0.5 µL forward primer (10 µM), 0.5 µL reverse primer (10 µM), 10 µL Amplicon Mix and 7 µL PCR-grade water. The PCR was run with the following protocol:

Tab. 3.3.1: Protocol used for the PCR.

Temperature [°C]	Time	Phase	Number of cycles
95	3 min	Enzyme activity	1
95	30 s	Denaturation	35
50	30 s	Annealing	35
72	90 s	Elongation	35
72	3 min	Inactivation	1
4	∞	Storage	1

After the PCR, gel electrophoresis was done to separate DNA extracts according to their size. DNA Ladder Mix 100-10,000 bp was used as marker. Marker and samples were loaded onto a 1.5 % agarose gel containing 50 µL/mL Rotisafe. TBE buffer was used for electrophoresis. The DNA was separated for 45 min at 100 V and the fluorescence staining of the gel was analyzed using UV light of the Gel Documentation System.

3.3.2 RNA isolation and Verso cDNA synthesis

3.3.2.1 RNA isolation

RNA was isolated from cells, soft tissue, e.g. spinal cord and brain, and firmer tissue, e.g. skin and melanoma. Different approaches were used for different tissues.

Cells were harvested and washed with PBS. The PBS was discarded after centrifugation and 400 µL TRI-reagent were added to the pellet. The pellet was vortexed vigorously and incubated for 10 min at RT.

For soft tissue 400 µL Tri-reagent were added to the tissue. Three ceramic beads were added, and the samples were homogenized with the BeadBug Microtube Homogenizer for 1 min and 2 cycles at 1200 g. The samples were then incubated for 10 min at RT.

The firmer tissue was treated with 400 µL TRI-reagent and homogenized with the Ultra-Turrax. The homogenization took approx. 30 s per tissue. The Ultra-Turrax was cleaned with 70 % ethanol and H_2O after each sample. The samples were incubated for 10 min at RT after homogenization.

After incubation, the treatment of the different tissues was the same. 80 µL chloroform were added. The samples were vortexed and incubated for another 10 min at RT. Then, the samples were centrifuged for 7 min at 16,100 g at RT. This led to a separation of the sample into three phases. The upper aqueous phase was transferred into a fresh tube, without disruption of the middle phase, which would lead to a phenol contamination. 200 µL isopropanol were added for precipitation of the RNA, the samples were vortexed and incubated for another 10 min at RT. Then, they were centrifuged for 10 min at 16,100 g at 4 °C. The supernatant was discarded, and the pellet was resuspended in 75 % ethanol. The samples were centrifuged for 7 min at 16,100 g at 4 °C and the supernatant was discarded. The pellet was left to air dry for 2-3 hours at RT. Then, it was resuspended in 30-40 µL RNAse-free H_2O. The RNA concentration was measured with the Nanodrop microvolume spectrophotometer.

3.3.2.2. Verso cDNA synthesis

For the reverse transcription of RNA to cDNA, the Verso cDNA Synthesis Kit was used. The manufacturer’s protocol was followed. Briefly, the kit was thawed on ice. A master mix for the total number of samples + 10 % was prepared.

Component	Volume [µL]
(5x) Synthesis Buffer	4
dNTP Mix	2
Hexamer Primer	0.7
OligodT Primer	0.3
Verso Enzyme Mix	1
RT-Enhancer	1
RNA	Corresponding 800 ng
RNAse-free H2O	Ad 20 µL

The sample volume corresponding to 800 ng RNA were pipetted into a PCR tube. 9 µL master mix were added. Then, RNAse-free H_2O was added to reach a volume of 20 µL. The program for the cDNA synthesis was 42 °C for 30 min, followed by 95 °C for 2 min. After that, the samples could be stored at 4 °C. Long-time storage was done at -20 °C. For further experiments, the samples were diluted to a concentration of 10 ng/µL with RNAse-free H_2O.

3.3.3 Real-time quantitative PCR

The expression of genes was analyzed on the mRNA level via quantitative real-time PCR (qPCR) on a Quant Studio 5 system. Primers for specific genes were designed and tested for specificity. The SYBR Select Mastermix was used according to the manufacturer's protocol. A master mix + 10 % was prepared with the SYBR Select reagent, forward and reverse primers, and RNAse-free H2O.

Component	Volume [µL]
SYBR Select	5
Forward Primer (10 µM)	1
Reverse Primer (10 µM)	1
RNAse-free H_2O	2
cDNA	1

The master mix without the cDNA was prepared and 9 µL were pipetted into every well of the 96- or 384-well plate. Then, 1 µL cDNA was added to every well. The samples were measured as triplicates. An unregulated housekeeping gene was measured to compare the amount of cDNA in each sample to other samples. Template-free samples were used as a negative control. The plate was closed with adhesive film and the samples were spun down in a tabletop centrifuge. Then, the qPCR was started with the Quant Studio 5. The following protocol was used:

Tab. 3.3.3: Protocol used for the qPCR.

Temperature [°C]	Time	Phase	Number of Cycles
50	2 min	Holding Stage	1
95	2 min	Activation	1
95	15 s	Denaturation	40
60	1 min	Annealing/Replication	40
95	15 s	Denaturation	1
60	1 min	Annealing/Replication	1
95	15 s	Dissociation	1
4	∞	Storage	1

The amplification of specific cDNA fragments was quantified by the intercalation of the SYBR Green cysteine dye into the double-stranded cDNA in real-time. Therefore, the increase of the fluorescence signal was proportional to the amount of cDNA in the sample. The fluorescence was plotted as a function of the number of cycles. For the calculation of

the relative mRNA amount, the $\Delta\Delta C_T$ method was used. The C_T-value is the number of cycles at which the fluorescence signal is higher than the background for the first time. The more of the specific mRNA corresponding cDNA is in the sample, the faster this threshold is reached. The QuantStudio Software calculated the C_T-value automatically. The unregulated housekeeping gene GAPDH was used as a reference gene.

The relative expression of the target gene relative to the reference gene was calculated as follows:

$$\Delta C_T = C_T \text{ (target gene)} – C_T \text{ (reference gene)}$$

$$\Delta\Delta C_T = \Delta C_T \text{ (sample)} – \Delta C_T \text{ (control)}$$

$$\text{Ratio} = 2^{-\Delta\Delta C_T}$$

3.3.4 Protein isolation and Bradford assay

Pefabloc was added to the phosphosafe buffer to achieve a final concentration of 1 mM. Then, 100 µL were added to the spinal cord or cell pellets. For larger tissue samples like melanomas larger volumes depending on the size of the sample were used. To homogenize the tissue samples and break down cells three ceramic beads were added, and they were homogenized for approx. 3 min at 25 Hz with the Mixer Mill. For cell pellets, it was enough to vortex the still frozen pellet with the phosphosafe buffer for approx. 10 s. For melanomas and skin tissue, the Ultra-Turrax was used. Then, the tissue samples were centrifuged for 60 min, and the cell samples for 30 min at 16,100 g at 4 °C. The supernatants were transferred to fresh tubes.

The protein concentration was assessed with the Bradford assay. For that, samples were diluted with H_2O, and Bradford reagent was added, which led to a color change. A 96-well plate was used for this assay. A standard curve was created by pipetting 0-5 µL 1 mg/mL BSA into the wells. 10-5 µL H_2O were added, respectively. This was done as a duplicate measurement. For the samples, 1 µL sample was added to 9 µL H_2O in the wells. This was done as triplicate. 200 µL Bradford reagent were added and the plate was shaken for 60 s. The absorption of the samples at 595 nm was measured in the microplate reader.

The protein concentrations of the samples were calculated by comparison with the standard curve.

3.3.5 Western Blot analysis

3.3.5.1 SDS gel preparation

The Western Blot (WB) is a method for the analysis and quantification of proteins. Before starting the WB, the proteins needed to be split up by size via a sodium dodecyl sulfate polyacrylamide gel electrophoresis (SDS-PAGE).

The percentage of polyacrylamide in the SDS gel was adjusted to the size of the proteins of interest. Smaller proteins, like α-Syn (14 kDa), needed a higher percentage gel (approx. 15 %), while larger proteins, like IKKε (80 kDa), needed a lower percentage gel (approx. 10 %). The higher percentage gel separates smaller proteins better than lower percentage gels, while lower percentage gels separate larger proteins better. A 10 % separating gel was prepared:

Substance	**Volume [µL]**
H_2O	2080
Tris, 1.5 M, pH 8.8	1230
Acrylamide	1640
SDS	49.2
APS	24.6
TEMED	2.46

The gel was filled between the glass plates of the gel cast and overlaid with isopropanol. This ensured a clean and smooth border of the separating gel. After about 30 min the gel solidified, and the collecting gel was prepared:

Substance	Volume [µL]
H_2O	1200
Tris, 0.5 M, pH 6.8	500
Acrylamide	250
SDS	20
APS	20
TEMED	2

The isopropanol was discarded, and the collecting gel was filled on top of the separating gel. A 10- or 15-pocket comb was pushed into the collecting gel. It took the gel another 30 min to solidify. After that, it could either be used directly for the SDS-PAGE or it could be stored, wrapped in a wet towel, at 4 °C.

3.3.5.2 SDS-PAGE

For the SDS-PAGE, a volume corresponding to 30 µg of total protein was pipetted into a tube. 5 µL of 4x Lämmli buffer/mercaptoethanol (5:1) were added to the tubes. They were briefly centrifuged and incubated at 95 °C for 5 min at 550 rpm in a heating block. This was done to denature the proteins. Meanwhile, the SDS gel was placed in a gel electrophoresis chamber, which was filled with SDS buffer. The comb was removed from the gel. After the 5 min denaturation period, the tubes were centrifuged again. Then, 3 µL protein marker and the complete samples were pipetted into the pockets of the gel. The chamber was closed, and an electrical current of 80 V was applied. After about 30 min the marker reached the separating gel and started to spread out. After this happened, the current was increased to 120 V. The run was finished when the bromophenol blue border reached the lower end of the gel.

3.3.5.3 Semi-dry blotting

This blotting technique was used as a standard method for all proteins, except for α-Syn. A piece of nitrocellulose membrane and two filter stacks were soaked in Blotting buffer for 5 min. The gel was taken out of the gel cast and the collecting gel was removed. The

separating gel was also placed in the Blotting buffer. Then, a filter stack was placed in the chamber of a semi-dry blotting device. The membrane was placed on top of it, then the gel. The second filter stack was put on top of that. Air bubbles were removed by pushing a roller over the blotting sandwich. The chamber was closed and inserted into the semi-dry blotting device. The program for mixed molecular weight proteins was used to achieve a good transfer of proteins between 20 and 100 kDa to the membrane. After it was finished, the chamber was taken out of the blotter and opened. The sandwich was removed, and the membrane was taken out of it. The filter stacks were cleaned with H_2O and were air-dried. The gel was discarded. The membrane was blocked with Blocking buffer for 1 h at RT with mild shaking.

3.3.5.4 Wet blotting

The wet blotting method was used for the detection of α-Syn to improve the transfer onto the membrane. No detection was possible with the semi-dry blotting method.

For this method, the nitrocellulose membrane and two membrane-sized pieces of blotting paper were soaked in Wetblot Buffer for 5 min. Then, the gel was also transferred into the buffer. A blotting sandwich was created between the two parts of the clamp as follows:

Cathode

Filter

Blotting Paper

Gel

Membrane

Blotting Paper

Filter

Anode

The clamp was closed and transferred into the blotting chamber. A cooling pack was placed next to it and the chamber was filled with Wetblot buffer. The electrodes were attached, and a voltage of 50 V was applied for 90 min.

After the blotting was done, the membrane was taken out of the sandwich and was transferred to 0.4 % PFA for 30 min at RT. This was done to help fixate small proteins to the membrane and was shown to increase the strength of the signal. After the incubation, the membrane was washed twice with PBS for 10 min. Then, the membrane was blocked with Blocking buffer for 1 h at RT with mild shaking.

3.3.5.5 Antibody staining

After blocking, the membrane was incubated with 2 mL of primary antibody solution. This was done according to Tab. 3.3.5.5. After the incubation, the membrane was washed twice for 10 min at RT with PBST. Then, it was incubated with the secondary antibody (Tab. 3.3.5.5). The membrane was washed twice for 10 min at RT with PBST after incubation and it was scanned with the Odyssey scanner to record the antibody signal. The next primary antibody was applied after scanning.

Tab. 3.3.5.5: Antibodies, dilutions, incubation time, and temperature used for WB.

Antibody (Host)	Dilution	Time [h]	Temperature [°C]
a-Syn (ms)	1:1000	24	4
IKKe (ms)	1:500	24	4
TBK1 (rb)	1:250	24	4
Actin (ms)	1:1200	1	22
Actin (rb)	1:2000	1	22
HSP90 (ms)	1:1000	1	22
LC3b	1:250	24	4
p62	1:400	24	4
CyclinD1	1:500	24	4
p53	1:250	24	4

p65	1:250	24	4
P-p65	1:250	24	4
p44-42	1:250	24	4
P-p44-42	1:250	24	4
p38	1:250	24	4
P-p38	1:250	24	4
Akt1	1:250	24	4
P-Akt1	1:250	24	4
Secondary	1:10,000	1	22

The relative amount of protein was calculated by densitometric analysis of the bands and comparison of the protein of interest with an unregulated housekeeping protein.

3.3.6 Immunohistochemistry

The specimen slides prepared beforehand were taken out of the -80 °C freezer and were brought to RT. Water drops were carefully removed and the tissue slices were surrounded with a Dako pen to create a fatty border, which reduced the amount of antibody needed for staining. The slides were washed for 10 min with PBSTx at RT with mild shaking. Then, they were taken out of the PBSTx and air-dried for 2-3 min. IHC blocking buffer was pipetted onto the slices and they were incubated for 2 h at RT. After that, the blocking buffer was removed and a solution of primary antibodies, diluted in IHC antibody buffer, was applied to the slices. The dilution, time, and temperature for every antibody are given in Tab. 3.3.6. The slices were covered with Parafilm for the time of the incubation.

After the incubation, the Parafilm was removed and the slides were washed three times for 10 min with PBSTx at RT. Then, a mix of secondary antibodies, diluted in IHC antibody buffer, was applied to the slices (Tab. 3.3.6).

After the last staining step, the slides were washed twice for 10 min with PBSTx and once with PBS at RT. Then, Aqua-Poly/Mount was added to the slices and they were covered with a glass slide.

The slices were analyzed using either the Axio Observer Z1 or the BIOREVO microscope.

Tab. 3.3.6: Antibodies, dilutions, incubation time, and temperature used for IHC.

Antibody (Host)	Dilution	Time [h]	Temperature [°C]
a-Syn	1:100	24	4
CGRP	1:200	24	4
IB4	1:50	24	4
GABA-A	1:500	24	4
TH	1:200	24	4
VGlut1	1:100	24	4
GAD67	1:200	24	4
Secondary	1:800	2	22

3.3.7 Glutamate measurement in the CSF

For the glutamate measurement in the spinal cord, Promega's Glutamate-Glo assay was used. The manufacturer's protocol was followed. Briefly, the kit was thawed, and a glutamate standard was prepared. The necessary amount of glutamate detection reagent was prepared. It consisted of a luciferin detection solution, reductase, reductase substrate, glutamate dehydrogenase, and NAD^+.

For CSF measurement, 5-10 µL of detection reagent were needed per reaction. The same amount of CSF and detection reagent was used.

The CSF sample was pipetted into the well of a white 96-well plate and the same amount of detection reagent was added. The same was done for the glutamate standard. The plate was shaken for 30-60 s and was incubated for 60 min at RT. Then, the luminescence was measured with the microplate reader.

The glutamate concentration of the samples was calculated by comparison with the standard curve.

3.3.8 Multiplex staining of human melanoma samples (Phenoptics)

Skin and melanoma samples from human patients were obtained from the university cancer center (UCT). The samples were already embedded in paraffin and were ready to be cut. The tissue was cut (4 µm) and placed on specimen slides. They were stored at 4 °C until used.

For the staining of these samples, PerkinElmer's Phenoptics approach was used. The slides were dewaxed and rehydrated by placing them two times for 5 min in xylol and then in a descending line of ethanol for 2 min each. In the end, they were placed twice in H_2O for 2 min each. Then, antigen retrieval was done. Depending on the primary antibody used for staining, the slides were placed in Antigen Retrieval Buffer 6 or 9. They were then boiled for 15 min in a microwave in the corresponding buffer. The buffer and slides were cooled down to RT.

Then, the slices were circled with a Dako pen. They were washed once with TBST for 2 min at RT. The TBST was discarded and they were blocked with Phenoptics Blocking Buffer for 15 min at RT. The blocking buffer was discarded, and the slices were incubated with the primary antibody as indicated in Table 3.3.8.

Tab. 3.3.8: Antibodies, dilutions, incubation time, and temperature used for Phenoptics.

Antibody (Host)	Dilution	Antigen Retrieval Buffer	Time [h]	Temperature [°C]
IKKe (ms)	1:400	AR6	24	4
TBK1 (rb)	1:400	AR6	24	4
CD3 (rb)	ready to use	AR6	0.5	22
Pan-Cytokeratin (ms)	1:100	AR9	0.5	22
PD1 (rb)	1:500	AR6	0.5	22
CD45(rb)	1:100	AR6	0.5	22
DAPI	1:5000	AR9	0.17	22
Ms + Rb HRP	ready to use	-	0.25	22

After the incubation, the primary antibody solution was discarded, and the slides were washed three times with TBST for 2 min each. Then, the opal polymer anti-rabbit anti-mouse HRP mix was applied to the slices and incubated for 15 min at RT. The secondary antibody mix was discarded, and the slides were washed three times with TBST for 2 min each. Then, the opal fluorophore, diluted 1:100 in PerkinElmer's Amplification Diluent, was applied to the slices and incubated for 10 min at RT. The fluorophore was discarded, and the slides were washed twice with TBST for 2 min each.

At this point, the antigen retrieval was repeated for the next primary antibody. After all antibodies were incubated, the last antigen retrieval was done, and the slices were stained with DAPI. The slides were washed three times with TBST for 2 min each. Aqua-Poly/Mount was applied, and a glass slide was added on top.

The slices were analyzed with the Vectra microscope and PerkinElmer's inForm software.

3.3.9 Statistical analysis

For the statistical analysis, GraphPad Prism 7 was used in this work. Data are presented as mean ± SEM.

Data were analyzed using two-way ANOVA for time courses and one-way ANOVA or t-Tests for single time point measurements. Significance was defined as *P < 0.05, **P < 0.01, ***P < 0.001 and ****P < 0.0001.

For the calculation of the p-value, Bonferroni's post hoc test for two-way ANOVA, Dunnett's post hoc test for one-way ANOVA and Student's two-tailed, unpaired t-Test were used. The number of animals used or repetitions (n) for every experiment are given in the figure legends.

4. Results

4.1 The role of IKKε and TBK1 in the pathogenesis of malignant melanoma

The first half of this work investigates the effect of IKKε and TBK1 on melanoma growth and invasiveness. *In vitro* experiments were done using the melanoma cell lines SK-Mel28 and A375M. Amlexanox was used for pharmacological inhibition of the IKKε/TBK1 complex. Furthermore, a xenograft mouse model was applied. The results shown here are already published in a peer-reviewed journal.

4.1.1 Expression of IKKε and TBK1 in human melanoma and melanoma cell lines

To find out if the protein kinase IKKε has a role in melanoma development and growth the expression of IKKε and its functional partner TBK1 was assessed in one melanocyte and two melanoma cell lines (Fig. 4.1.1 A-D), as well as in naevi and melanoma metastasis samples of patients (Fig. 4.1.1 E-F).

IKKε and TBK1 showed higher protein expression in the melanoma cell lines SK-Mel28 and A375M compared to the melanocyte cell line HERMES1 (Fig. 4.1.1 A-D). The same upregulation of protein expression was seen in the naevi and melanoma metastasis tissue samples of patients (Fig. 4.1.1 E-F) with relatively high inter-individual variations.

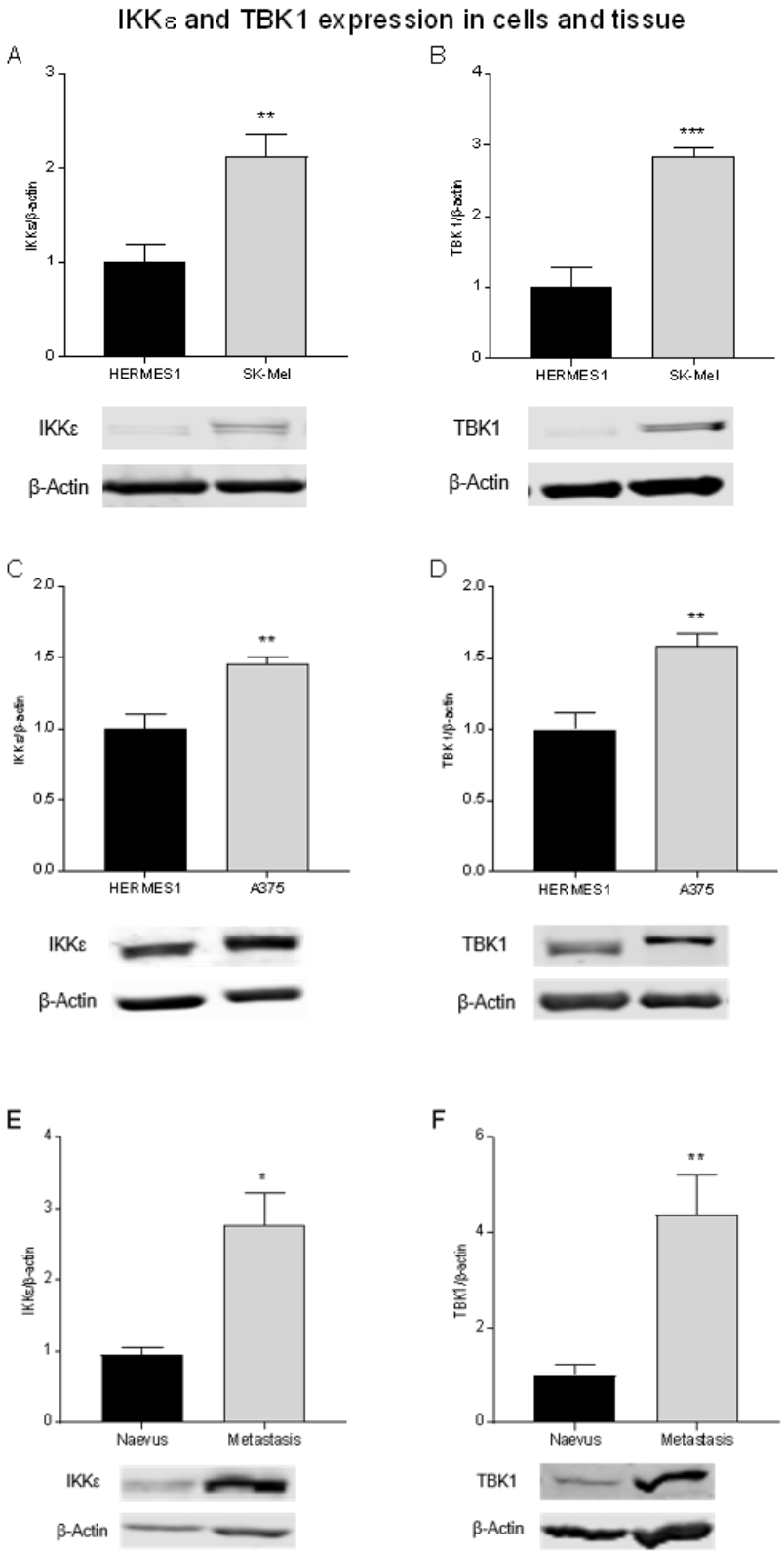

Fig. 4.1.1: Western Blot analysis of IKKε and TBK1 expression in melanoma cell lines and tissue samples compared to controls. Relative IKKε expression in SK-Mel28 cells compared to HERMES1 cells (A [n = 4]). Relative TBK1 expression in SK-Mel28 cells compared to HERMES1 cells (B [n = 5]). Relative

IKKε expression in A375M cells compared to HERMES1 cells (C [n = 4]). Relative TBK1 expression in A375M cells compared to HERMES1 cells (D [n = 8]). Relative expression of IKKε and TBK1 in patient samples of naevi and melanoma metastasis (E [n = 4-9], F [n = 3-6]). Blots show representative WB signal, the diagrams show the densitometric analysis of all blots. * p<0.05, ** p<0.01, *** p<0.001 (adapted from Möller et al. 2020[244]).

4.1.2 Proliferation of melanoma cells is inhibited by amlexanox treatment

The increase in IKKε and TBK1 expression shown in 4.1.1 is an indicator that these proteins have some impact on the characteristics of melanoma cells. Therefore, the proliferation of SK-Mel28 and A375M cells after treatment with 10, 20, 30, and 50 µM amlexanox and the vehicle DMSO was investigated.

The WST and SRB assays were performed for both cell lines and it was found that treatment with 20, 30, and 50 µM amlexanox resulted in a decreased proliferation in SK-Mel28 cells in the SRB assay (Fig. 4.1.2 B). In the WST assay, only the treatment with 30 and 50 µM amlexanox resulted in a significant decrease (Fig. 4.1.2 A). These results were obtained by my predecessor, Julia Wasel, and are shown to deliver a full overview of this project.

In A375M cells the WST assay showed no significant change of proliferation (Fig. 4.1.2 C), but the SRB assay showed a decreased cell number after treatment with 30 and 50 µM amlexanox (Fig. 4.1.2 D).

Since the highest effect on proliferation was seen after treatment with 30 and 50 µM amlexanox further experiments were done with these concentrations. The cell line SK-Mel28 was used for further experiments since it showed a promising effect on cellular proliferation after amlexanox treatment.

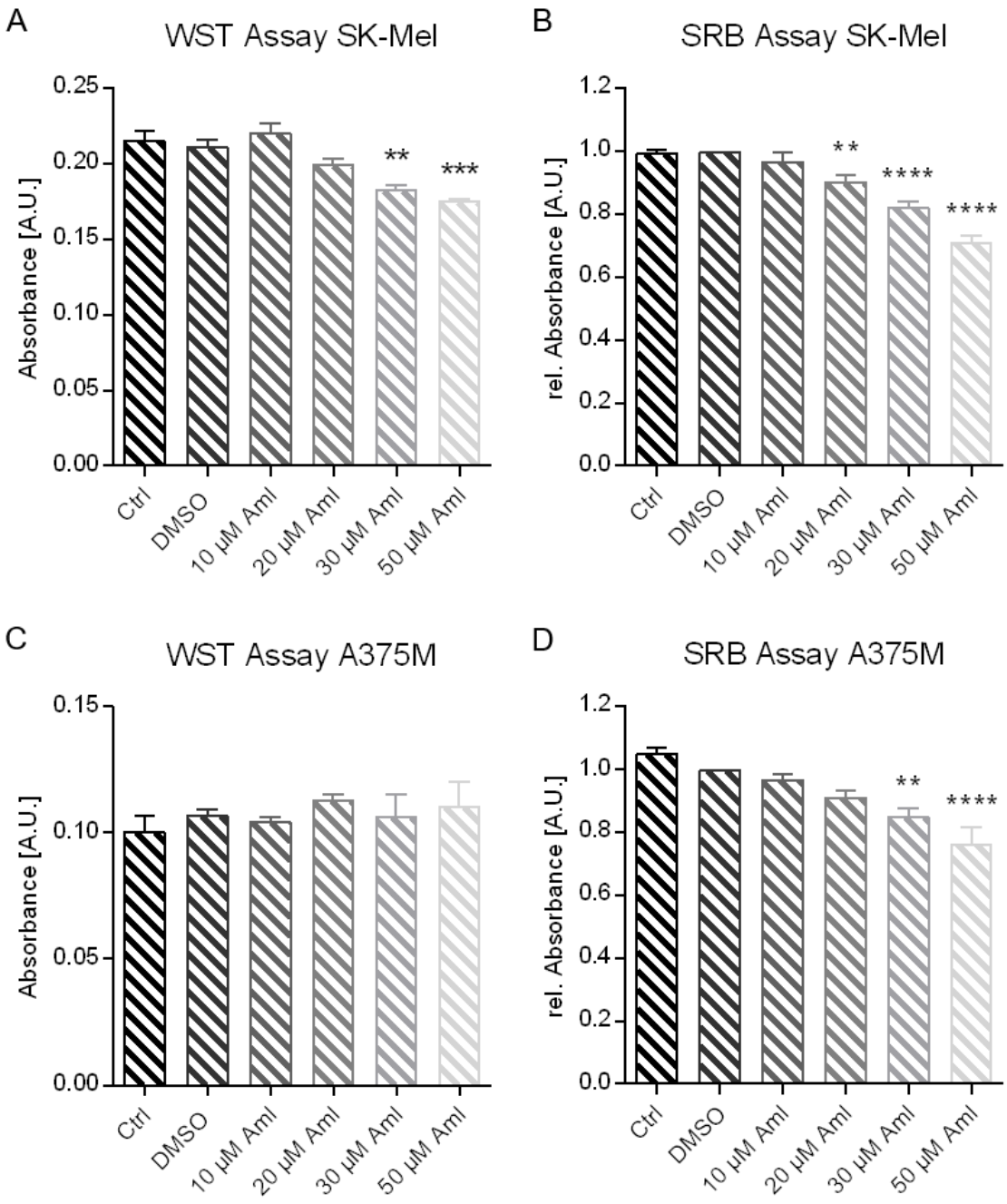

Fig. 4.1.2: Results of the WST and SRB assays of SK-Mel28 and A375M cells. The results of the WST assay show a significant decrease in the proliferation of SK-Mel28, but not A375M cells (A [n = 3], C [n = 3]). The SRB proliferation assay shows a significant decrease of proliferation in both cell lines (B [n = 9], D [n = 5]). ** $p<0.01$, *** $p<0.001$, **** $p<0.0001$ (adapted from Möller et al. 2020[244]).

4.1.3 Autophagy is inhibited in human melanoma cells after amlexanox treatment

One reason for the decreased proliferation shown in 4.1.2 could have been a change of autophagy after amlexanox treatment. Therefore, SK-Mel28 cells were treated with amlexanox for 24 h, and protein was isolated.

Autophagy is a process of cellular protection but can also influence the proliferation of cancer cells. The Western Blot revealed a decreased LC3b-II and an increased p62 expression after treatment with 30 and 50 µM amlexanox compared to vehicle-treated cells (Fig. 4.1.3 A, B). These proteins are indicators for autophagy in cells and are expected to be correlated inversely. LC3b-II is an important regulator protein for the formation of autophagosomes, while p62 constitutes an autophagy receptor, which is degraded during autophagy. The downregulation of LC3b-II after amlexanox treatment indicates an inhibitory effect of amlexanox on autophagy, which is supported by the upregulation of p62 after amlexanox treatment.

The same regulation of autophagic markers was seen in xenograft tumors, grown from SK-Mel28 cells in the flanks of nude mice. The animals were treated with the vehicle DMSO or with 25 mg/kg body weight amlexanox, respectively. The tumors from the amlexanox treated group showed autophagy inhibition compared to the tumors of the vehicle-treated group (Fig. 4.1.3 C, D). These results lead to the hypothesis, that inhibition of the autophagy pathway might be one of the main factors in influencing tumor characteristics, like proliferation und migration. To confirm this hypothesis, a cytotoxicity assay was done using a standard inhibitor of autophagy.

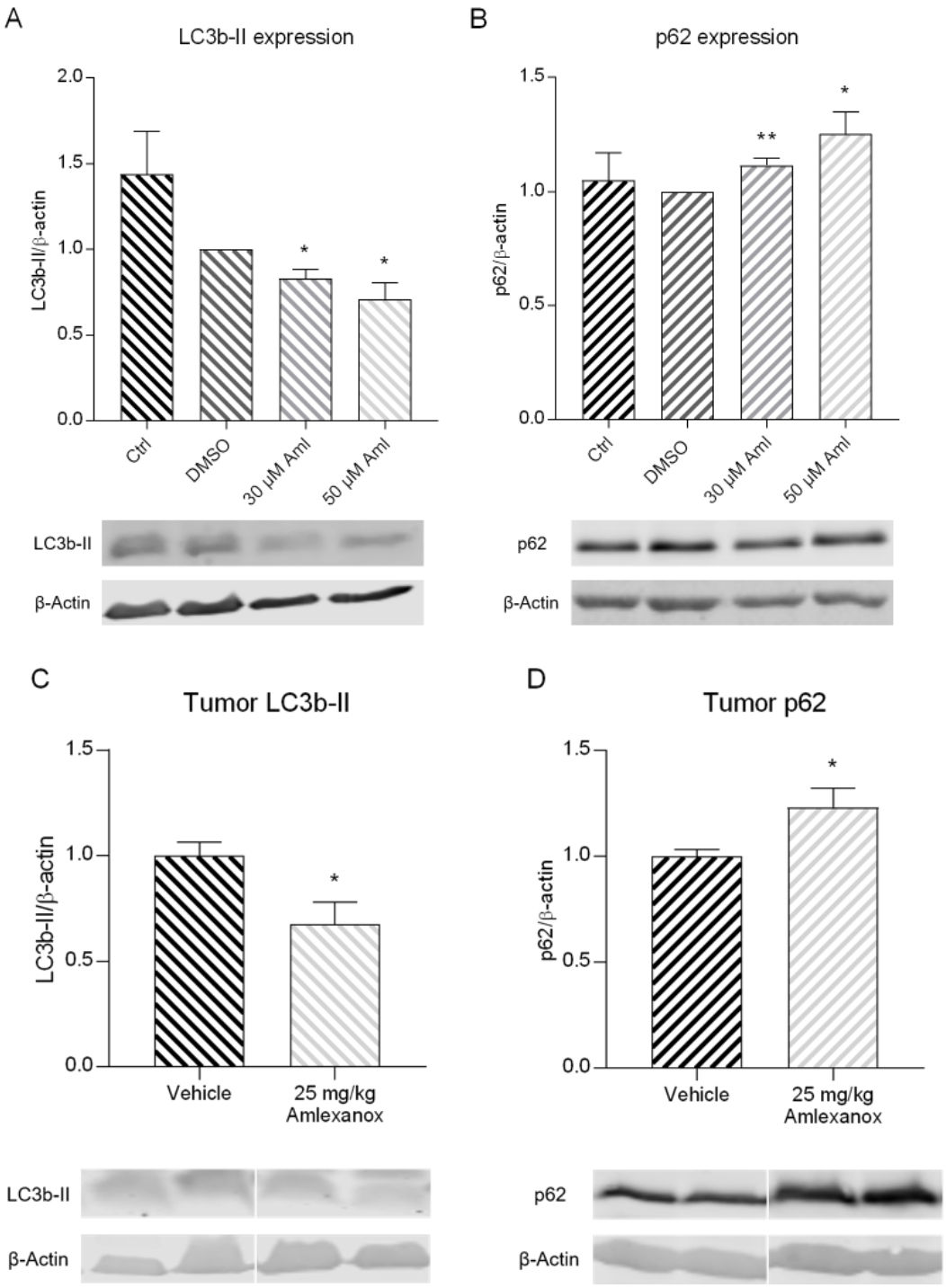

Fig. 4.1.3: Western Blot results of LC3b-II and p62 as indicators of autophagy. LC3b-II is downregulated after treatment with 30 and 50 µM amlexanox (A). p62 is upregulated after amlexanox treatment (B). n = 4. The same results were seen in the SK-Mel xenograft tumors of nude mice treated with DMSO or 25 mg/kg amlexanox, respectively (C, D). Blots show representative WB signal, the diagrams show the densitometric analysis of all blots. n = 5-6. * $p<0.05$, ** $p<0.01$ (adapted from Möller et al. 2020[244]).

4.1.4 Amlexanox has no impact on the cell cycle of SK-Mel28 cells

Next, the cell cycle of SK-Mel28 cells was investigated after amlexanox treatment to examine its impact on cell cycle progression. The cells were treated with amlexanox at the indicated concentrations or DMSO, stained with PI and the cell cycle distribution was measured via FACS analysis.

The percentages of cells in the different phases were compared between the different groups (Fig. 4.1.4 A). There was no significant difference in the relative distribution of cells between the G1, S, G2, <G1, and >G2 phase of the vehicle and amlexanox treated groups.

To confirm these results the CyclinD1 and p53 expression on the protein level were analyzed via WB and no significant differences between untreated, vehicle-treated, and amlexanox treated cells were found (Fig. 4.1.4 B). CyclinD1 acts as a regulatory subunit of CDK4, and CDK6. This regulation is required for the G1/S phase transition. p53, which also impacts the cell cycle via various mechanisms, was also not regulated after amlexanox treatment (Fig. 4.1.4 C). A simplified representation of the cell cycle shows how and where CyclinD1 and p53 influence the cell cycle progression (Fig. 4.1.4 D). While CyclinD1 is the key regulator of G1-phase to S-phase transition p53 inhibits a large number of cell cycle regulatory proteins, like CyclinD1/CDK4/6 complex, and CDC2.

Since no significant difference was seen in the relative cell cycle-specific distribution of cells and CyclinD1 and p53 expression, it seems very likely that amlexanox had no effect on the cell cycle and didn’t lead to a cell cycle arrest in SK-Mel28 cells. These results were obtained by my predecessor, Julia Wasel, and are shown to deliver a full overview of this project.

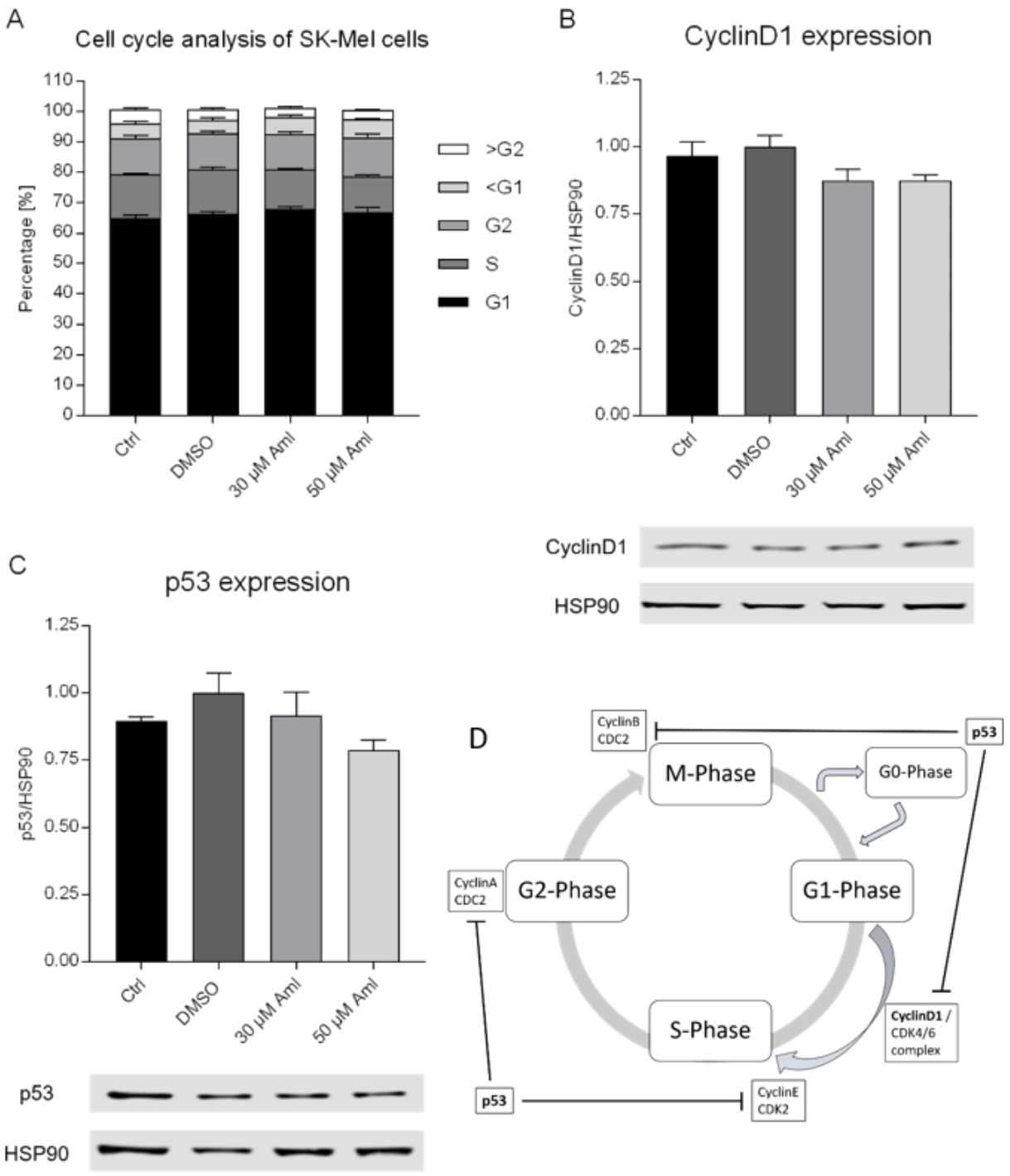

Fig. 4.1.4: Cell cycle analysis of SK-Mel28 cells. The percentages of 100,000 measured SK-Mel28 cells that are in the G1, S, G2, <G1, and >G2 phases are shown. There is no significant difference between the different treatments (A [n = 3]). Expression of the cell cycle relevant protein CyclinD1 was analyzed with WB. No difference was detected (B [n = 4]). p53 was also analyzed and showed no difference after amlexanox treatment (C [n = 4]). A simplified representation of the cell cycle and the points where CyclinD1

and p53 interact. Blots show representative WB signal, the diagrams show the densitometric analysis of all blots (adapted from Möller et al. 2020[244]).

4.1.5 Regulation of MAPK proteins after treatment with amlexanox

Several IKKε/TBK1 target genes have already been associated with melanoma initiation and progression. Therefore, the expression and activation of important proteins of the NF-κB, MAPK, and Akt pathways were investigated. They were shown to play an important role in tumor proliferation and progression via activation of a variety of target genes.

Cells were treated with 30 and 50 µM amlexanox and reduced activation of p65 and p44-42 were detected in cells treated with 50 µM amlexanox (Fig. 4.1.5 A, B). No difference was seen in untreated cells or cells treated with 30 µM amlexanox compared to vehicle-treated cells.

Also, no change in activation was seen at the level of MAPK pathway p38, and Akt1, no matter the treatment (Fig. 4.1.5 C, D). Even though, a trend to a significantly decreased Akt1 activation was seen after treatment with 50 µM amlexanox. These results were obtained by my predecessor, Julia Wasel, and are shown to deliver a full overview of this project.

The impact of amlexanox on the NF-κB and MAPK pathways is shown here. These regulations may influence the proliferation, as it was seen in 4.1.2, as well as migrative and invasive properties of melanoma cells, as seen in 4.1.6. To confirm this hypothesis a cytotoxicity assay was done using standard inhibitors of p42/44 and NF-κB. The results indicate that the inhibitory effect of amlexanox on the autophagy pathway has a much more prominent effect than the inhibition of the NF-κB and MAPK pathways (Fig. 4.1.7).

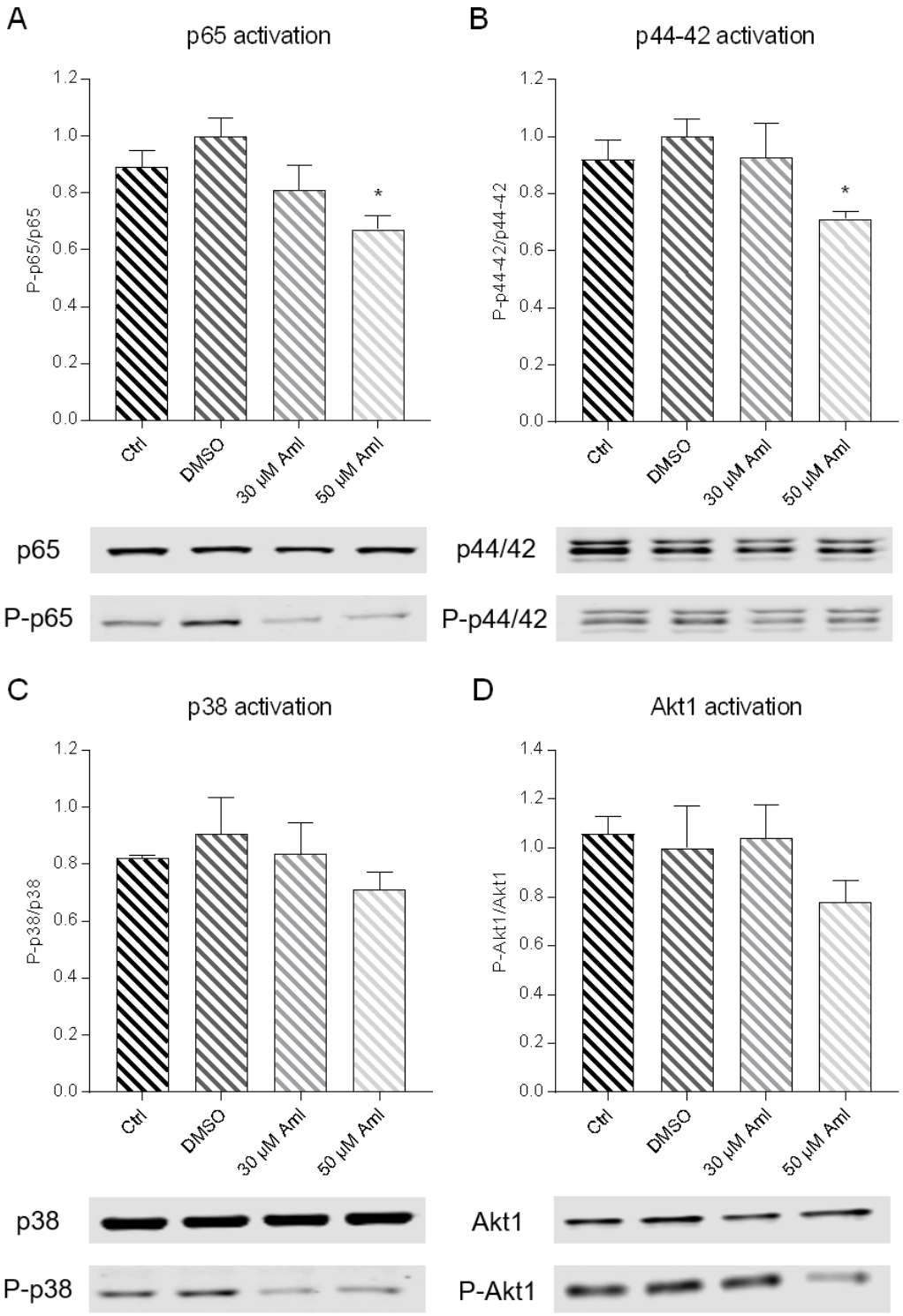

Fig. 4.1.5: Western Blot results of protein activation involved in melanoma development in SK-Mel28 cells. The expression of NF-κB-p65, MAPK, Akt1, and the phosphorylated proteins was measured, and the ratio was calculated. This was used as an indicator of protein activation. p65 and p44-42 activation is reduced after treatment with 50 µM amlexanox (A [n = 3] and B [n = 4]). No significant difference is seen in

p38 and Akt1 activation (C [n = 3] and D [n = 4]). Blots show representative WB signal, the diagrams show the densitometric analysis of all blots. * p<0.05 (adapted from Möller et al. 2020[244]).

4.1.6 Migrative and invasive capacities of SK-Mel28 cells are inhibited by amlexanox treatment

In the next step, the effect of amlexanox on the migrative and invasive capacities of SK-Mel28 cells was investigated. My predecessor on this project used the Transwell migration assay and the scratch migration assay. In the Transwell migration assays, the cells have to overcome a physical barrier and migrate in the direction of an increasing FCS gradient. In the scratch migration assay, a defined scratch is created in a confluent cell layer and cells have to migrate into the scratch. To confirm the results of these assays I used ibidi's migration assay. Here, cells are grown in a two-chamber insert in a cell culture plate. After they settled down the insert is removed, and the cells migrate into the cell-free gap. The difference to the scratch migration assay is that no cells are damaged or killed in the process of gap creation. Therefore, each assay investigates different aspects of migration. From the migration through a physical barrier, over the migration into a cell-free gap, to the migration in a cell-free gap in the company of damaged cells which secrete a variety of transmitter molecules.

The Transwell migration assay showed a significant decrease in the number of migrated cells after the treatment with 30 and 50 µM amlexanox compared with vehicle-treated cells (Fig. 4.1.6.1 A). The effect was more pronounced with the higher amlexanox concentration. The negative control showed that almost no cells migrated without the FCS cue, which confirmed the method.

Ibidi's migration assay confirmed these results. SK-Mek28's migrative capacities decreased after amlexanox treatment compared to vehicle treatment, with a slightly stronger effect at higher concentrations (Fig. 4.1.6.1 B). The same result was observed with the scratch migration assay (not shown). Representative images of the cell growth are shown at the beginning of the experiments and after 6 h, which were used for calculation (Fig. 4.1.6.1 C).

The Transwell migration assay was performed by Julia Wasel. ibidi's migration assay was performed by me in cooperation with Dr. S. Schiffmann from the Fraunhofer IME-TMP, Frankfurt, Ger. Julia Wasel's results are shown to give a full picture of the different assays.

With the combination of the different assays and the same results confirming each assay, it is likely that amlexanox inhibits the migrative capacities of SK-Mel28 melanoma cells *in vitro*.

After the migration assay, an invasion assay was also done. This assay was based on the Transwell assay. 0.3 mg/mL Matrigel was divided into the Transwell insert. Matrigel adds a second, complex physical barrier on top of the already existing porous membrane. Then, the cells and the different treatments were put on top of the Matrigel. This assay resulted in a decrease in the invasive capacity of SK-Mel28 cells after treatment with 50 µM amlexanox compared to vehicle-treated cells. No significant decrease was observed after treatment with 30 µM amlexanox. The negative control showed no invasion of cells without the FCS cue (Fig. 4.1.6.2). This assay was performed by Julia Wasel, and the results are shown to deliver a full picture of this project.

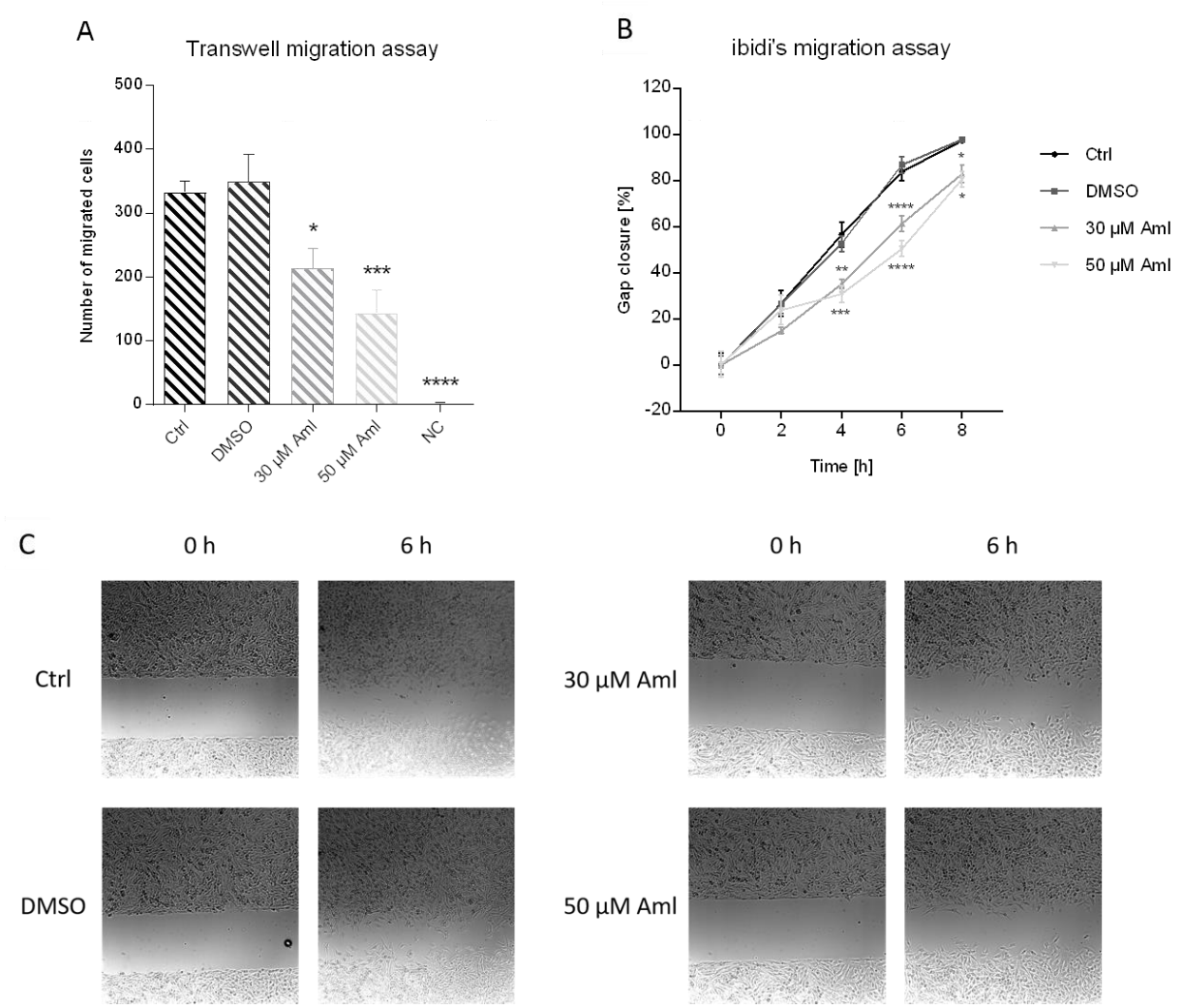

Fig. 4.1.6.1: Migration assays of SK-Mel28 cells. Transwell migration assay of SK-Mel28 cells after amlexanox treatment. The number of migrated cells was counted (A [n = 5]). ibidi's migration assay was done to confirm the results of the Transwell assay. The percentage of gap closure was measured at different time points (B [n = 3]). Representative pictures used for the analysis of ibidi's migration assay. Cell-free gap = 500 µM (C). * p<0.05, ** p<0.01, *** p<0.001, **** p<0.0001 (adapted from Möller et al. 2020[244]).

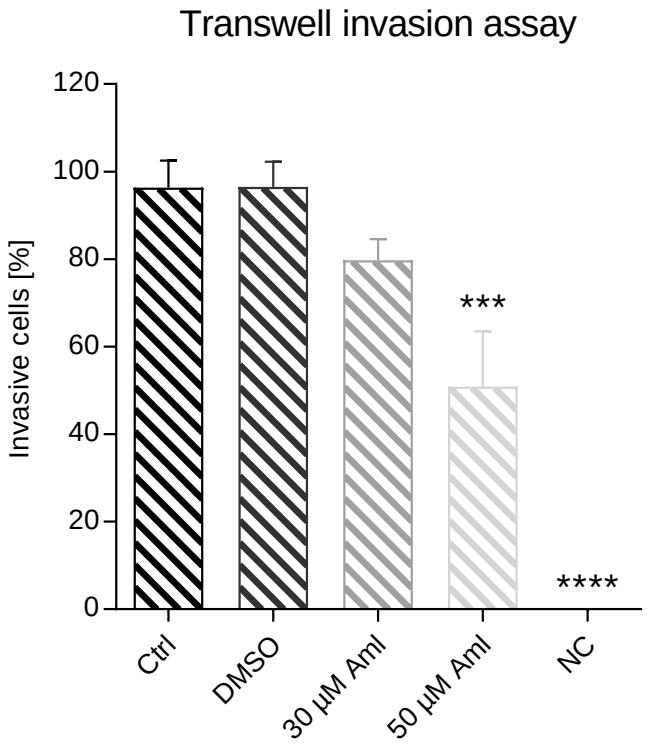

Fig. 4.1.6.2: Transwell invasion assay. The percentage of invaded cells compared with migrated cells was calculated. 50 µM amlexanox showed a significant decrease in invasive capacity. n = 5. *** p<0.001, **** p<0.0001 (adapted from Möller et al. 2020[244]).

4.1.7 The inhibition of the autophagy pathway is the most prominent effect of amlexanox treatment

To evaluate the importance of amlexanox-mediated inhibition of the NF-κB, MAPK, and autophagy pathways the WST and SRB assays were used. Cells were treated with DMSO, 30 µM amlexanox, and 2.5 nM of the autophagy inhibitor Bafilomycin A1 (BafA), 10 µM the MAPK inhibitor PD98059, or 100 µM of the NF-κB inhibitor PDTC, respectively. Cell growth was measured 48 h after treatment.

The SRB assay didn't show significant results, but a trend to an inhibition of cell growth by 30 µM amlexanox treatment. A similar effect was seen after treatment with the autophagy inhibitor BafA and the MAPK inhibitor PD98059. No difference between these treatments and additional amlexanox treatment, as well as the treatment with PDTC, was

seen (Fig. 4.1.7 B). The WST assay resulted in strongly significant inhibition of cell growth after treatment with BafA, and a significant difference after treatment with PDTC. No additional effects after amlexanox treatment were seen (Fig. 4.1.7 A).

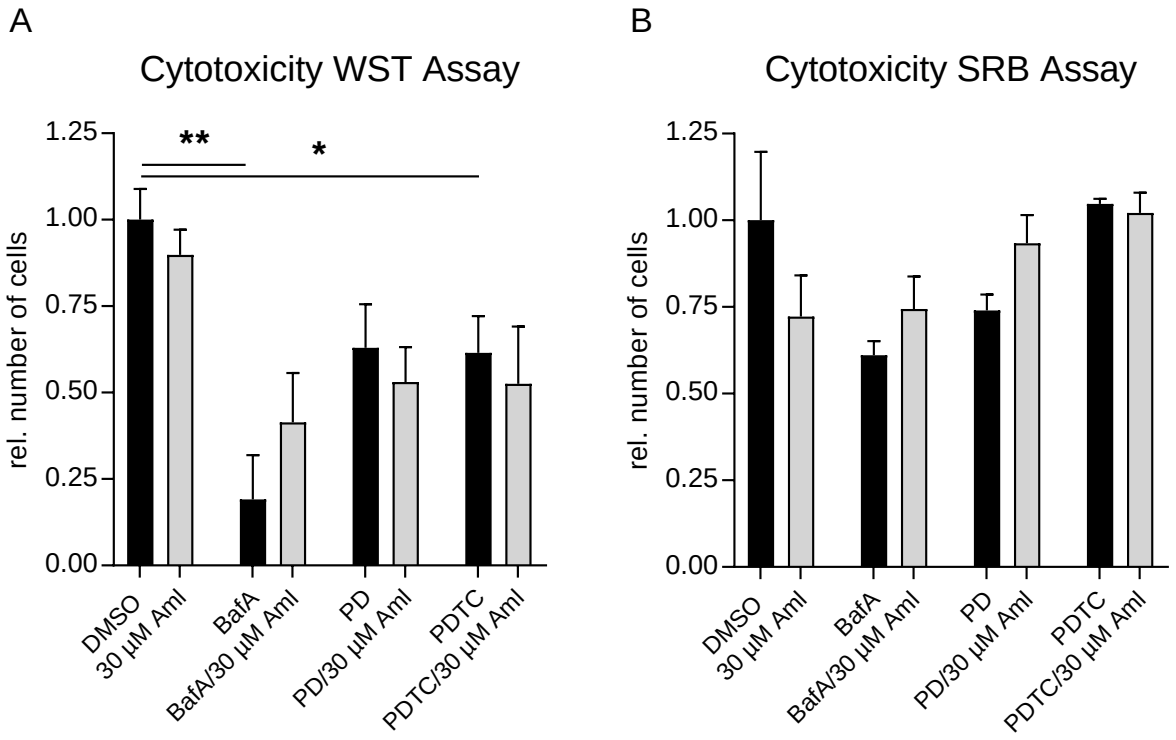

Fig. 4.1.7: Cytotoxicity assay. Effects on cell growth of SK-Mel28 cells after treatment with amlexanox, BafA, PD, PDTC, and combinations of these. Results of the WST (A) and SRB (B) assay. n = 3-4. * $p<0.05$, ** $p<0.01$ (adapted from Möller et al. 2020[244]).

These were the first results to evaluate which amlexanox-mediated effect is the most important for the results that were seen earlier. The strong effect of autophagy inhibition, together with the fact that amlexanox didn't exert additional effects, implies that the autophagy pathway is the most important one of the three pathways investigated so far. The NF-κB inhibitor also showed a significant reduction in cell growth with no additional amlexanox-mediated effect. This implies that the NF-κB is also an important pathway in the amlexanox-mediated effects, even though not as important as the autophagy pathway. The inhibition of the MAPK pathway with PD98059 didn't result in any significant results,

but a trend is seen. This pathway may add some importance to the amlexanox-mediated effects, but not nearly as strong as the other two pathways.

4.1.8 Xenograft model in nude mice

After the already promising *in vitro* results, the experiments were continued *in vivo*. The SK-Mel28 cells were injected into the flanks of immunodeficient Foxn1 nude mice. The tumor growth was measured for 28 days. Then, the animals were sacrificed, and the tumor was dissected.

The animals were treated by feeding them with cornflakes which were soaked either with DMSO or with 25 mg/kg amlexanox. Both groups showed slow tumor growth in the beginning. Most likely during this time, the tumor had to settle and acted on its microenvironment. After approx. seven to nine days the growth rate of the control group increased until day 25. Between days 25 and 28 the growth rate decreased again. The amlexanox treated animals showed a lower rate of tumor growth and a trend to a significantly decreased tumor volume at the end of the experiment (Fig. 4.1.8 A, C). The growth rate was similar up to day 21, at which the growth rate already decreased. Between days 21 and 23, and days 25 and 28 no tumor growth at all could be detected. The calculation of the AUC confirmed the decrease in tumor volume (Fig. 4.1.8 B). The tumor volume was reduced by 32 % (DMSO: 623 mm^3 ± 93; Aml: 423 mm^3 ± 59) with amlexanox treatment.

The tumor was weighed directly after dissection. The tumors of treated animals tended to be lighter than the tumors of untreated animals. Even though the result was not statistically significant, the reduction of the weight was 36 % (DMSO: 95.84 g ± 23.87; Aml: 61.37 g ± 10.02) (Fig. 4.1.8 C, D).

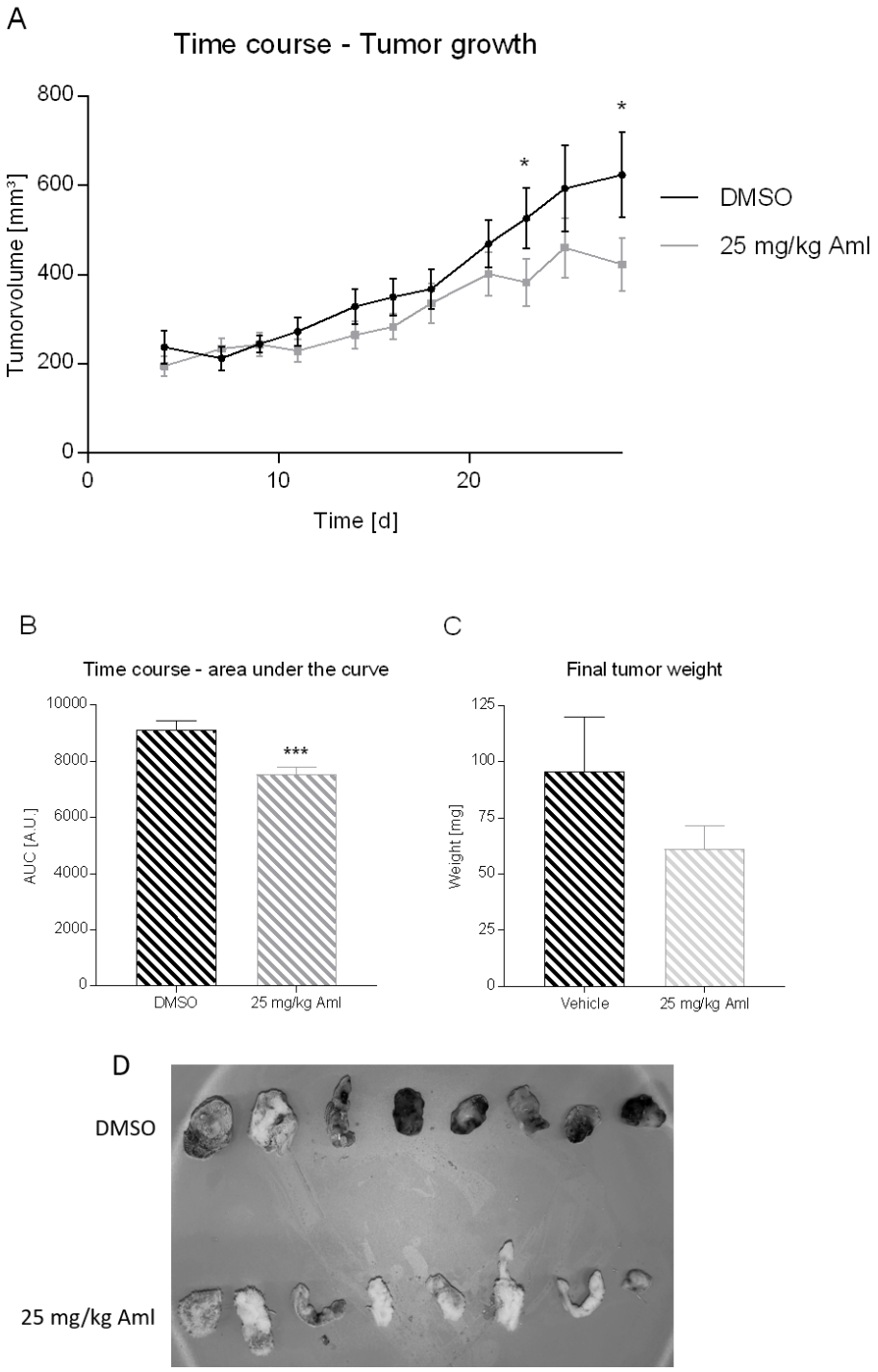

Fig. 4.1.8: Reduction of melanoma size after amlexanox treatment. The treatment of nude mice with amlexanox at a dose of 25 mg/kg body weight led to a significant reduction in the size of the tumor, compared to DMSO treatment (A). This is confirmed by the calculation of the area under the curve. Calculation of the area under the tumor volume vs. time curve (B). After sacrificing the animals, the tumor was dissected and weighed. The weight of the tumors dissected from amlexanox treated animals tended to be lower than the

weight of the control group (C). Representative pictures of eight tumors per group after dissection (D). n = 12-18. * p<0.05, *** p<0.001 (adapted from Möller et al. 2020[244]).

4.1.9 Expression of IKKε and TBK1 in human melanoma tissue

This experiment was started with the staining of IKKε, TBK1, and DAPI alone. The melanoma was well-defined and strong IKKε expression was just found in the melanoma. TBK1 expression was found in the melanoma, as well as the epidermis of the healthy skin (Fig. 4.1.9 A, B). After the enlargement of the antibody panel, the phenoptics tissue stainings of the primary melanoma samples revealed a strong colocalization of IKKε and the T-cell marker CD3, as well as IKKε and the tumor treatment marker PD1 (Fig. 4.1.9 C, E). PD1 is mostly expressed in cytotoxic T-cells and the inhibition of PD1 by antibody therapy is mostly used for non-removable, and metastasizing melanomas[245]. Combinational therapy of PD1 inhibitors and IKKε inhibitors may be a useful approach for melanoma therapy. Barely any colocalization of IKKε and the leukocyte marker CD45 was seen (Fig. 4.1.9 D). This is likely due to the staining intensity of the antigens since IKKε and CD3 are colocalized, and CD3 has to be colocalized with CD45. TBK1 was more widely distributed than IKKε and weak colocalizations with CD45 and PD1, but none with CD3 were found (Fig. 4.1.9 F-H). IKKε and TBK1 showed some colocalizations, but not in every cell (Fig. 4.1.9 I). The representative picture was taken directly in the melanoma (Fig. 4.1.9 H). A CD3 and CD45 colocalization was expected but is barely seen. Most likely the exposure time for the CD45 staining should have been longer to increase the signal. In this case, an overlay of CD3 and CD45 markers should have been seen.

The stainings showed that CD3 and CD45 positive leukocytes infiltrate the malignant melanoma and that IKKε as well as TBK1 are expressed in the tumor. IKKε was barely expressed at all in healthy skin, while TBK1 was expressed in the epidermis. An additional finding is that IKKε and CD3 are often colocalized, which indicates an effect of IKKε on the immune system in the tumor microenvironment.

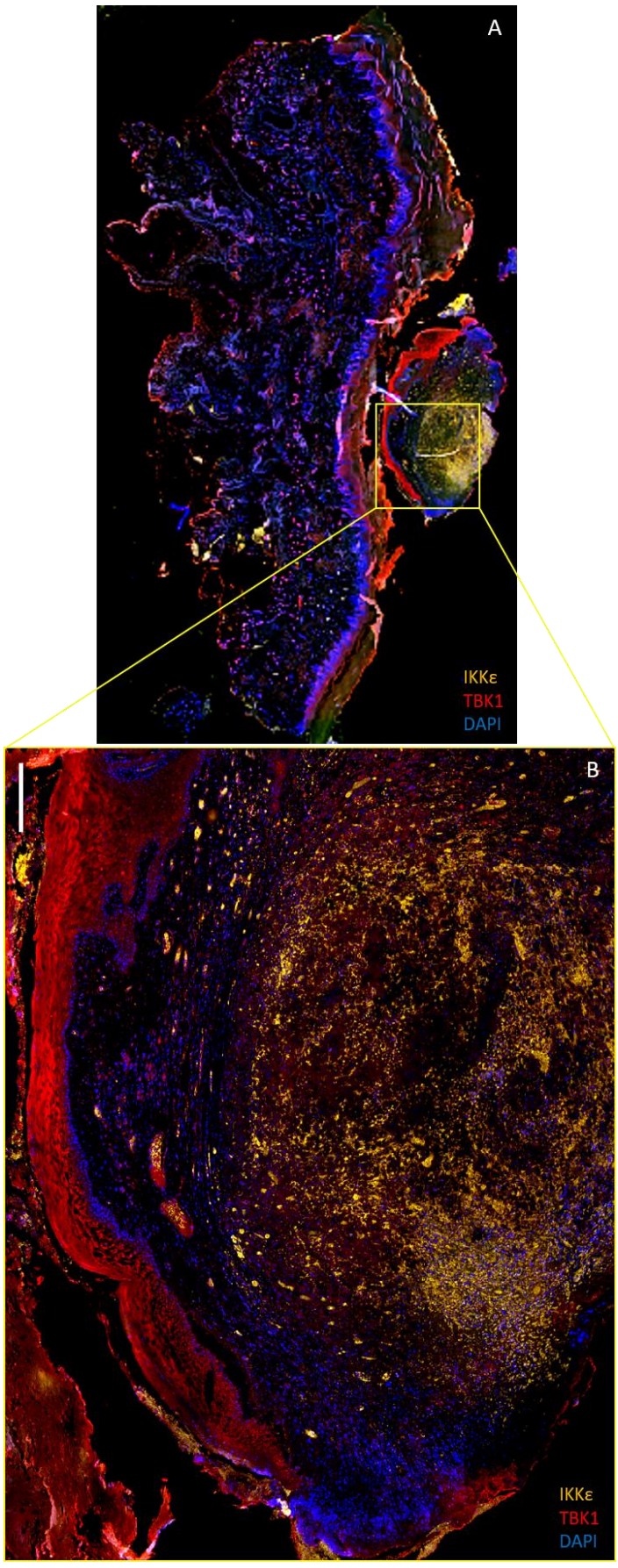
A
IKKε
TBK1
DAPI
B
IKKε
TBK1
DAPI

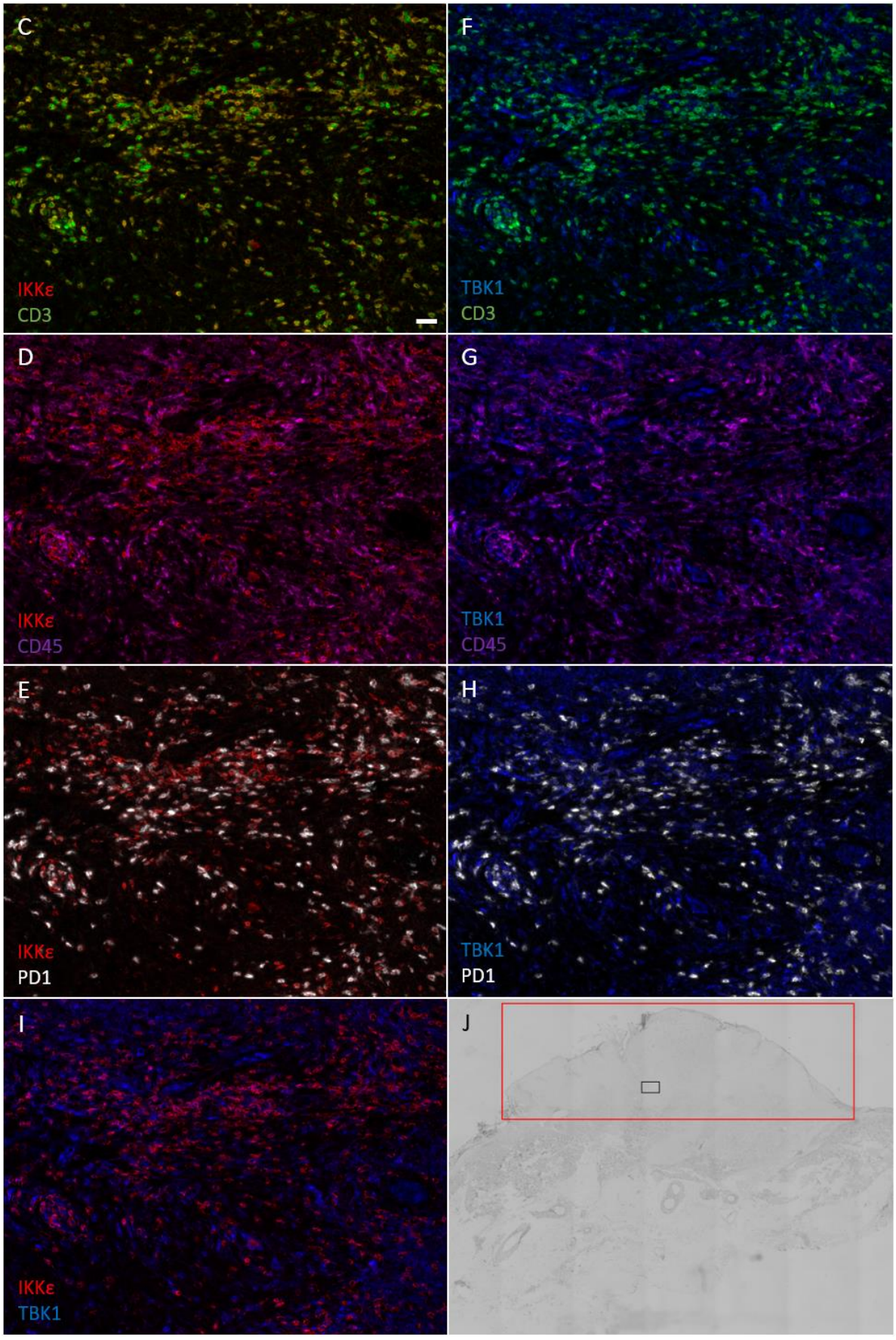
C
IKKε
CD3
F
TBK1
CD3
D
IKKε
CD45
G
TBK1
CD45
E
IKKε
PD1
H
TBK1
PD1
I
IKKε
TBK1
J

Fig. 4.1.9: Multiplex IHC staining of human malignant melanoma. Staining of IKKε (orange), TBK1 (red), and DAPI (blue) in the primary melanoma sample of a patient. Scale bar = 300 µM. Colocalization of IKKε (red) and CD3 (green) (A), IKKε and CD45 (magenta) (B), IKKε and PD1 (white) (C), TBK1 (blue) and CD3 (D), TBK1 and CD45 (E), TBK1 and PD1 (F), IKKε and TBK1 (G), and a transmitted light image of the tissue sample (H). The tumor is marked with the red square and the position where the picture was taken is marked with the black square. Scale bar = 100 µM. Representative images out of 5 different patient samples (adapted from Möller et al. 2020[244]).

4.2 The role of alpha-Synuclein in the nociceptive system

4.2.1 Control of α-Syn knockout in SNCA$^{-/-}$ animals

The knockout of α-Syn in the SNCA$^{-/-}$ animals was controlled by Western Blot and IHC analysis. Additionally, the α-Syn antibody specificity was established.

Western Blot results of the spinal cord (Fig. 4.2.1 A) of WT and SNCA$^{-/-}$ mice resulted in a signal at approx. 16 kDa only in WT tissue. No signal was detected in SNCA$^{-/-}$ tissue. The height of the band correlates with the manufacturer's description.

Similar results were obtained with the IHC. Staining was seen in the dorsal horn of the spinal cord of WT (Fig. 4.2.1 B), but not SNCA$^{-/-}$ animals (Fig. 4.2.1 C). The specificity of the secondary antibody was tested by staining of the spinal cord without the primary antibody. No signal was detected from the secondary antibody alone (Fig. 4.2.1 D).

The focus on the spinal cord in this experiment is because later experiments focus almost entirely on changes in the spinal cord. This areal of the CNS is one of the most important and regulated in the entire nociceptive pathway.

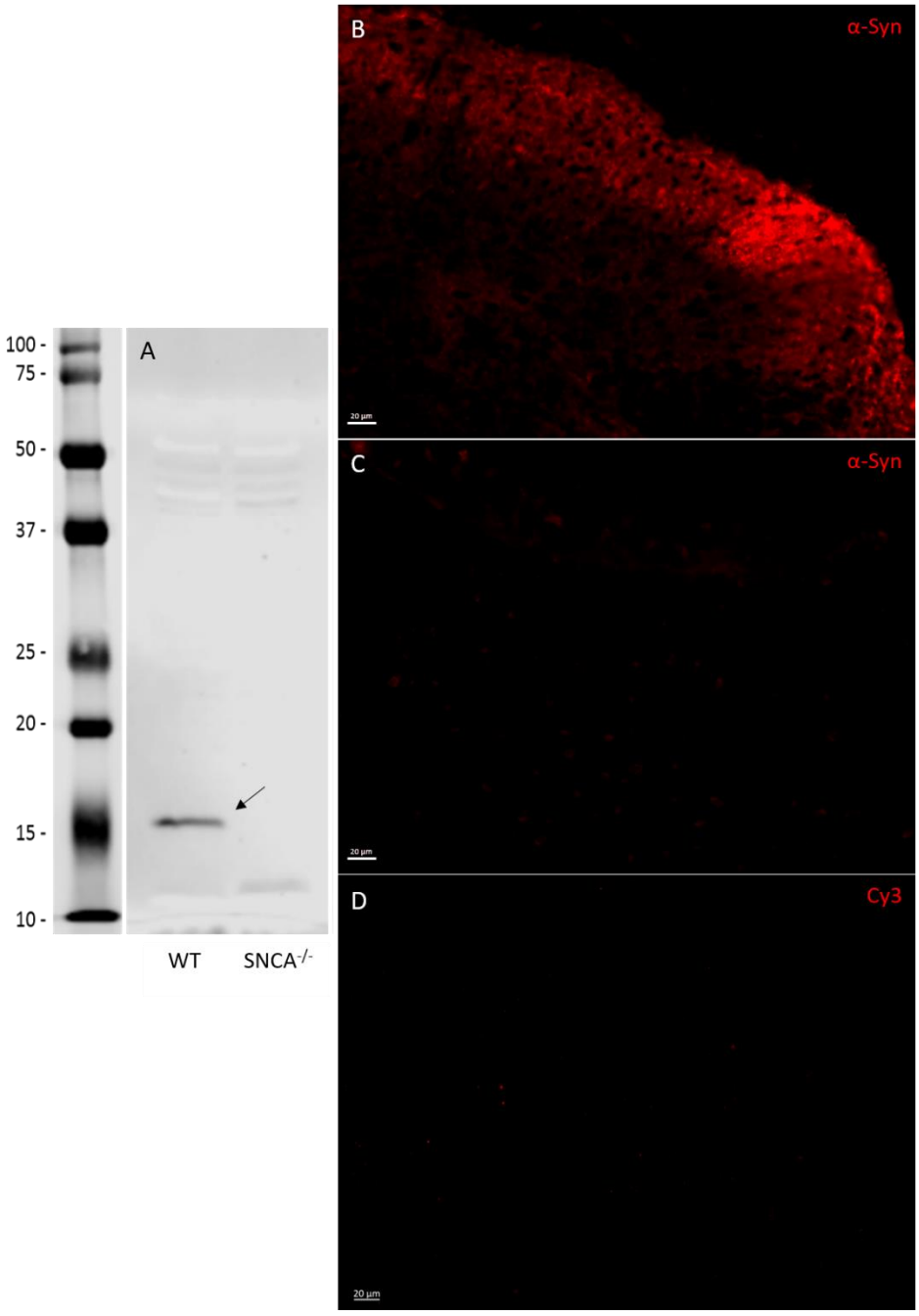

Fig. 4.2.1: Western Blot and IHC results of α-Syn knockout animals. WB results of WT vs SNCA$^{-/-}$ animals showed no signal in the spinal cord (A) of knockout animals. IHC staining of α-Syn in the spinal cord of WT (B) and SNCA$^{-/-}$ (C) animals resulted in no staining of the SNCA$^{-/-}$ spinal cord. The negative control of the secondary antibody didn't show any signal (D). Scale bar = 20 µM. The blot shows a representative WB signal.

4.2.2 Expression of α-Syn in the spinal cord of mice

The upper laminae of the dorsal horn are one of the most important areas in the CNS for nociceptive transmission. Most of the nociceptive signal transmission is transmitted from first-order neurons to second-order neurons in laminae I and II of the dorsal horn. The exclusive expression of α-Syn in these laminae indicates the participation of it in the nociceptive pathway.

IHC staining of α-Syn in the SC showed an exclusive localization in the dorsal horn. Staining of CGRP as a marker for lamina I and IB4 as a marker for lamina II revealed a co-localization of α-Syn with these markers. However, α-Syn is also expressed in even deeper laminae of the dorsal horn and is not limited on laminae I and II (Fig. 4.2.2.1) No other expression than in the dorsal horn was found in the cross-section of the SC (Fig. 4.2.2.1 B).

After finding α-Syn exclusively expressed in the dorsal horn of the SC different neuronal population markers were stained for a co-localization with α-Syn. Co-localizations of α-Syn with some of these populations would place it in the corresponding neurons and might shed light on the mechanism of how α-Syn influences the nociceptive pathway.

IHC of α-Syn and four different neuronal population markers revealed a co-localization of α-Syn with inhibitory interneurons. A co-localization with GAD67 and GABA-A was found. GAD67 is a glutamate decarboxylase that catalyzes the decarboxylation of glutamate to GABA. GABA-A is a receptor for the inhibitory neurotransmitter GABA.

No co-localization of α-Syn with markers for excitatory neurotransmitters was seen. The spinal cord was stained for tyrosine hydroxylase (TH), the enzyme that catalyzes the reaction of L-tyrosine to L-3,4-dihydroxyphenylalanine, also known as the precursor of dopamine L-DOPA. The expression of α-Syn in glutamatergic neurons via expression of the vesicular glutamate receptor VGlut1 was also investigated. Barely any co-localization between α-Syn and VGlut1 was seen. The co-localization that is seen is most likely artificial due to a strong α-Syn signal. Therefore, barely any to none co-expression or co-localization of α-Syn and excitatory neurons was detected (Fig. 4.2.2.2).

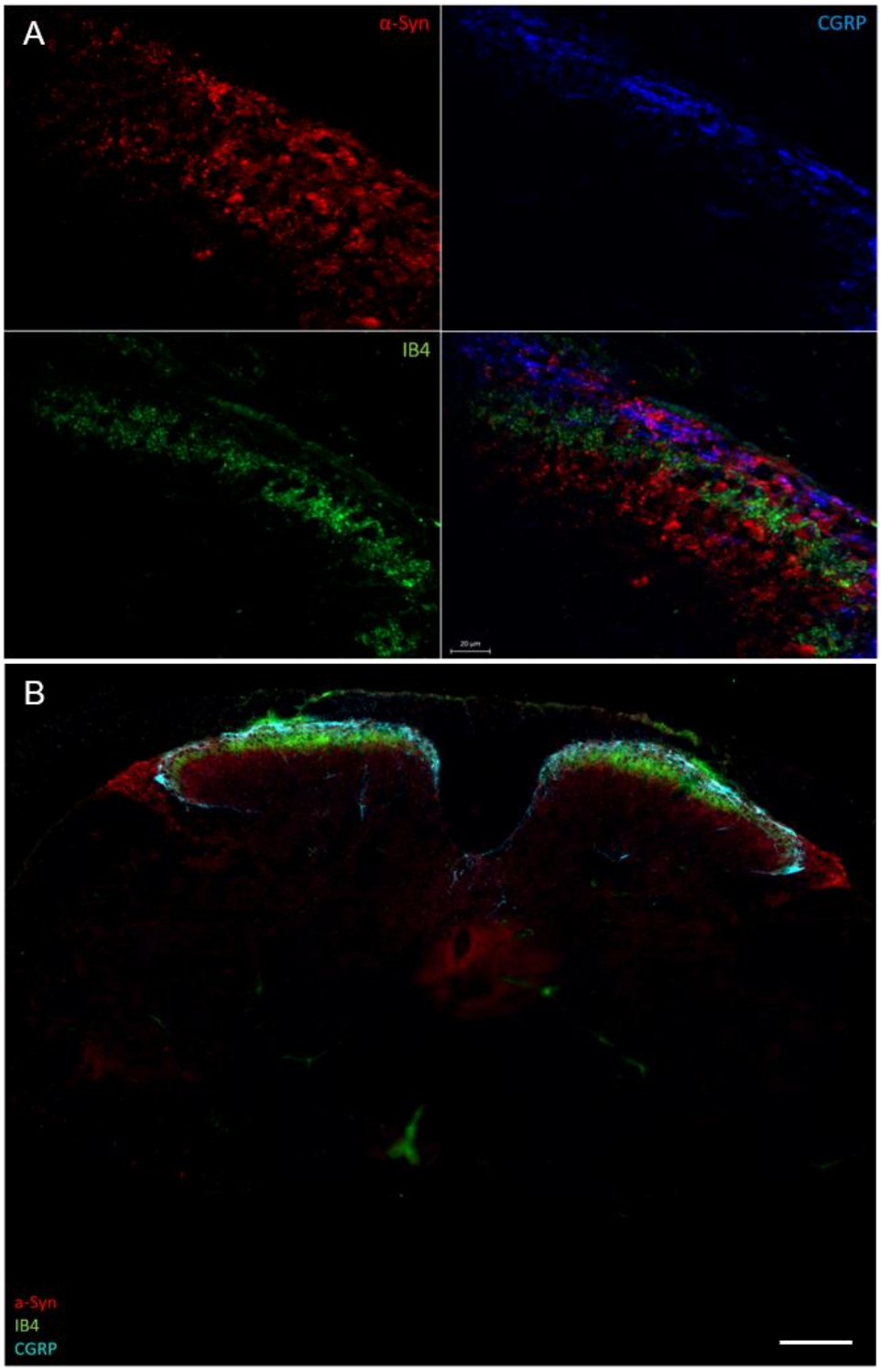

Fig. 4.2.2.1: Expression of a-Syn in the murine spinal cord. Expression of α-Syn (red), CGRP (blue) and IB4 (green) in the dorsal horn of the spinal cord. 40x magnification (A). Scale bar = 20 µM. Expression of α-Syn (red), CGRP (turquoise) and IB4 (green) in a complete cross-section of the spinal cord (B). α-Syn is exclusively expressed in the dorsal horn. Scale bar = 200 µM.

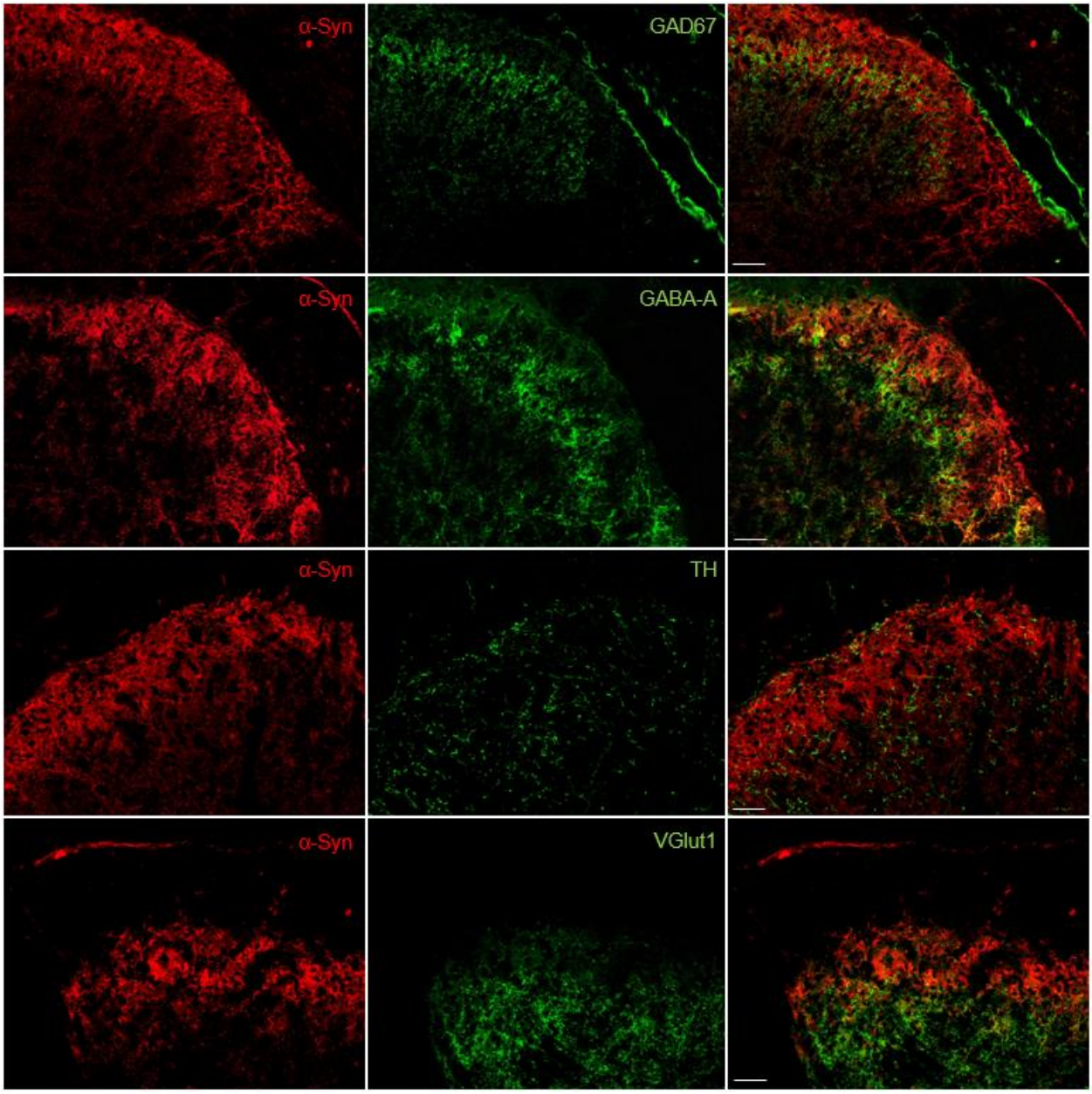

Fig. 4.2.2.2: IHC co-staining of α-Syn and a variety of neuronal markers. Cross-sections of the spinal cord are stained for α-Syn (red) and GAD67, GABA-A, TH, and VGlut1 (green), respectively. The merged image on the right-hand side indicates a co-localization of α-Syn with GAD67 and GABA-A, but barely to no co-localization with TH and VGlut1. Scale bar = 20 µM.

4.2.3 α-Syn's impact on tumor-associated pain

To investigate if α-Syn has an impact on tumor-associated pain and tumor growth, as indicated for malignant melanoma, B16 mouse melanoma cells were harvested and injected subcutaneously into the left hind paw of the animals. The animals developed a tumor in this paw. The tumor started to grow between days 3 and 7 and grew with an increasing growth rate until the end of the experiment. The mechanical pain threshold (Δ PWL) and the paw volume were measured over a time course of 21 days.

There was no difference in the Δ PWL between both groups on days 0-14. At day 21 the Δ PWL of WT animals increased further, while it stayed constant in SNCA$^{-/-}$ animals. The difference at day 21 between the genotypes was highly significant ($p < 0.01$) (Fig. 4.2.3.1 A). The paw volume between the genotypes was the same for the complete experiment, even though there seemed to be a trend to a decreased volume in SNCA$^{-/-}$ animals at day 21 (Fig. 4.2.3.1 B). Representative pictures of four WT and four SNCA$^{-/-}$ animals show a decreased tumor size in SNCA$^{-/-}$ animals (Fig. 4.2.3.1 C). The increase in the sample size from four to eight animals per group revealed no difference in tumor development. Therefore, the decrease of Δ PWL is most likely due to the effects of α-Syn on the nociceptive pathway and not on tumor development.

To start the exploration of the mechanisms involved an analysis of nociceptive relevant genes was done. The SC was dissected 21 days after B16 inoculation. The investigated genes are frequently regulated in nociceptive models and have a high implication in regulating nociception. The analysis is often used in projects investigating these types of experiments.

COX-2 encodes the PG producing enzyme COX-2. This enzyme is one of the basic regulators in all nociceptive pathways. The screening revealed a significant decrease of COX-2 in the SC of SNCA$^{-/-}$ animals compared to WT (Fig. 4.2.3.2 A). iNOS encodes the inducible nitric oxide (NO) enzyme iNOS. NOs lead to vasodilatation and are a reliable marker for the activation of the immune system. Additionally, diabetic neuropathy is often caused by a reduced blood flow, which is regulated by NO. Nevertheless, even with its large implication in nociception and immune activation no regulation of this gene was seen here. The same is true for IL1B, which encodes for the cytokine interleukin-1β (IL-1β). IL-

1β activates the immune system via different pathways and can even induce the expression of COX-2 (Fig. 4.2.3.2 B, C). TNFA encodes for the cytokine TNF-α. This cytokine modulates the immune response and is a key regulator in inflammation and inflammatory nociception. A trend to downregulation of TNFA was seen in SNCA$^{-/-}$ animals compared to WT (Fig. 4.2.3.2 D). MMP9 encodes for the enzyme matrix metalloproteinase 9. The modulating role of this enzyme is often connected with neutrophil action, such as activation of IL-1β. Elevated levels are also found in patients with rheumatoid arthritis. Additionally, this enzyme is described to possess potential implications in tumor development. The screening revealed a significant decrease of MMP9 in the SC of SNCA$^{-/-}$ animals compared to WT (Fig. 4.2.3.2 E). AKT1 encodes for the enzyme Akt1. This enzyme is the key regulator of the Akt pathway and additionally modulates other, adjacent pathways. All these pathways influence nociception, the immune response, and tumor development. A significant increase was seen in the expression of Akt1 in the SC of SNCA$^{-/-}$ animals compared to WT (Fig. 4.2.3.2 F). DOR encodes for the δ-opioid receptor (DOR). The DOR is an inhibitory GPCR, which is expressed in the CNS. Activation of this receptor produces analgesia. The receptor is activated by enkephalins. A trend to downregulation of DOR is seen in SNCA$^{-/-}$ animals compared to WT (Fig. 4.2.3.2 G). CB1-R, which encodes for the cannabinoid receptor 1 (CB1-R) is a GPCR, mostly with an inhibitory subtype. In rare cases, it can be an excitatory subtype, though. The CB1-R is expressed in the PNS and CNS and its activation produces analgesia in the nociceptive system. The receptor is activated by endocannabinoids. No regulation of the CB1-R was seen (Fig. 4.2.3.2 H). FAAH encodes for the fatty acid amide hydrolase enzyme. It is responsible for the production of bioactive fatty acid amides. The most important member of this group for this work is the endocannabinoid 2-arachidonoylglycerol. No regulation of this gene was seen in this experiment (Fig. 4.2.3.2 I). CD11b encodes a cell adhesion molecule, which is expressed on the surface of dendritic cells, monocytes, macrophages, and granulocytes. Therefore, CD11b is often used as a marker for immune cell invasion and immune system activation, which frequently happens during and after nociception. No regulation of this marker was seen after tumor inoculation (Fig. 4.2.3.2 J). Iba1 encodes the ionized calcium-binding adapter molecule 1, which is expressed in microglia and circulating macrophages. Like CD11b, Iba1 is a marker for immune activation. No regulation of this marker was seen here (Fig. 4.2.3.2 K). c-FOS encodes the transcription

factor c-Fos and is described as a proto-oncogene. It is upregulated by a variety of stimuli, like tumor-promoting signals and pain. This makes it a great nociceptive marker to analyze in the melanoma model. A trend to a downregulation was seen in WT animals compared to SNCA$^{-/-}$ (Fig. 4.2.3.2 L).

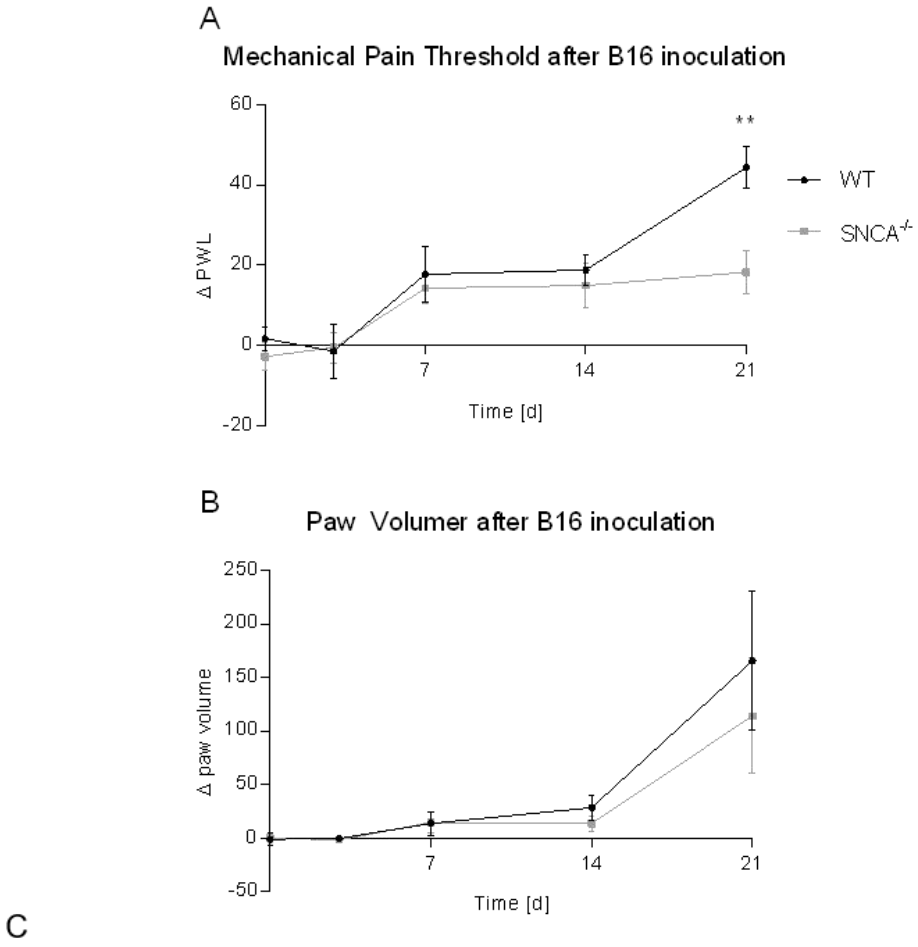

Fig. 4.2.3.1: Results of tumor-associated pain after B16 inoculation. The mechanical pain threshold was measured with the Dynamic Plantar test over a time course of 21 days (A [n = 10]). $SNCA^{-/-}$ animals showed a higher mechanical pain threshold 21 d after tumor inoculation compared to WT. The paw volume was measured directly after the Dynamic Plantar test to verify tumor growth (B [n = 8]). Representative pictures of four WT and four $SNCA^{-/-}$ animals are shown, with an arrow indicating the injected paw (C). ** $p<0.01$.

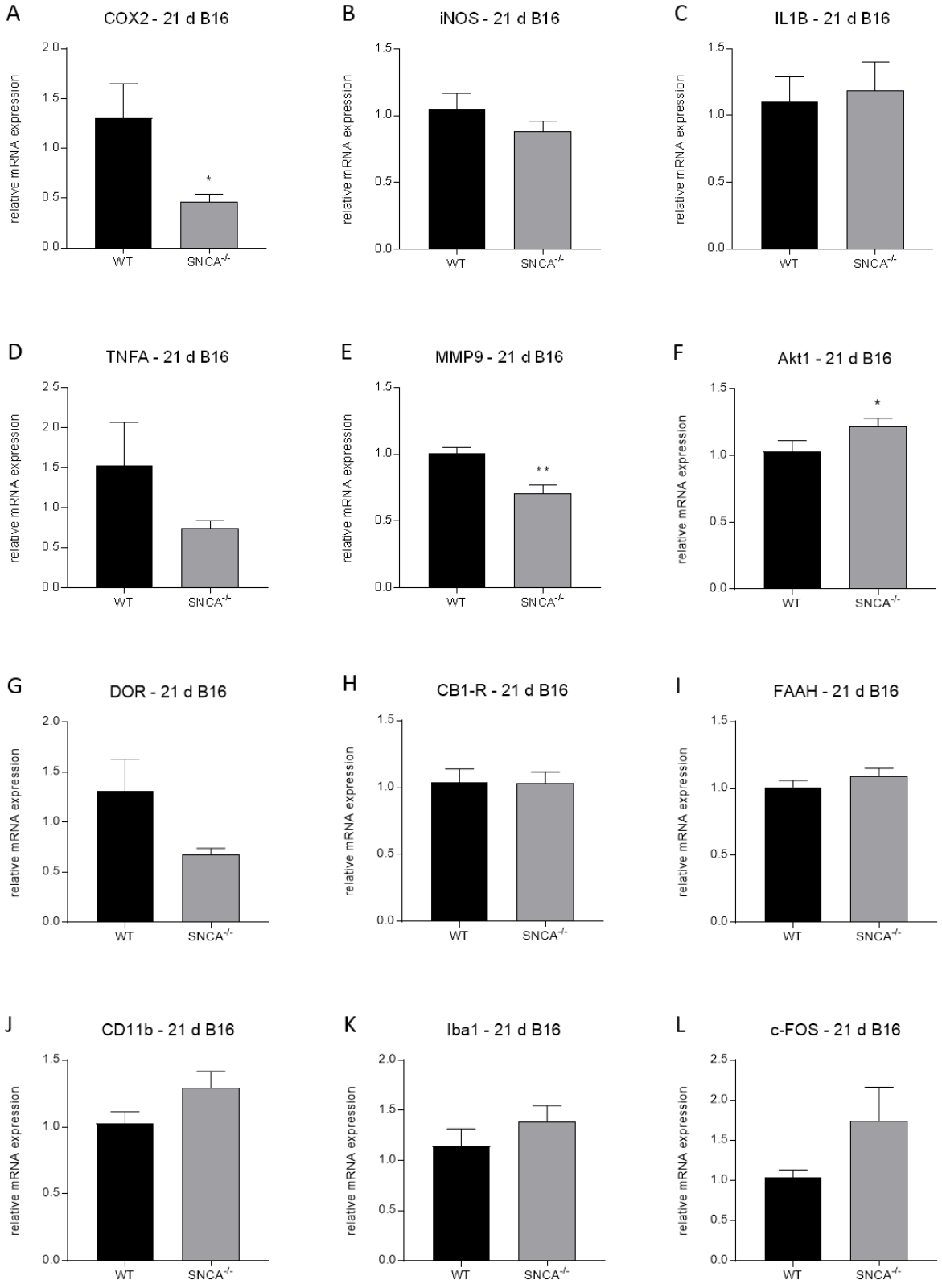
A
COX2 - 21 d B16
relative mRNA expression
2.0
1.5
1.0
0.5
0.0
*
WT
SNCA-/-
B
iNOS - 21 d B16
relative mRNA expression
1.5
1.0
0.5
0.0
WT
SNCA-/-
C
IL1B - 21 d B16
relative mRNA expression
1.5
1.0
0.5
0.0
WT
SNCA-/-
D
TNFA - 21 d B16
relative mRNA expression
2.5
2.0
1.5
1.0
0.5
0.0
WT
SNCA-/-
E
MMP9 - 21 d B16
relative mRNA expression
1.5
1.0
0.5
0.0
**
WT
SNCA-/-
F
Akt1 - 21 d B16
relative mRNA expression
1.5
1.0
0.5
0.0
*
WT
SNCA-/-
G
DOR - 21 d B16
relative mRNA expression
2.0
1.5
1.0
0.5
0.0
WT
SNCA-/-
H
CB1-R - 21 d B16
relative mRNA expression
1.5
1.0
0.5
0.0
WT
SNCA-/-
I
FAAH - 21 d B16
relative mRNA expression
1.5
1.0
0.5
0.0
WT
SNCA-/-
J
CD11b - 21 d B16
relative mRNA expression
1.5
1.0
0.5
0.0
WT
SNCA-/-
K
Iba1 - 21 d B16
relative mRNA expression
2.0
1.5
1.0
0.5
0.0
WT
SNCA-/-
L
c-FOS - 21 d B16
relative mRNA expression
2.5
2.0
1.5
1.0
0.5
0.0
WT
SNCA-/-

Fig. 4.2.3.2: Expression of nociceptive relevant genes in the SC of the melanoma model. Compared are the SC of WT and SNCA$^{-/-}$ animals 21 d after B16 mouse melanoma cell inoculation into the left hind paw. Relative mRNA expression is shown for COX-2 (A), iNOS (B), IL1B (C), TNFA (D), MMP9 (E), Akt1 (F), DOR (G), CB1-R (H), FAAH (I), CD11b (J), Iba1 (K), and c-FOS (L). n = 3, except for WT IL1B (n = 2) and WT TNFA (n = 2). * $p<0.05$, ** $p<0.01$.

The significant decrease of COX-2 and MMP9 expression in SNCA$^{-/-}$ animals suggests some analgesic effects in SNCA$^{-/-}$ animals. This is supported by the trend seen in the TNFA expression. There are still pro-nociceptive effects, like the significant increase in Akt1 expression and the trend to DOR downregulation in SNCA$^{-/-}$ animals, which imply that there is a variety of different mechanisms involved. On top of that, the trend to c-FOS upregulation in SNCA$^{-/-}$ animals implies that the tumor had stronger effects on these animals. Additionally, the sample size of three, and in two cases just two, animals makes it necessary to add more samples to this analysis. Nevertheless, this screening highlighted some pathways that need to be researched thoroughly to understand the mechanisms involved. One example in particular is the COX-2 pathway. First results were already obtained with a PGE_2 ELISA. No difference of PGE_2 concentration between the genotypes was found in the protein samples of three spinal cords per group (results not shown). Therefore, the regulation of COX-2 in this model might not explain the difference in nociception between the genotypes.

4.2.4 α-Syn's impact on motor function and nociception of acute pain

The motor system of SNCA$^{-/-}$ animals was tested before behavioral experiments were done. All nociceptive behavior tests that were done are based on a motor reaction, e.g. lifting the paw. An intact motor system is crucial for these tests. The Rotarod and the Hanging Wire tests were used to assess basic motor functions in all nociceptive models.

SNCA$^{-/-}$ animals showed no motor impairment in either the Rotarod (Fig. 4.2.4.1 A) or the Hanging Wire test (Fig. 4.2.4.1 B). The systemic knockout of α-Syn expressed no consequences for the motor systems in these animals. Also, these results confirmed that the animals were able to perform behavioral experiments.

After that, the Hot Plate and the Cold Plate test to assess the latency time until the first reaction for nociceptive heat and cold were done. The animals were placed on a 52 °C or 4°C heated plate and the time until they reacted towards this thermal stimulus was recorded. There was no difference between WT and SNCA$^{-/-}$ animals in the Hot Plate test (Fig. 4.2.4.1 C). The Cold Plate test showed a higher tolerance for the nociceptive cold of SNCA$^{-/-}$ animals (Fig. 4.2.4.1 D). They reacted later to this noxious thermal stimulus than the WT animals. In other words, SNCA$^{-/-}$ animals were less sensitive for cold pain than their WT counterparts.

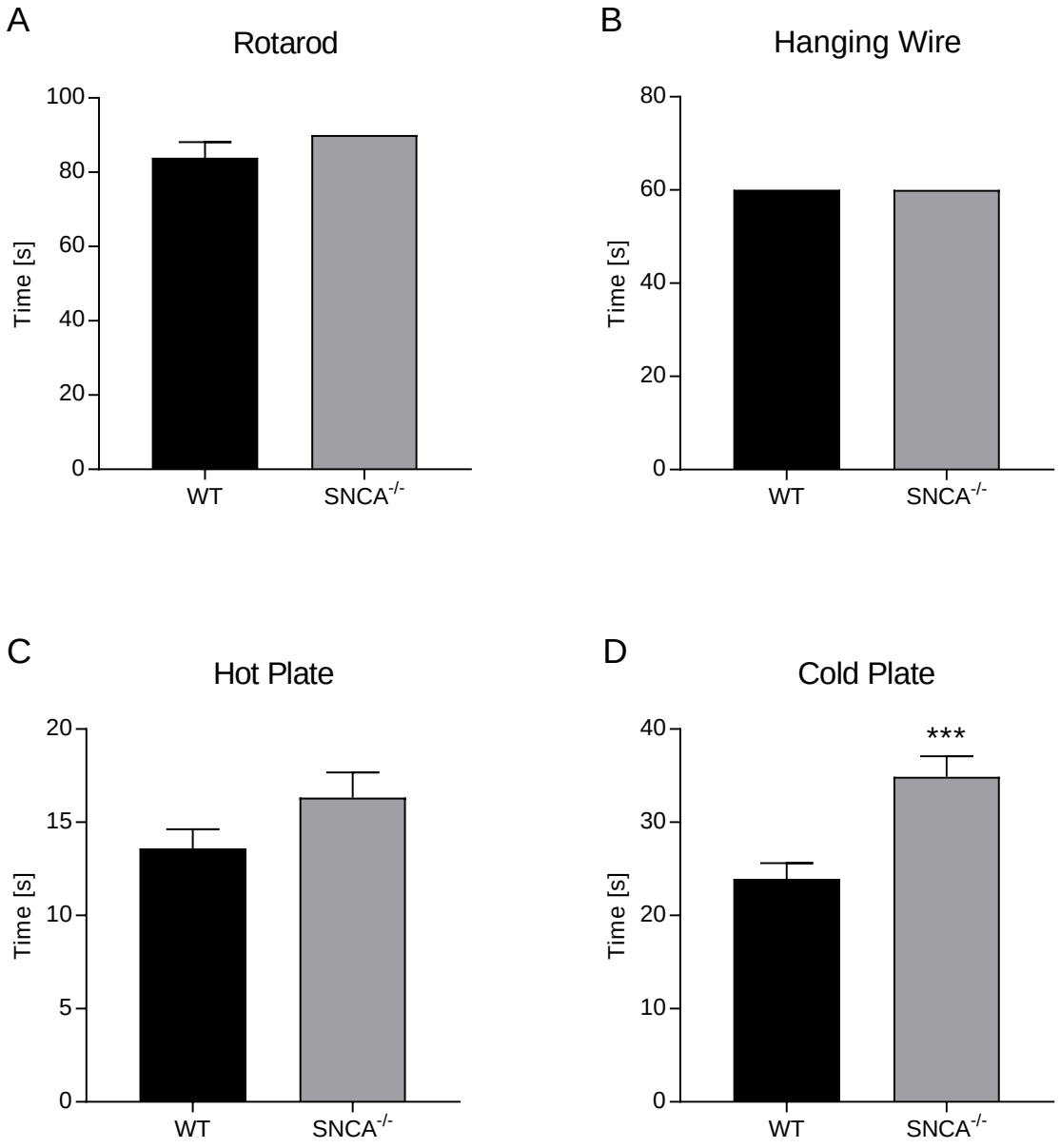

Fig. 4.2.4.1: Motor and acute pain tests. The motoric function of SNCA$^{-/-}$ mice is not impaired in comparison to the respective WT mice (A [n = 12], B [n = 12]). There is no difference of reaction latency between WT and SNCA$^{-/-}$ animals in the Hot Plate test (C [n = 12]), but a highly significant difference in the Cold Plate test (D [n = 11]). *** p<0.001.

To find an explanation for this behavioral difference the expression of the TRPM8 receptor was investigated. A decreased expression of TRPM8 in the paw of SNCA$^{-/-}$ animals (Fig. 4.2.4.2) was found. TRPM8 is the channel most often described for the registration of cold and a downregulation leads to a decreased sensitivity to noxious cold stimuli.

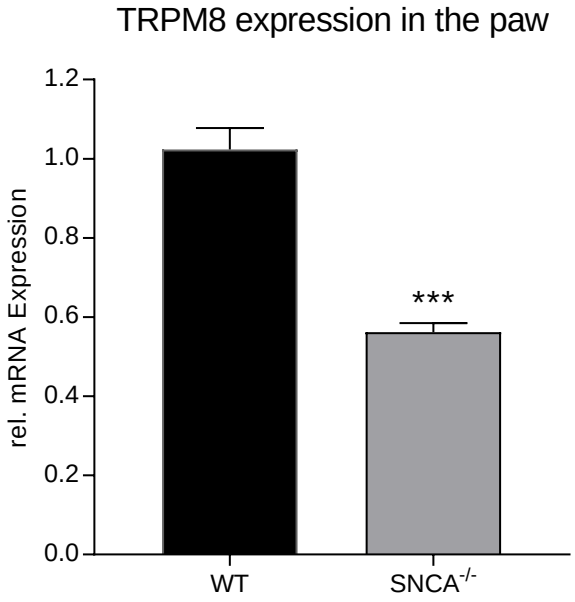

Fig. 4.2.4.2: TRPM8 expression in the paw. The mRNA expression of TRPM8 is significantly decreased in the paw of SNCA$^{-/-}$ animals. n = 3-4. *** p<0.001.

Since the effects of the α-Syn knock-out might differ between adolescent and older animals some experiments were done with 6-7-month-old mice. First of all, the motor system and acute pain were tested. These preliminary results with three animals per group didn't reveal any significant differences of the motor system or acute pain nociception between the genotypes yet (results not shown).

4.2.5 α-Syn's impact on inflammatory nociception

The next step was to investigate the reaction to inflammatory nociception. For that, the formalin and the Zymosan A tests as models for inflammatory nociception were used. While the effect of formalin lasts for about 45-60 min, the effect of Zymosan A lasts for about 24 h.

While the SNCA$^{-/-}$ group showed results like they are often described for the formalin test, this means an biphasic reaction with an acute phase I with higher licking and an inflammatory phase II, followed by a decrease of licking time at the end of the test, the WT group behaved non-typically. They showed a longer lasting and very strong phase I, which barely declined before becoming phase II. Since different mouse strains behave differently in this test it is possible, that this is normal for this strain. The formalin test showed no significant difference between the genotypes in the time course (Fig. 4.2.5.1 A), but the calculation of AUC revealed a difference. The AUC for the total time course was significantly decreased in the SNCA$^{-/-}$ group (Fig. 4.2.5.1 B). After splitting the time course into phase I (0-10 min) and phase II (10-45 min) a strongly decreased AUC was observed in phase I in the SNCA$^{-/-}$ group, while there was no difference in the AUC of phase II (Fig. 4.2.5.1 C, D). This showed that the nociception of acute pain (phase I) was different between the genotypes, while there was no difference in the nociception of inflammatory pain (phase II). This was also seen as a trend in the time course. Additionally, it is important to mention that the animals showed a strong inter-individual variety in this test. This is not uncommon in murine behavioral tests, and n=11 should be large enough to compensate this, but this variety still influences the results. Especially the time course and the statistics there. Since some animals revealed a large difference between the genotypes further experiments were done to investigate inflammatory nociception.

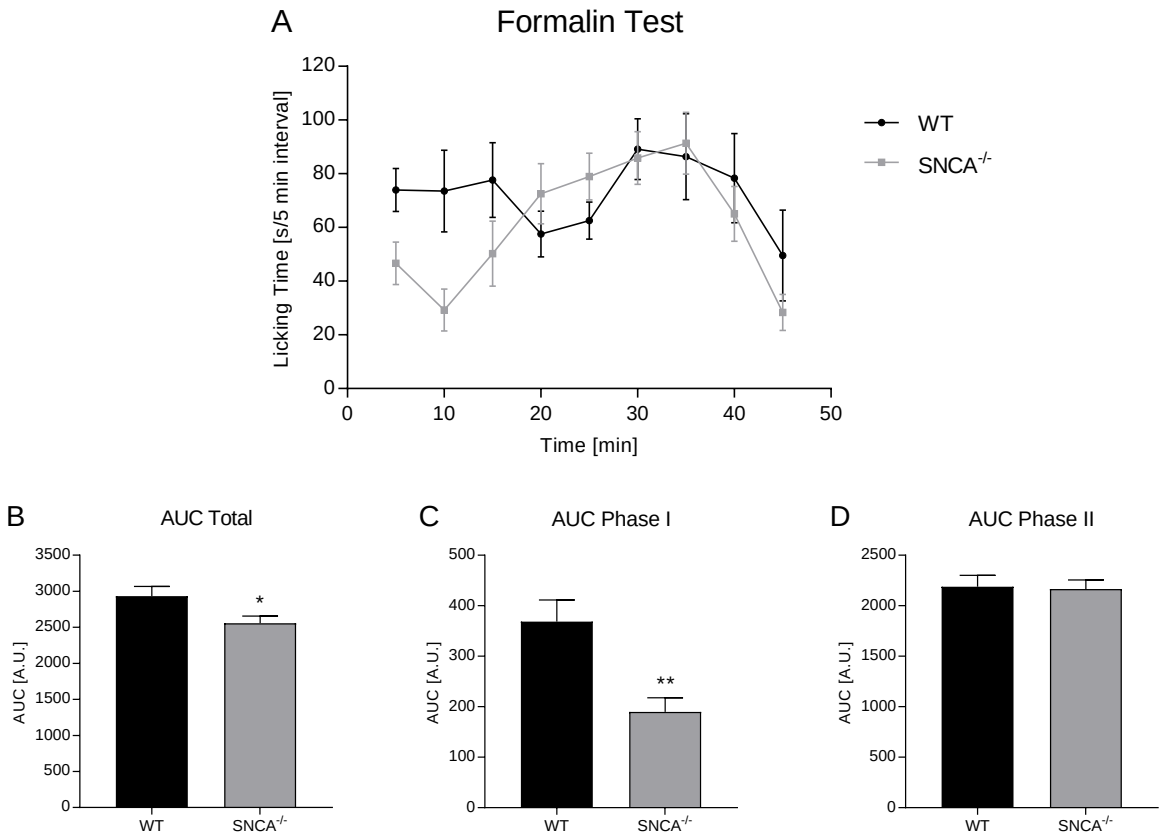

Fig. 4.2.5.1: Behavioral results of the formalin test. The time mice spent licking the formalin-injected paw is blotted against the 5 min intervals. Statistical analysis with two-way ANOVA didn't result in significant differences between the genotypes (A). The calculation of the AUC resulted in a significant decrease in the total licking time (B). The calculation of the AUC of phase I resulted in an even more significant licking time (C). The calculation of the AUC of phase II resulted in no differences between the genotypes. AUC is calculated with the area under the curve of the licking time vs. time curve. n=11. * $p<0.05$, ** $p<0.01$.

Further analysis of the formalin model revealed an effect of formalin injection on α-Syn expression. The protein expression of α-Syn in the spinal cord was increased 2 h after formalin injection into the paw. The level went back to baseline at 8 h after injection (Fig. 4.2.5.2 A).

After that, the glutamate concentration in the CSF 30 min after formalin injection was measured to see if there was a difference between the genotypes. Glutamate is the most important and abundant excitatory neurotransmitter in the nociceptive pathway. A regulation of this transmitter might be a reason for differences in nociceptive behavior.

The glutamate concentration after formalin injection showed a 10-fold increase compared to baseline (WT: 21.35 ± 5.76 µM; WT 30' F: 253.11 ± 15.58 µM; SNCA$^{-/-}$: 20.66 ± 2.90 µM; SNCA$^{-/-}$ 30' F: 226.44 ± 39.30 µM), but there was no difference between the genotypes (Fig. 4.2.5.2 B). This experiment revealed that the glutamate level in the CSF is not influenced by α-Syn expression. The differences in inflammatory nociception that were seen are most likely due to other mechanisms.

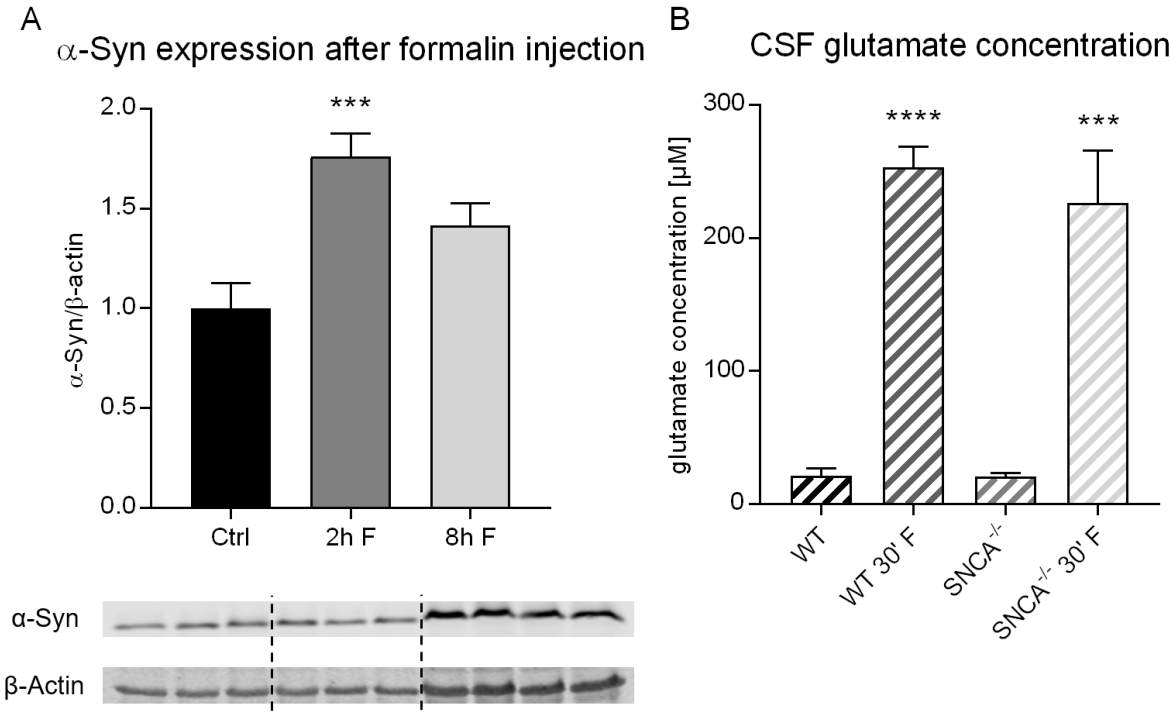

Fig. 4.2.5.2: Molecular changes after formalin injection. α-Syn expression in the SC of WT mice in untreated animals (Ctrl), 2 h, and 8 h after formalin (F) injection. One representative WB is shown (A [n = 6-8]). The expression of α-Syn is highly increased 2 h after the injection. The glutamate concentration in the CSF is highly increased 30 min after formalin injection (B [n = 5-6]). There was no difference between the genotypes. Blots show representative WB signal, the diagrams show the densitometric analysis of all blots. *** p<0.001, **** p<0.0001.

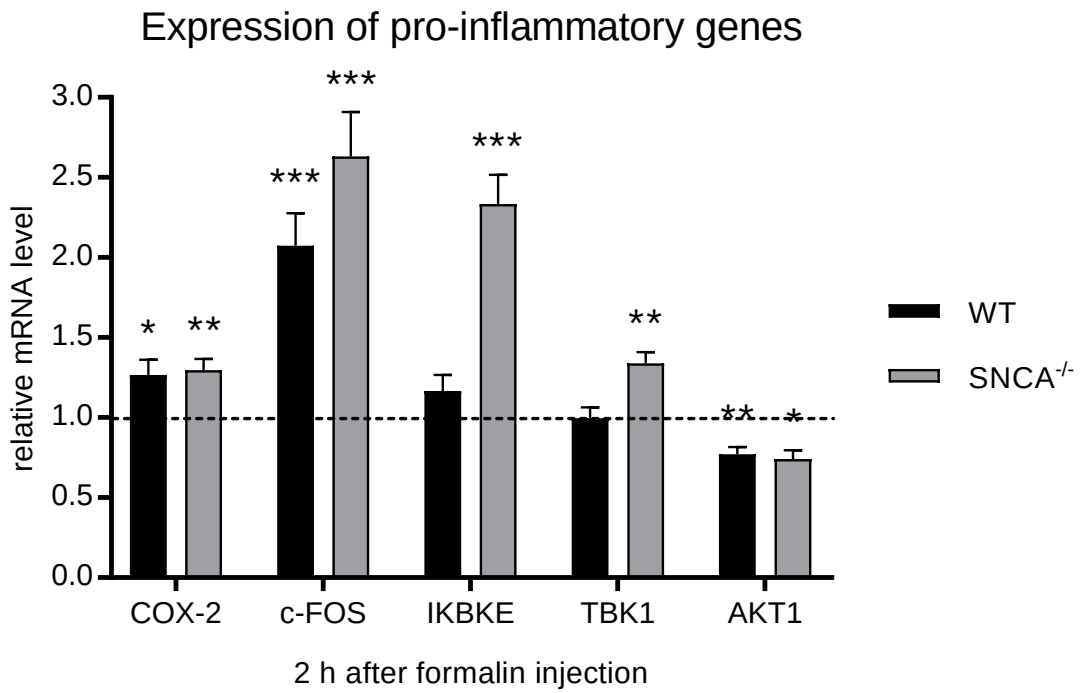

Fig. 4.2.5.3: Regulation of pro-inflammatory genes in the spinal cord 2 h after formalin injection. Relative mRNA expression of the pro-inflammatory genes COX-2, c-FOS, IKBKE, TBK1, and AKT1 in the spinal cord of WT and SNCA$^{-/-}$ mice 2 h after formalin injection. Untreated controls of the corresponding genotype are set to 1 and indicated by the dotted line. Statistical significance is calculated between control and formalin treated samples of the same genotype. n = 8-12. * $p<0.05$, ** $p<0.01$, *** $p<0.001$.

The expression of pro-inflammatory genes in the SC was measured via qPCR. Compared were untreated controls versus animals with formalin injection 2 h before the dissection. The untreated controls were set to 1 for a relative representation of data. The investigated genes COX-2, c-FOS, IKBKE, TBK1, and AKT1 are all important key proteins in inflammatory processes, which are either regulated by, or actively regulate the NF-κB, MAPK, and Akt pathways.

qPCR results of the expression of pro-inflammatory genes in the SC showed very similar results in their regulation between WT and SNCA$^{-/-}$ animals. Some differences were still seen. While COX-2 was upregulated in both genotypes 2 h after formalin injection, the upregulation revealed a higher significance in SNCA$^{-/-}$ animals. No difference in the significance was seen in the upregulation of c-FOS between the genotypes after formalin

injection but the relative upregulation was higher in SNCA$^{-/-}$ animals. IKBKE and TBK1 were upregulated in SNCA$^{-/-}$, but not in WT animals. AKT1 was downregulated in both genotypes after formalin injection compared to the untreated controls. This is curious since AKT1 is expected to be upregulated in inflammatory processes. Slightly more significant downregulation of AKT1 was seen in WT animals compared to SNCA$^{-/-}$ animals (Fig. 4.2.5.3). Taken together, it seems that the inflammatory status of SNCA$^{-/-}$ animals after formalin injection is increased stronger than in WT animals. Even though no difference on a behavioral level was seen between the genotypes. A difference in α-Syn expression in the SC was seen 2 h after formalin injection compared to untreated controls, though. The α-Syn protein was upregulated (Fig. 4.2.5.2 A). Additionally, the individuals used for qPCR were checked for their results in the formalin test. A correlation is seen between a strong reaction in the behavior test and the upregulation of pro-inflammatory genes. Even without a significant difference in behavior in the inflammatory phase of the formalin test, it seems that a correlation between the inflammatory status and α-Syn expression is plausible.

To confirm some of these results with another inflammatory model the Zymosan A behavior test was done. This model acts in a slightly different way than the formalin model. While formalin mainly initiates a central sensitization via inflammatory processes, Zymosan A creates a local inflammation around the injection side with the typical symptoms. Tumor, the swelling of the tissue, and rubor, the reddening of the tissue, can easily be observed. Calor, the increase in temperature, and dolor, the pain, can be measured. Only the function laesa, the decrease in physiological functions, is harder to confirm. The mechanical nociception was measured over a time-course of 8 h with the dynamic plantar test. The results are shown as the difference of paw withdrawal latency between the treated and untreated hind paws (Δ PWL). A typical result would be the increase of Δ PWL up to 5-6 h, and a decrease after that.

The results of the formalin test were confirmed with the Zymosan A test. The Δ PWL was the same between the genotypes and the calculation of the AUC confirmed that there was no difference in this inflammatory model between WT and SNCA$^{-/-}$ mice (Fig. 4.2.5.4 A, B).

The results of the inflammatory nociceptive models showed that α-Syn has no impact on the behavioral level of inflammatory nociception, but it is itself regulated by formalin-

induced inflammatory nociception. Additionally, animals lacking α-Syn showed an increase in some pro-inflammatory genes (IKBKE, TBK1), which were not seen in WT animals and a stronger increase in c-FOS, compared with their WT littermates. Molecular data for the Zymosan A-induced inflammatory nociception are still missing.

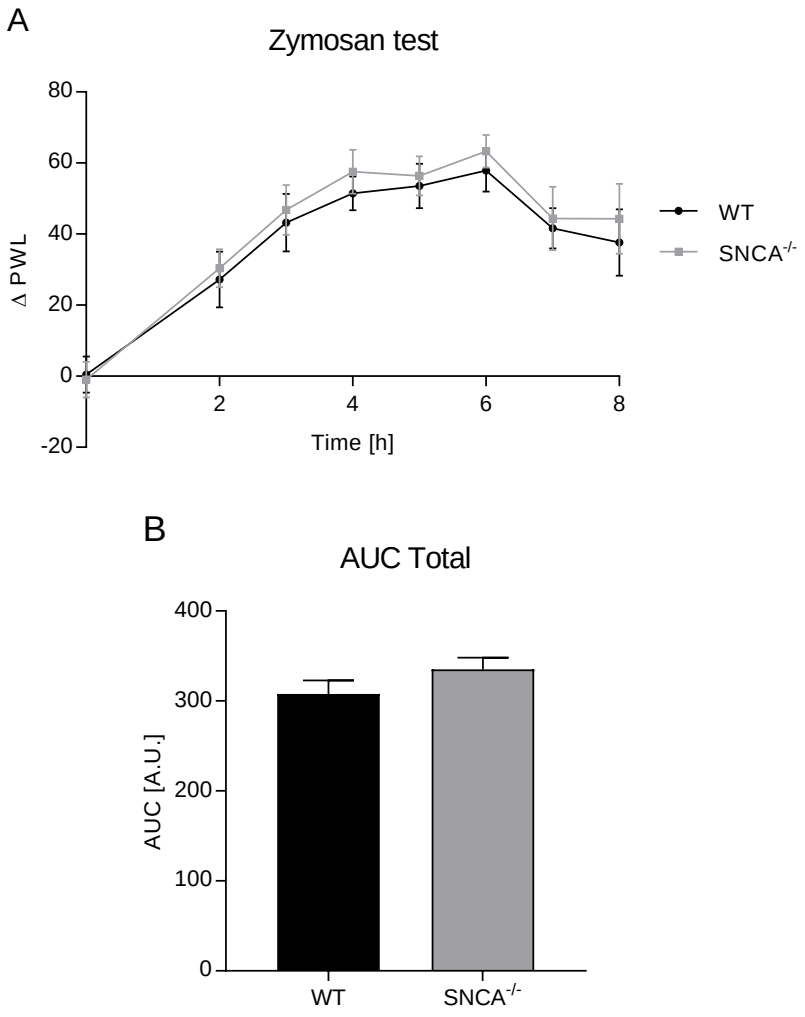

Fig. 4.2.5.4: Zymosan test as a second inflammatory model. Results of the mechanical hyperalgesia of the paw after injection of Zymosan A (A). An increase in Δ PWL means stronger nociception in this behavioral model. The AUC shows no differences between the genotypes. AUC is calculated with the area under the curve of the Δ PWL vs. time curve. (B). n = 7-8.

4.2.6 α-Syn's impact on nociception in a model of neuropathic pain

SNI was applied to WT and SNCA$^{-/-}$ animals and the mechanical pain threshold of the naïve and the operated paw were measured with the Dynamic Plantar test.

The difference between the paws (Δ PWL) of both genotypes was approx. 0 before the SNI surgery. 3 days after SNI, the operated left paw became more sensitive and the Δ PWL increased in both groups. 7 days after the operation, the Δ PWL of the WT animals increased slightly, while it decreased in the SNCA$^{-/-}$ animals. The difference was significant with $p < 0.05$. The WT group reached a plateau phase at day 14 and remained relatively stable until day 28. The sensitivity of the SNCA$^{-/-}$ group increased again at day 14 and then decreased until day 28. At days 14 and 21, there was no difference between the genotypes, however, on day 28 the Δ PWL in the SNCA$^{-/-}$ group was significantly lower than in the WT group (Fig. 4.2.6.1 A).

The AUC over 28 days was significantly lower in the SNCA$^{-/-}$ group than the AUC of the WT group (Fig. 4.2.6.1 B). The time course was split in an acute phase I (0-7 days) and a neuropathic phase II (7-28 days). No difference was seen in phase I (Fig. 4.2.6.1 C), while the difference between the groups was highly significant in phase II (Fig. 4.2.6.1 D). These results indicate, that SNCA$^{-/-}$ animals have a decreased neuropathic nociception compared with their WT counterparts.

The α-Syn expression in the SC of WT animals after SNI was also examined. No significant difference was seen at day 7 and 14, but a significant decrease of α-Syn expression was observed at day 28 (Fig. 4.2.6.3 A). These results were confirmed by IHC staining of α-Syn expression in the SC. Animals underwent Sham (Fig. 4.2.6.3 B) or SNI (Fig. 4.2.6.3 C-E) treatment and a decrease in the staining intensity was seen at day 28 after SNI.

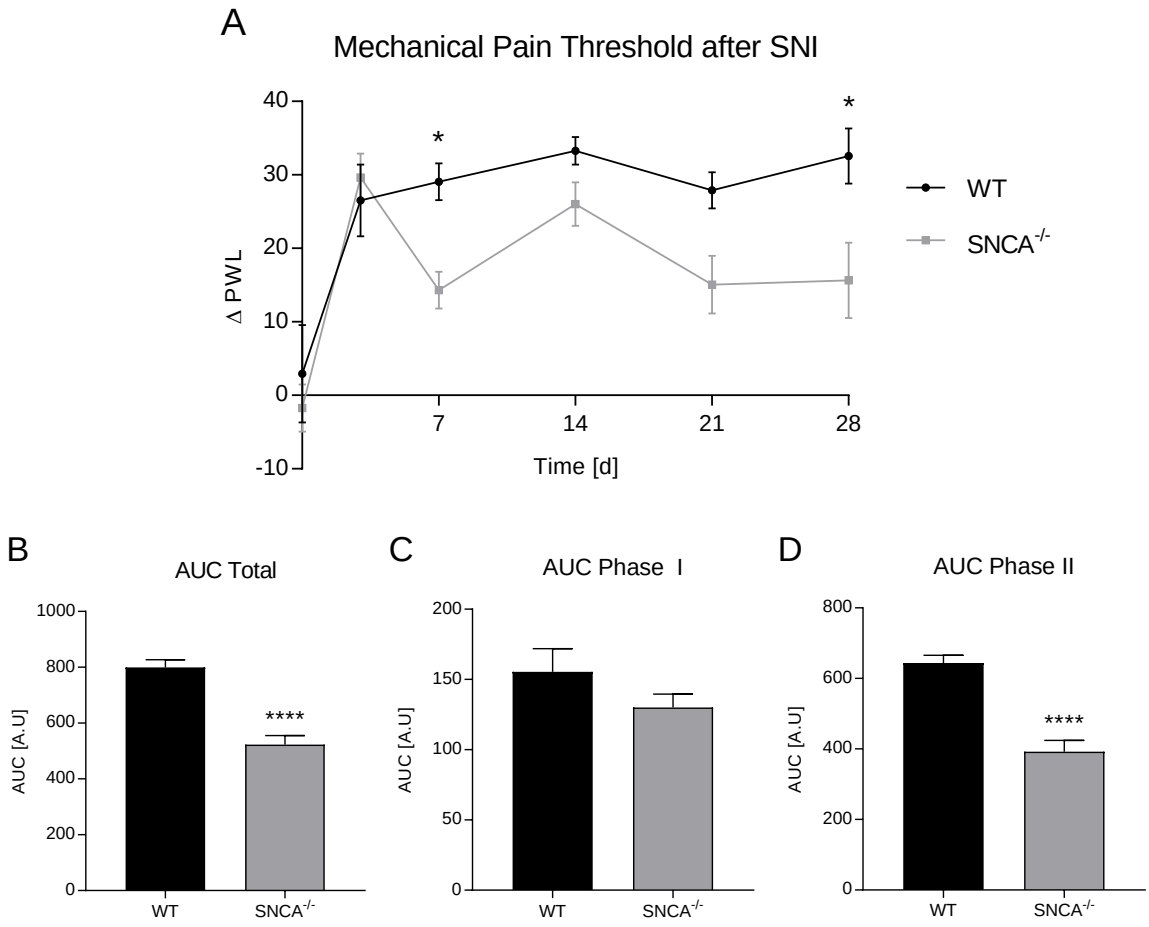

Fig. 4.2.6.1: Time course and AUC of WT and SNCA$^{-/-}$ animals after SNI. PWL was measured with the Dynamic Plantar test before and 3, 7, 14, 21, and 28 d after SNI. Significant differences between the genotypes were seen on day 7 and day 28 (A). AUC was calculated for phase I (0-7 d) (C) and phase II (7-28 d) (D). The total AUC (B) is significantly different between the genotypes, as well as the AUC of phase II. Phase I shows no difference between the genotypes. AUC is calculated with the area under the curve of the Δ PWL vs. time curve. n=10. * $p<0.05$, **** $p<0.0001$.

The same experiment was done with the older animals, which were already used for the acute nociceptive models. The WT group increased its Δ PWL up to day 7, then decreased it again on day 14 and stayed stable after that until the end of the experiment. The SNCA$^{-/-}$ group exhibited a more fluctuating behavior, with an increase at day 3, a decrease at day 7, another increase at day 14, another decrease at day 21, and a stable behavior at the end. The calculation of the AUC confirmed that there were no significant differences in the behavior (Fig. 4.2.6.2 A-D).

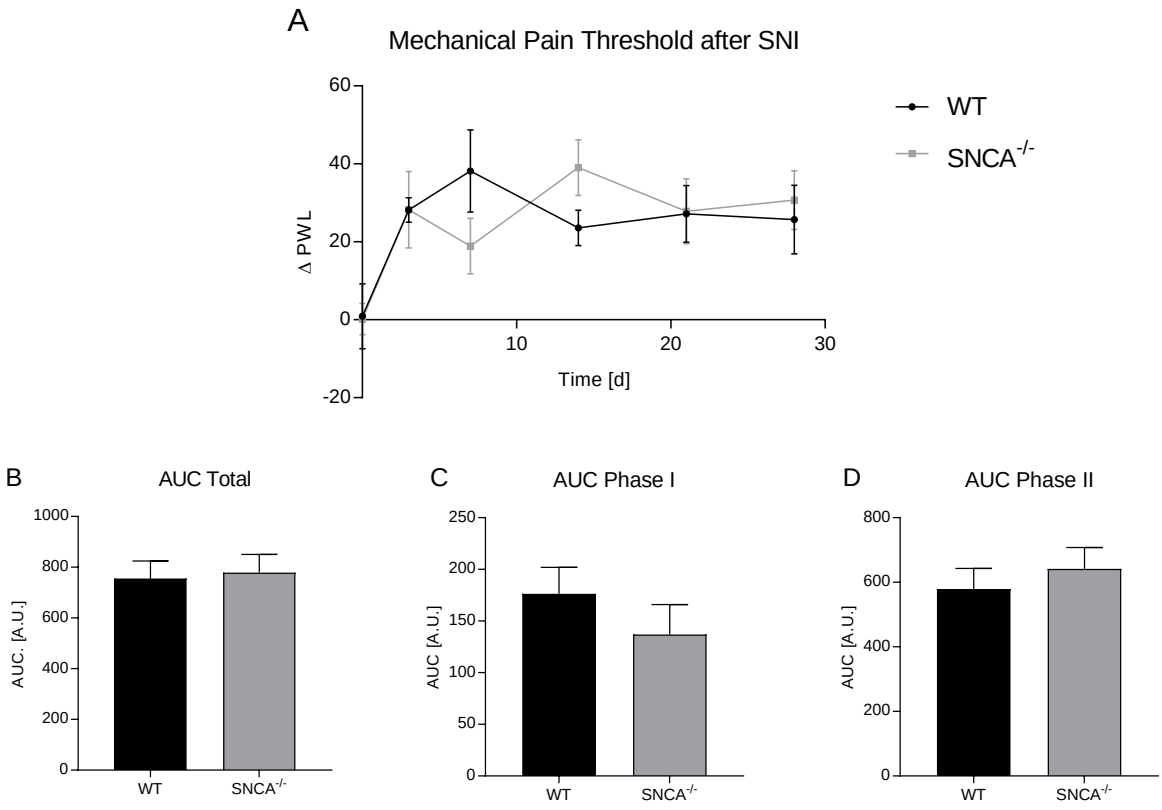

Fig. 4.2.6.2: Time course and AUC of older (> 6 months) WT and SNCA$^{-/-}$ animals after SNI. PWL was measured with the Dynamic Plantar test before and 3, 7, 14, 21, and 28 d after SNI. No significant differences between the genotypes were seen (A). AUC was calculated for the total time course (B), phase I (0-7 d) (C), and phase II (7-28 d) (D). The AUCs show no difference between the genotypes. AUC is calculated with the area under the curve of the Δ PWL vs. time curve. n = 3.

Taken together, SNCA$^{-/-}$ animals experienced less pain at day 7 and day 28. The calculation of the AUC also shows a reduction of the nociception in the complete neuropathic phase II. These results are not confirmed in a smaller group (n = 3) of older animals (> 6 months), where no significant difference was seen. Also, α-Syn expression in the SC is significantly decreased 28 d after SNI of WT animals.

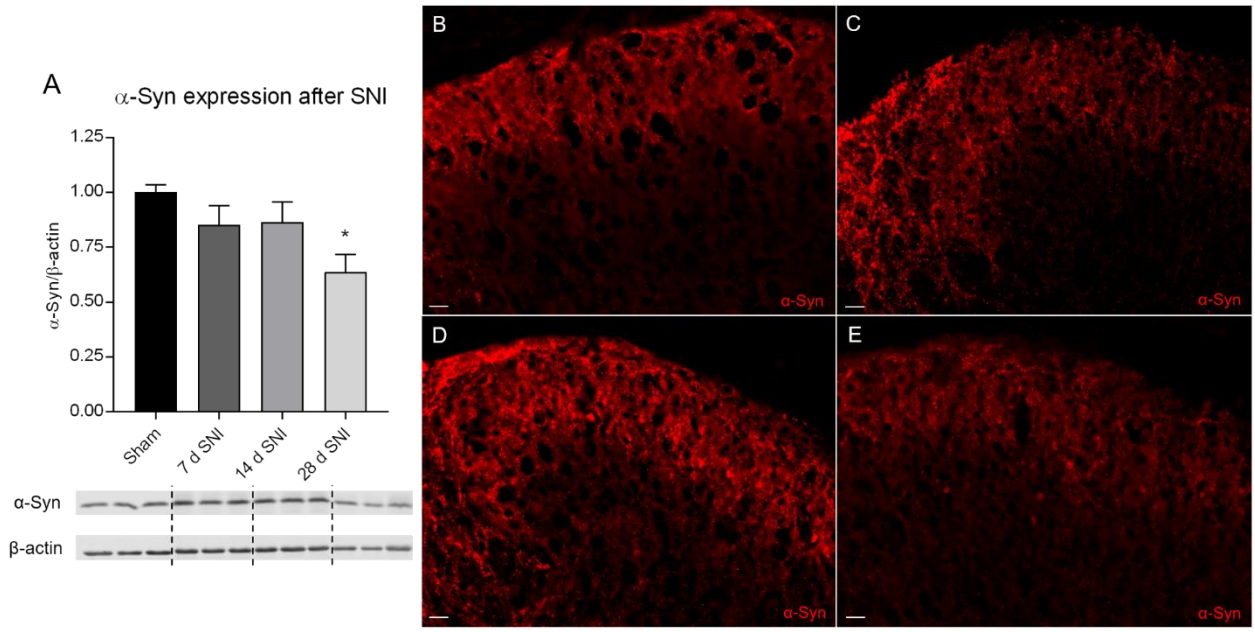

Fig. 4.2.6.3: a-Syn expression in the spinal cord of WT animals at different time points after SNI. Western Blot analysis shows the downregulation of a-Syn 28 d after SNI (A [n = 5-6]). IHC staining of a-Syn of the dorsal horn of WT animals shows no difference between Sham (B), 7 d SNI (C), and 14 d SNI (D), but a decrease of intensity at 28 d after SNI is seen (E). IHC is shown as representative pictures. Scale bar = 20 µM. Blots show representative WB signal, the diagrams show the densitometric analysis of all blots. * $p<0.05$.

To start the investigation into relevant molecular pathways the mRNA expression of a variety of genes was measured in the SC. The initiation and progression of neuropathic pain is a precisely tuned mechanism, which is not yet fully understood. The expression of a large part of the genes, which were already investigated in the tumor model, were measured over the time course of the SNI model for neuropathic pain.

qPCR results of the expression of these genes revealed a highly significant downregulation of COX-2 in the SC of SNCA$^{-/-}$ animals compared to WT at 7 and 14 d after SNI operation. While the expression of COX-2 tended to increase in WT at days 7 and 14 it decreased in the SNCA$^{-/-}$ animals. The comparison of baseline levels of COX-2 expression showed an increased expression in SNCA$^{-/-}$ animals (Fig. 4.2.6.4 A). There is no significant difference in iNOS expression between the genotypes, even though SNCA$^{-/-}$ animals tend to express less iNOS than WT 14 d after SNI. iNOS expression in

both groups decreases until day 14 and increases back to the baseline level at day 28 (Fig. 4.2.6.4 B). IL1B expression is significantly decreased 7 and 28 days after SNI in the SC of SNCA$^{-/-}$ animals compared to WT. Even though the baseline levels of IL1B are significantly increased in SNCA$^{-/-}$ animals compared to WT. IL1B expression in WT increases at 7 d after SNI and then decreases back to the baseline level. In SNCA$^{-/-}$ animals IL1B expression decreases at 7 d after SNI and then fluctuates around this decreased level (Fig. 4.2.6.4 C). TNFA baseline expression is significantly increased in SNCA$^{-/-}$ animals compared to WT animals. It is also significantly decreased 7 days after SNI in SNCA$^{-/-}$ animals compared to WT. The expression in SNCA$^{-/-}$ animals decreases on day 7, increases back to baseline at day 14, and decreases on day 28. In WT animals TNFA expression is increased on day 7 and goes back to baseline level on day 14. This is stable at day 28 (Fig. 4.2.6.4 D). The MMP9 baseline level of SNCA$^{-/-}$ animals is significantly decreased compared to WT animals. The expression of MMP9 is significantly increased in SNCA$^{-/-}$ animals at days 7 and 28 compared to WT. The expression levels in WT animals are decreased at day 7, 14, and 28, while it is just decreased at day 14 in SNCA$^{-/-}$ animals (Fig. 4.2.6.4 E). There is no difference in Akt1 baseline expression between the genotypes. Akt1 is significantly increased at day 7, and significantly decreased at day 14 in SNCA$^{-/-}$ compared to WT. Except for that, no significant difference is seen in Akt1 expression (Fig. 4.2.6.4 F). Basal DOR expression levels are significantly increased in SNCA$^{-/-}$ animals compared to WT. DOR expression levels are significantly decreased at days 7, 14, and 28 in SNCA$^{-/-}$ animals compared to WT. A decrease of DOR expression is seen at days 7 and 14 in both genotypes. At day 28 this recovers slightly in SNCA$^{-/-}$ animals, and completely in WT animals (Fig. 4.2.6.4 G). No difference or significant changes between the genotypes and over the time course are seen in CB1-R expression, except for a significant decrease at day 14 in SNCA$^{-/-}$ animals compared to WT (Fig. 4.2.6.4 H). The same is seen in FAAH expression, but with an added significant increase of FAAH expression in SNCA$^{-/-}$ animals compared to WT at day 28 (Fig. 4.2.6.4 I).

Taken together it seems that many factors influence the neuropathic nociception and the SNI model. Strong antinociceptive effects were seen in SNCA$^{-/-}$ animals in the regulation of COX-2, IL1B, and TNFA. But there were also pro-nociceptive effects in the regulation of MMP9, DOR, CB1-R, and FAAH. The decreased nociceptive response in the behavior

experiment implies that the antinociceptive effects outweigh the pro-nociceptive effects, though. The sample size of n=3 makes it necessary to increase the number of samples for the experiment.

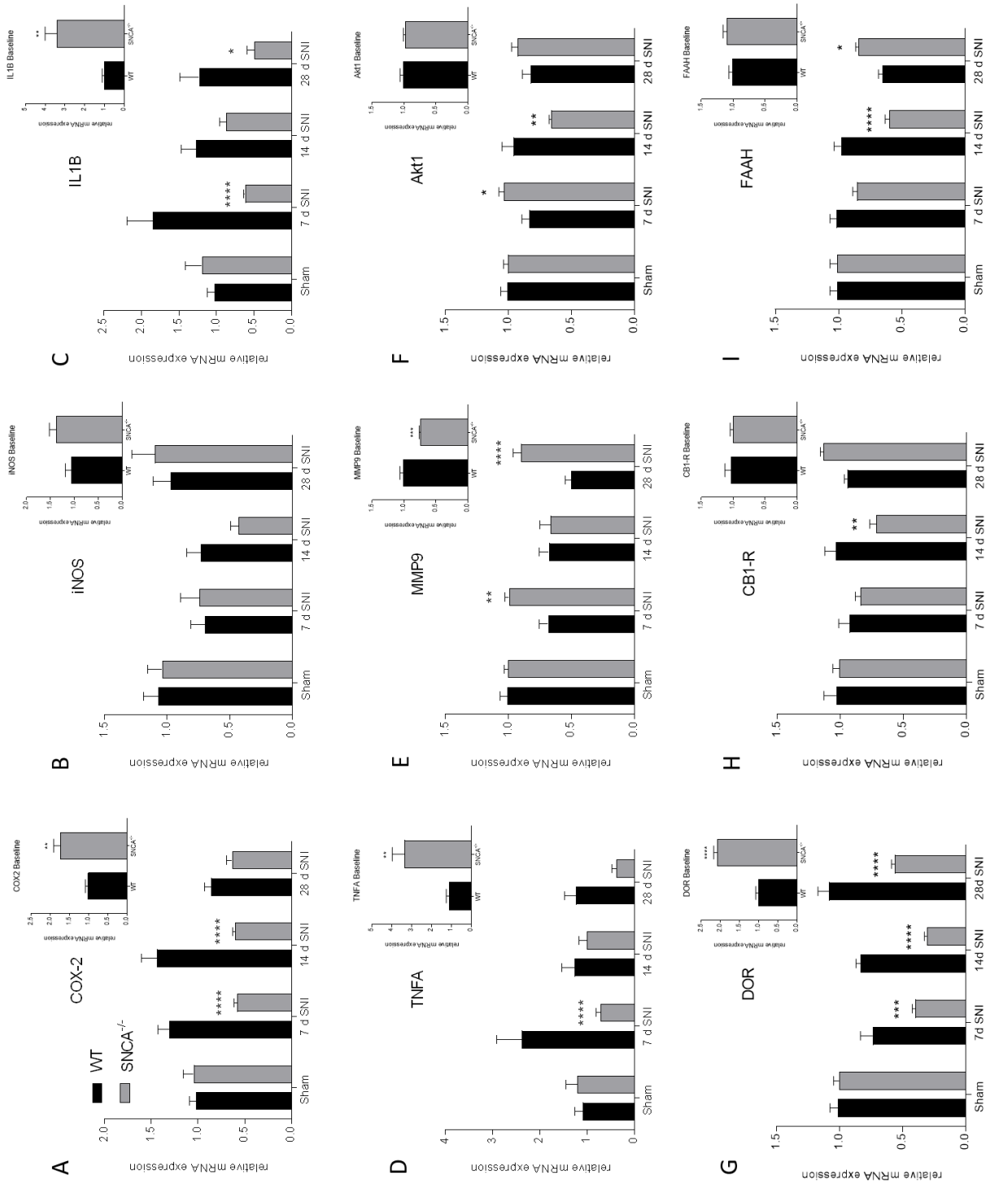

Fig. 4.2.6.3: Expression of nociceptive relevant genes in the SC of the SNI model. Compared is the mRNA expression in the SC of WT and $SNCA^{-/-}$ animals. In the large graphs, the treatments are compared relative to the Sham operation of the corresponding genotype. In the inserted graph the baseline levels are compared between the genotypes. Relative mRNA expression is shown for COX-2 (A), iNOS (B), IL1B (C), TNFA (D), MMP9 (E), Akt1 (F), DOR (G), CB1-R (H), and FAAH (I). n = 3. * $p<0.05$, ** $p<0.01$, *** $p<0.001$, **** $p<0.0001$.

5. Discussion

The present work investigates the function of IKKε, TBK1, and α-Syn in the pathogenesis of melanoma and pain. A previous study was able to show a correlation between PD and malignant melanoma[41,42] and one of the key factors in PD is the accumulation of α-Syn fibrils. Additionally, pain is one of the main non-motor symptoms in PD, as well as in tumor diseases. Furthermore, α-Syn is described to affect tumor progression[246]. A possible correlation and maybe even causality between these phenomena are plausible. This work intends to increase the understanding of these topics. The first half of this work tested the effect of IKKε and TBK1 in human malignant melanoma and the effect of the IKKε/TBK1 inhibitor amlexanox on the properties of malignant melanoma. The second half focused on the effect of α-Syn in the murine nociceptive system.

5.1 Expression of IKKε and TBK1 in human malignant melanoma

Recent studies showed that IKKε is upregulated in a variety of different tumors, e.g. breast cancer, glioma, and ovarian cancer. The kinase IKKε is reported as an important oncoprotein and promotes tumor growth, migration, and invasion. An inhibitory effect on tumor growth is described for different types of cancer (reviewed in [88]). Since the origins of malignant melanoma can be diverse and it is a ‘difficult to treat’ tumor a possible effect of IKKε/TBK1 inhibition on tumor characteristics could be a promising therapeutic option. Additionally, a previous study from our group already established an inhibition of melanoma growth by IKKε knock-out in murine melanoma cells[106]. This work confirms these findings for human malignant melanoma.

In this work it was observed that IKKε and its functional partner, TBK1, are both upregulated in SK-Mel28 and A375M cells compared to non-malignant HERMES1 melanocytes. Additionally, both kinases show overexpression in samples of malignant melanoma compared to healthy naevi. Similar results were already seen in gastric and non-small cell lung cancer[96,247].

In slices from primary human melanoma, multiplex immunofluorescence analysis was performed and expression of both IKKε and TBK1 in the melanoma was observed. This confirms the Western Blot results of IKKε and TBK1 expression in melanoma metastases.

IKKε showed a strong colocalization with CD3-positive cells while TBK1 colocalized partially with CD45- but not with CD3-positive cells. Some of the TBK1 and IKKε stained cells showed additional immunoreaction with PD1. It seems that IKKε and TBK1 are also expressed in tumor-infiltrating immune cells and can, therefore, modulate the immune reaction. Additionally, the expression pattern implies that IKKε is primarily expressed in T-cells, while TBK1 is expressed in leukocytes in general. The expression of IKKε in T-cells was already published before for murine tissue. This group also found inhibition of tumor growth after IKKε knock-out in T-cells[107]. The importance of TBK1 in the immune system is also extensively discussed and investigated (reviewed in [248]). The findings of this work support these findings for the microenvironment of malignant melanoma. Additionally, the multiplex staining revealed that barely to no expression of IKKε is seen in non-tumor tissue and that TBK1 is only expressed in the epidermis of healthy skin. Both kinases are not only expressed in melanoma cells but also in the tumor environment. The tumor environment itself has an extremely strong impact on the regulation of tumor characteristics[249]. These results do not necessarily show that IKKε and TBK1 have an impact on tumor characteristics, but they show that the kinases are regulated during tumor progression, or that their deregulation leads to the formation and progression of malignant melanoma.

5.2 Effects of amlexanox on tumor characteristics

As mentioned before, it is published that IKKε acts as an oncoprotein and promotes the progression of tumor growth, migration, and invasion. This is known amongst others for breast cancer, glioma, and ovarian cancer[90,250,251]. The effect of IKKε and TBK1 in malignant melanoma was at first evaluated via *in vitro* inhibition with the specific IKKε/TBK1 inhibitor amlexanox[109].

Both, the WST and SRB proliferation assays, resulted in an amlexanox dose-dependent decrease in proliferation of SK-Mel cells. The results for the A375 cells were not as clear. While there was no change in proliferation seen in the WST assay, the SRB assay resulted in a decrease in proliferation at 30 µM and 50 µM amlexanox. This is most likely due to the function of the two tests. The WST assay is based on the metabolic activity of living

cells, while the SRB assay stains the total cell mass adherent to the bottom of the well. If no difference in the WST assay, but a difference in the SRB assay, is seen, it means that the same number of cells show a metabolic activity, but that there are fewer total cells in the amlexanox-treated wells. This could still indicate an amlexanox induced decrease in proliferation of A375 cells. After obtaining these imprecise results for the A375 cells it was decided to limit further experiments to the SK-Mel28 cell line.

Since no publication up to this point mentions the effect of amlexanox on autophagy, and since the regulation of autophagy might be an explanation for the change in proliferation after amlexanox treatment, the LC3b-II and p62 expression, as recommended by Klionsky et al[252], were investigated. TBK1 is crucial for the maturation of the autophagosome by phosphorylation of the necessary autophagy receptors optineurin, NDP52, TAX1BP1, and p62[253,254]. This makes TBK1 a key regulator of autophagy. IKKε is also investigated in the context of autophagy. The screening of a library of activated kinases revealed IKKε as a positive regulator in autophagy. Additionally, it was postulated that IKKε-regulated autophagy is necessary for breast cancer progression[87]. Western Blot results showed a downregulation of LC3b-II and an upregulation of p62 after amlexanox treatment. These results support each other since the expression of LC3b-II and p62 are inversely correlated. This expression pattern led to the conclusion that autophagy is inhibited in melanoma cells after amlexanox treatment. The literature agrees that autophagy is downregulated during and briefly after the transformation of melanocytes into malignant melanoma cells but is highly upregulated after the tumor established itself. This characteristic is also associated with a poor prognosis[47,255,256]. Therefore, malignant melanoma belongs to the kind of tumors where autophagy has a promoting effect on growth, survival, and oncogenesis. The inhibition of autophagy in this kind of tumor can lead to a decrease in these characteristics and makes the treatment with chemotherapy more effective[257–259]. The result that amlexanox treatment inhibits autophagy in malignant melanoma cells is the first step to show the effectiveness of amlexanox treatment and explains also on a mechanistic level why amlexanox treatment inhibits proliferation and migration *in vitro*.

Another important aspect is the inhibition of p65 and p44-42 after amlexanox treatment. The results of this project were able to show that amlexanox inhibits the phosphorylation

of p65. Since amlexanox specifically inhibits IKKε and TBK1 this happens via this pathway. The inhibition of p65 results in an inhibition of NF-κB and subsequent expression of oncogenic genes. It is already known that inhibition of NF-κB leads to a decrease in angiogenesis and the promoting factor CXCL8 expression[260]. Angiogenesis is an important mechanism in cancer progression to ensure blood flow in the tumor and the inhibition of this mechanism limits tumor growth. Other studies showed that NF-κB activity is upregulated in melanoma, which influences the regulation of apoptosis, angiogenesis, and tumor cell invasion[261]. Additionally, the results showed that not only p65 but also p44-42 is inhibited by amlexanox treatment. The MAPK p44-42, also known as ERK1/2, is one of the main regulators of the MAPK pathway. This pathway is described as maybe the most important driver of human cancers. One of the basic therapies of BRAF-mutated melanomas is the treatment with MAPK inhibitors. This pathway is a key player in the regulation of cell proliferation, survival, and differentiation. The dysregulation of this pathway is known to be involved in oncogenesis[262] (reviewed in [72]). The modulation of the MAPK pathway via p44/42 inhibition after amlexanox treatment is most likely an anti-tumor mechanism. The effects of inhibition of p65 and p44-42 added to the inhibited autophagy are most likely the main reasons for the inhibition of tumor characteristics after amlexanox treatment.

Besides the inhibition of proliferation, and inhibition of migration and invasion of SK-Mel cells after amlexanox treatment is seen. Three different types of assays were used for the investigation of migrative abilities. The scratch assay, which resulted in cellular growth into a cell-free gap after damaging a confluent cell layer, was done first and showed inhibition of migration after amlexanox treatment. But since the cell-free gap is created by scratching cells away many cells are damaged and die. The process of cell death releases a variety of signal molecules which in turn influence the cells around them[263]. Therefore, the results were verified with a similar assay. The ibidi setup creates a cell-free gap without damaging the cells. No cell death transmitters are released, and the migration of tumor cells into the cell-free gap can be observed over a time course. The Transwell assay added a physical barrier to the migrative setup and was additionally used to measure invasive abilities. The Transwell assay resulted in an endpoint measurement of migrative and invasive abilities. In all three assays, amlexanox inhibits the migration of SK-Mel cells. A reason for that is likely the inhibition of the NF-κB and the MAPK pathways by

amlexanox. These pathways do not only affect the proliferation of cells, but also migrative and invasive abilities[261,262]. A similar result was already found. Amlexanox inhibits prostate tumor metastasis, which is highly dependent on migrative and invasive abilities, by modulation of the IKKε/TBK1 regulated NF-κB pathway[86]. This work confirmed some of these results for melanoma cells.

To evaluate which pathway is the most influential for these characteristics first results were obtained to clear this up. The cytotoxicity assay showed that the inhibition of autophagy by BafA resulted in a strong decrease in cell growth. This effect was not further increased by amlexanox treatment. Inhibition of the MAPK and NF-κB pathways tended to show some trend to growth inhibition, but not nearly as strongly pronounced as during the inhibition of autophagy. These results imply that amlexanox's inhibitory effect on autophagy is the main driving force behind all the other effects that were seen after amlexanox treatment. Since these experiments just started to hint on the autophagy pathway, more experiments in a similar manner should be done. For example, the same treatments used in this cytotoxicity assay should be used in the migration and invasion assay to see if these results are confirmed.

Taken together, it was found that treatment of melanoma cells with amlexanox inhibits proliferation, migration, and invasion of these cells. A reason for this observation is very likely the inhibition of autophagy and the inhibition of the NF-κB and MAPK pathway by amlexanox, even though the autophagy pathway proofed to be the most influential one. Dose-dependent effects were observed. Additionally, it was found that there was no effect on the cell cycle progression after amlexanox treatment. No literature for the effect of IKKε on the cell cycle was found, and only one recent study for the influence of TBK1 on the cell cycle. This study described TBK1 as a driving force of the cell cycle[264], which could not be confirmed by this work. One reason for the different results could be the cell lines used. While Sarraf et al. worked with HTC116 and HeLa cells, SK-Mel28 cells were used for this work. Additionally, they found the involvement of TBK1 after PINK1/Parkin knock-out, while TBK1 was directly inhibited with amlexanox in this project.

5.3 Amlexanox inhibits malignant melanoma growth in an *in vivo* xenograft model

For the investigation of the *in vivo* significance of IKKε and TBK1, a xenograft model in athymic nude mice was performed as described before[265,266]. Animals were fed either with a vehicle or with 25 mg/kg body weight amlexanox. It was shown in a previous study that the method of feeding cornflakes with the treatment results in stable and comparable serum levels of amlexanox. The authors measured ~ 1 µM amlexanox approx. 4 h after the last feeding. This concentration of amlexanox inhibits IKKε and TBK1 effectively *in vitro* and doesn't affect other kinases, e.g. IKKα or IKKβ[109,241].

The *in vivo* experiment resulted in a significantly reduced tumor size of the amlexanox treated group, as well as a trend to significantly decreased tumor weight compared with the vehicle-treated group. The calculation of the area under the curve confirmed the results of the time course measurement. Similar results were already published for glioblastoma and prostate tumor[86,104]. These results of amlexanox inhibiting tumor growth in a xenograft model were confirmed for malignant melanoma.

The reduction of tumor size and weight in a xenograft model is a further development from *in vitro* studies. Amlexanox influencing tumor development and growth is now not only shown in an artificial *in vitro* setup but also in an *in vivo* model. The reason for this reduction in tumor size might very well be the inhibition of autophagy, which is urgently needed for melanoma progression, and the inhibition of the NF-κB and the MAPK pathways[244].

Amlexanox was used as a paste for the treatment of aphthous ulcers, allergic rhinitis, and asthma because of its effect on the immune system. Like with every therapeutic, possible allergy is a risk factor, even though no mentioned cases were found by the author. Amlexanox is not contraindicated for the use in children and data for the use in older age groups are still missing. This could be a problem for the possible treatment of melanoma with amlexanox since the incidence of the disease rises with age. Another important factor in the pharmacology of therapeutics is the risk of intake during pregnancy. For amlexanox, pregnancy is not defined as a contraindication, but the data situation is sparse. Additionally, no data is available for the risk of the infant during breastfeeding. More

clinical trials for the case of pregnancy and breastfeeding would be needed if amlexanox should be used as a therapeutic for tumor treatment. Already known side effects of amlexanox paste treatment are diarrhea, burning, or stinging where the paste is applied, nausea, and inflammation of mucous membranes[267]. Some of these less common side effects may only appear when amlexanox is used as a paste, which would be likely for superficial melanoma treatment. Compared to the possible gain the risks are very low. Furthermore, amlexanox was shown not to be a mutagen, and even doses up to 200-times the human daily-dose were not harmful in *in vivo* experiments[268].

Overall, amlexanox seems to be a safe and compatible therapeutic for use in humans. In the past, it was used for the treatment of ulcers, allergic rhinitis, and asthma, but was just moderately effective. New studies repurposed amlexanox and found it to be effective in non-alcoholic fatty liver disease[109], type 2 diabetes[269], and different types of cancer[86,104,244]. This makes amlexanox a promising target for additional therapeutic options for these diseases.

5.4 Summary and outlook of the first part

At this point, the results show that treatment of SK-Mel28 melanoma cells with amlexanox inhibits typical tumor characteristics such as proliferation, migration, and invasion. Amlexanox does not affect the cell cycle nor apoptosis induction. It was shown that treatment with amlexanox inhibits autophagy in SK-Mel cells *in vitro*. Amlexanox also reduces the activation of p65 and p44-42, which inhibits the activation of the NF-κB and MAPK pathways. Influencing these pathways, especially the autophagy pathway, is the most likely reason for the inhibition of tumor characteristics seen in this project. It was able to confirm the inhibition of tumor growth by amlexanox both *in vitro* and *in vivo*.

So far, it is still unclear if the treatment with amlexanox influences the tumor characteristics specifically via IKKε or TBK1, or via the IKKε/TBK1 complex. IKKε is described as an oncogene, but so is TBK1[270,271]. The inhibition of both kinases by amlexanox likely causes the observed effects. To examine if just one of the kinases is responsible for these results a knock-out of each kinase is necessary. Another interesting trial would be a chemotherapy of melanoma cells. It has been described that the chemosensitivity of tumor

cells is mediated via the autophagy mechanism[258,259]. Since melanoma cells depend on autophagy and it was shown that amlexanox treatment inhibits autophagy the cells should react stronger to chemotherapy after amlexanox treatment.

Taken together, this work was able to show that the treatment of malignant melanoma with the already approved drug amlexanox has positive effects on the outcome. Amlexanox inhibits important tumor characteristics, e.g. proliferation and migration, and finally reduces tumor size. Since right now the standard treatment for malignant melanoma is the removal of the tumor and the pharmacological treatments don't act on every type of malignant melanoma the possibility to treat the patient with a safe drug like amlexanox significantly increases the possibilities of malignant melanoma treatment.

5.5 Expression of α-Syn in nociceptive relevant areas of the spinal cord

The IHC stainings of the SC showed that α-Syn is exclusively expressed in the dorsal horn. Co-stainings with CGRP, a marker for lamina I, and IB4, a marker for lamina II, revealed an expression of α-Syn in these laminae, but also further inward. Therefore, the expression of α-Syn in the spinal cord is limited to laminae I – III of the dorsal horn.

The marginal nucleus of the spinal cord (Lamina I), substantia gelatinosa of Rolando (Lamina II), and nucleus proprius of the spinal cord (Lamina III) all exhibit first-order synapses for the transmission of nociceptive stimuli from the periphery via the spinothalamic tract to the thalamus[272,273]. The localization of α-Syn exclusively in this area indicates its role specifically in the nociceptive signal transmitting pathway.

To further identify neuronal subtypes that express α-Syn, it was searched for colocalizations of α-Syn with neuronal population markers. No colocalization with the excitatory marker TH or VGlut1 was seen. But α-Syn was expressed in inhibitory interneurons positive for GAD67 and GABA-A. These findings are contrary to a recently published study by Taguchi et al[274] which describes the expression of α-Syn in VGlut1 positive neurons but saw different expression profiles of GAD positive neurons. This group found colocalizations of α-Syn and GAD in the external plexiform layer of the olfactory bulb, the lateral globus pallidus, medial globus pallidus, and substantia nigra pars

reticulate. No colocalization was found in the cerebral cortex, hippocampus, subthalamic nucleus, and thalamus. The difference between the two studies is, that α-Syn expression in the SC was assessed in this work, while they performed *ex vivo* hippocampal cell culture and then IHC of the brain. Nevertheless, Taguchi et al. show in their study some colocalizations of GAD positive neurons and α-Syn. Their data supports the findings of GAD and α-Syn positive neurons in this work. The IHC of the spinal cord even implies that all GAD positive neurons express α-Syn. This leads to the hypothesis that the expression of α-Syn differs between the spinal cord and the brain, even though both areas are part of the CNS. The fact that α-Syn is expressed in nociceptive relevant areas of the spinal cord and is expressed in inhibitory interneurons strongly suggests that it has some impact on the nociceptive transmission.

5.6 α-Syn influences cold nociception and neuropathic pain, but has no impact on other nociceptive models

The phenotype of SNCA$^{-/-}$ animals is not different from WT. They are viable, fertile, normal in size, weight, and do not display any gross abnormalities. Additionally, no differences were seen in social behavior or motor function. They exhibit a reduction in total striatal dopamine, though[146]. The animals have a 129X1/SvJ background, which is known to develop a progressive hearing loss, starting at three months of age, and which have a 1-3 % chance to develop testicular teratomas[275,276]. Mogil et al. tested different mouse strains for their behavior in a variety of nociceptive tests. They also used the 129 strain and the formalin test, which can now be used to compare the data. The group found that the 129 mouse strain reacts similar to the early phase pain of the formalin test, but significantly less to the late phase pain compared to the often used C57Bl/6 strain[277]. The acute nociceptive models in this work revealed a difference in thermal cold nociception between the genotypes. SNCA$^{-/-}$ animals are significantly less sensitive to this type of noxious stimulus. A similar trend for noxious heat was also seen, but it didn't become significant. Further investigations of the difference in noxious cold behavior revealed a decreased expression of TRPM8 in the paw of SNCA$^{-/-}$ animals. This indicates that the difference in nociceptive cold behavior originates in the TRPM8 expression levels and that it is directly or indirectly influenced by α-Syn expression. The paw was investigated in this

experiment since modulation of cold nociception is likely due to the TRPM8 channel, which is exclusively expressed in primary nociceptive afferents. They start in the peripheral tissue, e.g. the paw, and transmit into the SC.

The TRPM8 channel is widely accepted as the most important sensor for noxious cold[278], and TRPM8$^{-/-}$ mice exhibit severe behavioral deficits in response to cold stimuli[279]. Therefore, the downregulation of this sensor in the paw might contribute to a decrease in cold nociception. The search for α-Syn or SNCA and TRP channels didn't reveal any publications describing this phenomenon. It might be interesting to look further into the subject of how TRP channel expression is regulated by α-Syn. At this point, it can just be said that the TRPM8 receptor is downregulated in the paw of SNCA$^{-/-}$ animals. Additionally, since the whole paw was investigated and no IHC was performed it is still unclear for which exact cell types this result is relevant. TRPV1 and TRPA1 channel expression were also investigated in the paw but no differences were found (data not shown).

After performing the acute nociceptive models, inflammatory nociception with the formalin test and the zymosan A test were investigated. The zymosan A test didn't reveal any differences between the genotypes. In the formalin test a significant difference in nociceptive behavior during the acute phase I, but not during the inflammatory phase II was detectable. Furthermore, α-Syn expression in the spinal cord was upregulated 2 h after formalin injection. This shows an effect of α-Syn on the acute phase I of the formalin test, but not on the inflammatory phase II. The WT animals showed a very different time-course in the formalin test compared to the often used C57Bl/6 mice. If the data is compared to existing publications for this mouse strain the total licking time of the acute phase I is similar between the SNCA$^{-/-}$ animals and the existing data, but the WT animals behaved too strong compared with this data (WT: ~ 145 s; SNCA$^{-/-}$: ~ 75-80 s, Mogil: ~ 74 s). The inflammatory phase II was similar between the genotypes in this work but is strongly increased compared with Mogil's data (WT/SNCA$^{-/-}$: ~ 480 s, Mogil: ~ 140 s)[277]. These results make the comparison with external data hard, and it makes more sense to just compare both genotypes in this work. At this point, a change in glutamate release into the CSF was a possible reason for the different phase I between the genotypes. Glutamate is the most important excitatory transmitter during nociception. A highly

significant increase in glutamate concentration was measured 30 min after formalin injection. But there was no difference in CSF glutamate concentration between the genotypes. This correlates well with the fact, that the animals didn't exhibit a difference in their behavior during phase II of the formalin test but can't be a reason for the difference in phase I. Similar results for the glutamate release were found in another study. The authors describe similar glutamate levels in the brain of different α-Syn mutated mouse strains. The only difference they found was that α-Syn participates in the regulation of the neurotransmitter reserve pool[280].

It is published that α-Syn supports the release of neurotransmitters by promoting cargo discharge and reducing pore closure, while it also inhibits exocytosis when overexpressed[147]. The localization of α-Syn in the nociceptive relevant areas of the spinal cord and the overexpression 2 h after formalin injection leads to the conclusion that it may be upregulated as an answer to the inflammatory stimulus. This upregulation could inhibit the release of different neurotransmitters. Dependent on the neurons which express α-Syn and are therefore affected by the upregulation, this would either lead to an increase or a decrease of the nociceptive signal. It was already shown in this work that α-Syn seems to be expressed in inhibitory interneurons of the SC. Following this hypothesis, the release of the inhibitory neurotransmitter GABA should be reduced after α-Syn upregulation. This hypothesis is confirmed by a study that showed a reduction of GABAergic transmission in α-Syn overexpressing mice[281]. Furthermore, it is observed that the painful behavior of WT animals declines approx. 30-35 min after formalin injection, while the glutamate concentration in the SC shows a 10-fold increase. It is not clear if there is a causality between a possible reduction in GABA release and increased glutamate levels, but it seems that there might be a correlation. One publication supporting a correlation of this regulation investigated whisker-trimmed cats and found a glutamate upregulation and a GABA downregulation in the CNS[282]. Other studies describe similar correlations but propose the regulation of glutamate and GABA receptors as a possible reason (reviewed in [283]).

The context of this network still needs to be investigated. Right now it is known that inhibitory interneurons act as a gate to prevent innocuous stimuli from activating nociceptive pathways within the spinal cord and that disinhibition in the dorsal horn is

accompanied by hypersensitivity to mild stimuli[284,285]. α-Syn was found to be expressed in inhibitory interneurons, which means this part of this complex nociceptive network is influenced. An inhibition of exactly this population of interneurons, and subsequent hypersensitivity, by α-Syn, is unlikely since a decline in painful behavior is seen. Another option for inhibitory interneurons to influence the nociceptive pathway is by modulation of the descending pathway. This pathway modulates the nociceptive transmission by releasing noradrenaline and serotonin[286]. The α-Syn expressing inhibitory interneurons may modulate the descending pathway via inhibition of adrenergic and serotonergic neurons. At this point, inhibition of these interneurons by α-Syn upregulation would lead to disinhibition of these modulating neurons and therefore to a stronger antinociceptive modulation. It is also possible that α-Syn is expressed in other neuronal populations which was not investigated further, though.

After the formalin test, the animals were sacrificed, and a variety of pro-inflammatory markers were investigated in the spinal cord. Overall, a stronger expression of pro-inflammatory markers was seen in $SNCA^{-/-}$ animals compared to WT. Studies in the context of α-Syn and immunity do not provide clear results. It is suspected that the activation of the immune system can lead to α-Syn misfolding, which in the end can lead to the development of synucleinopathies. But studies investigating the effect of α-Syn on the immune system show everything from no effect to strong activation of the immune system by microglial α-Syn uptake. This is reviewed by Lema Tomé[287] and Reish[288]. The results of this work add to this spectrum by showing that the expression of pro-inflammatory markers after immune activation is stronger in mice lacking α-Syn. Since most studies used α-Syn overexpression, mutated α-Syn, or fibrils more studies with an α-Syn knock-out need to be done. For this part of the work, there is the conclusion that there was no change in painful behavior during phase II of the formalin test, even though $SNCA^{-/-}$ animals showed an increased immune response after formalin injection. But since the SC analyzed for the immune response was dissected 2 h after formalin injection and the formalin test only lasted for 45 min this increased inflammatory effect in $SNCA^{-/-}$ mice was not necessarily the case during the test. Further experiments could investigate the immune status approx. 30 min after formalin injection, when the painful response is at its maximum.

The SNI model for neuropathic pain revealed a decreased nociception of SNCA$^{-/-}$ mice. Additionally, α-Syn was downregulated in the spinal cord of WT animals at 28 d after SNI operation. As discussed before in the formalin model, α-Syn may influence the descending antinociceptive pathway. The absence of α-Syn leads to an impaired neurotransmission[147]. The impairment of inhibitory interneurons modulating the descending pathway leads to a disinhibition of this pathway and therefore to increased antinociceptive effects via noradrenergic and serotonergic neurotransmission. This hypothesis also correlates well with the observation, that α-Syn is downregulated in the spinal cord 28 d after the start of the experiment. What undermines this hypothesis is the finding that in genetic models of Parkinson's disease rodents exhibit a loss of inhibitory interneuron activity and a decreased reaction to thermal pain (reviewed in [289]). Since the overexpression, as well as the knockout of α-Syn, impair neuronal transmission these findings support each other. The only difference is that this review also describes hyperactivity of the nociceptive pathway, while a decrease in nociceptive behavior is seen in this work. This could either be due to the additional investigation of neurotoxic Parkinson's disease models, which are based on a completely different method and cannot be included in this hypothesis or due to an activation of the descending pathway, which is not included in most studies.

The mRNA expression in the spinal cord was investigated at different time points after SNI. Sham treated SNCA$^{-/-}$ animals showed an increase of COX-2, IL1B, TNFA, and DOR and a decrease of MMP9. Most publications focus on the effect of pathological α-Syn on the immune system and they all find that the pathological protein activates immune response, which leads to neuroinflammation[290] (reviewed by [288]). It was also found that physiological α-Syn activates the immune response of peripheral blood macrophages[291]. Only one study was found which focuses on the effect of α-Syn knock-out and the immune response in the CNS. They conclude that the knock-out leads to the cell death of dopaminergic neurons, which finally leads to an immune response. The authors didn't find a response after knock-out of α-Syn in glutamatergic neurons[292]. All these studies have an immune response after α-Syn modulation in common. Either due to pathological forms or due to a cascade of events. This is different from what is seen here. The molecular data of Sham-operated animals show that some immune markers, like COX-2 and IL1B, are regulated by the absence of physiological α-Syn. This indicates the presence of a still

unknown mechanism of α-Syn. The upregulation of these pro-inflammatory and pro-nociceptive markers implies that SNCA$^{-/-}$ animals should show increased nociceptive behavior, which they don't. It could be that a reason for this is the downregulation of these markers at a different time point after SNI. Since the upregulation is the baseline for the SNCA$^{-/-}$ animals, the new "normal", only the downregulation influences the nociceptive behavior during the neuropathic pain model. Interestingly, the analgesic marker DOR and FAAH, which produces endocannabinoids, are upregulated at baseline measurements and are downregulated during the SNI model. It is not clear how these regulations influence the nociception, and if they are at all translated into protein levels, but they act as a starting point for further mechanistic studies.

Old (< 6 months) animals were also used for motor tests, and tests of acute and neuropathic nociception. The high inter-individual variance in the motor test was not due to animals not being able to do this test, but due to them being intelligent enough to just end the test by jumping down from the rod. Their motor behavior was intact. The old animals didn't show significant differences in the models for acute nociception. A reason for the non-existing significance might be the low number (n = 3) of test subjects. A trend of a decreased cold nociception is seen in old SNCA$^{-/-}$ animals, which might become significant after testing more animals. Furthermore, the neuropathic pain model also didn't reveal significant differences. A trend to decreased nociception in SNCA$^{-/-}$ animals seen on day 7, but it didn't become significant probably due to the low n-number. The hypothesis behind these experiments was that α-Syn may act neuroprotective and that the differences seen in previous experiments are due to neuronal cell death in SNCA$^{-/-}$ animals. Therefore, the older animals were expected to show an even stronger effect than the younger animals. It was shown that α-Syn has a protective effect on the mitochondria and that α-Syn knock-out leads to a decrease in cellular respiration and fragmented mitochondria[293]. These effects automatically lead to less robust cells and support the hypothesis. Additionally, α-Syn is described to inhibit apoptosis in response to pro-apoptotic stimuli (reviewed in [144]). Still, the hypothesis for this part of the project was not confirmed. Likely, the effects seen in the nociceptive models are not due to neuronal cell death, but due to a regulatory effect of α-Syn on neuronal transmission.

5.7 Tumor growth may be inhibited in the absence of α-Syn

The connection of malignant melanoma and the role of α-Syn in the nociceptive pathway was investigated with the nociceptive melanoma model. Mouse melanoma cells were used to create a local tumor in one of the hind paws. The tumor leads to increased pain sensitivity due to damage to nerves and inflammation in the affected areas. As expected, increasing nociceptive responses were observed in the WT group. SNCA$^{-/-}$ mice started the same, but from day 14 mechanical hypersensitivity was lower than in WT animals. The paw volume of SNCA$^{-/-}$ animals tends to be smaller, which indicates reduced tumor growth.

High inter-individual differences prevented a significant result. However, these results indicate that decreased nociception is most likely not due to an effect of α-Syn on the nociceptive system, but rather due to reduced tumor growth.

Additionally, molecular changes were investigated similar to the SNI model, except that the spinal cords of WT and SNCA$^{-/-}$ animals were investigated 21 d after B16 inoculation. Some parallels to the SNI spinal cords are seen. COX-2 and Akt-1 are downregulated in SNCA$^{-/-}$ animals after experiencing pain. A trend to a downregulation is seen in TNFA and DOR mRNA. These regulations were significant in SNI treated SNCA$^{-/-}$ animals. MMP9 shows an opposed regulation to the SNI model. Since there is barely any publication concerning the topic of CNS immune regulation via physiological α-Syn it is not easy to compare these data with existing ones. The only thing found in the study showing that dopaminergic cell death leads to the immune response, and not α-Syn knock-out[292]. What is known is that pro-nociceptive markers like COX-2 and TNFA should be up- and not downregulated after nociceptive tests[294,295]. This regulation in SNCA$^{-/-}$ animals indicates an additional reason for the reduced nociceptive behavior at the end of the B16 melanoma model. Some of the experiments need more samples to confirm these results, but like the analysis of the SNI treated spinal cords some starting points for the mechanistic involved are found.

Different studies already established a connection between α-Syn and tumor growth. It was found that α-Syn drives the progression of meningioma via the Akt/mTOR pathway. In this study, the depletion of α-Syn significantly decreased tumor cell proliferation and colony formation[246]. Another study by Israeli et al. also used murine B16 cells, as well as

two other tumor cell lines. The result was that overexpression of α-Syn led to an acceleration of proliferation and an increase of tumorigenesis[296]. A mechanism was not found at this point, but this work can confirm the results of this group by showing that α-Syn knockout leads to impaired tumor growth. Interestingly, a study by Shekoohi et al. showed that SNCA KO in SK-Mel28 cells leads to a significantly reduced tumor growth in a xenograft model[297]. They conclude their study with the idea that α-Syn may be a potential target for the therapy of malignant melanoma.

5.8 Summary and outlook of the second part

The second part of this work is focusing on a possible effect of α-Syn on the nociceptive system. It was shown that α-Syn indeed plays a role in acute and neuropathic nociception, as well as in tumor growth. Additionally, α-Syn has some impact on inflammatory mechanisms.

α-Syn localization was investigated in the spinal cord and it was found expressed in the dorsal horn approx. in laminae I-III. The IHC stainings also revealed colocalization with markers for inhibitory interneurons, but not with markers for excitatory neurons. The results show that knockout of α-Syn leads to an inhibition of noxious cold nociception, associated with a downregulation of the cold-sensing TRPM8 channel in the paw. Furthermore, α-Syn knockout led to a decreased acute nociceptive response to chemical stimulation as seen in phase I of the formalin test. Except for that, $SNCA^{-/-}$ animals didn't show differences in motor function and other models of acute nociception in comparison to wild-type mice. In models for inflammatory nociception, there was no difference in the nociceptive behavior between WT and KO mice although a-Syn was upregulated in the spinal cord after inflammatory stimulation and pro-inflammatory genes were altered.

In the SNI model for neuropathic pain, $SNCA^{-/-}$ animals showed less nociception and a decrease of α-Syn in the spinal cord, which became significant 28 d after SNI induction. In a model for tumor-associated pain, $SNCA^{-/-}$ animals revealed decreased nociception and inhibition of tumor growth. A variety of studies support these findings, but this work shows for the first time that the knockdown of α-Syn has such effects on nociceptive behavior. The resulting hypothesis for this is a modulation of the descending

antinociceptive pathway, where α-Syn seems to be expressed. α-Syn may regulate the neurotransmission of inhibitory interneurons, which inhibit the descending antinociceptive pathway. Additional functions of α-Syn may be the tissue-specific modulation of TRPM8 expression and a positive effect on tumor growth. Furthermore, mRNA expression analysis in the spinal cord of a variety of inflammatory and nociceptive genes revealed a regulation in $SNCA^{-/-}$ animals with and without nociceptive treatment. The investigation of the regulation of these genes might lead to a mechanistic conclusion on α-Syn's impact on the nociceptive and tumor-related system.

Further experiments to confirm the expression of α-Syn in this pathway should be done. Either optogenetic approaches to be able to investigate this pathway or tissue-specific inducible knock-outs of α-Syn. Additionally, pharmacological or RNA inhibition of α-Syn could be done to further confirm these findings. Electrophysiological recordings of specific neurons would also be a great approach to see the effect of α-Syn in this particular neuronal subset.

6. Summary

The goal of this work was to further increase the knowledge of the role of IKKε, TBK1, and α-Syn in the pathogenesis of melanoma and pain. It was shown that inhibition of IKKε and TBK1 with the small molecule inhibitor amlexanox inhibits tumor growth, proliferation, migration, invasion, and autophagy *in vitro* and *in vivo*. One reason for the effect on tumor characteristics might be the inhibition of autophagy seen after amlexanox treatment. Malignant melanoma cells become dependent on autophagy after tumor establishment for further progression. Therefore, the inhibition of this process can modulate tumor characteristics like proliferation and migration. An additional reason might be the decrease in p65 and p44/42 activation after amlexanox treatment. These proteins of the NF-κB and MAPK pathway strongly influence proliferation, migration, and invasion of cells. Further experiments revealed that the cell cycle and the relevant proteins Cyclin D1 and p53 are not affected by amlexanox treatment. The *in vivo* xenograft model confirmed that amlexanox treatment also influences tumor growth *in vivo*. Amlexanox administration resulted in a significantly smaller tumor compared to vehicle-treated mice. In addition to cell culture and mouse experiments, tissue material from melanoma patients was assessed. Samples of healthy skin, naevi, and melanoma metastases were investigated for IKKε and TBK1 expression. Both kinases were upregulated in the metastases compared to healthy tissue. In primary melanoma, IKKε and TBK1 were expressed in tumor cells as well as immune cells further pointing to their regulatory role. Expression of IKKε was not seen in non-melanoma tissue, and expression of TBK1 was just seen in the epidermis beside of the melanoma cells.

Concerning the role of α-Syn in nociception, it was found that α-Syn promotes TRPM8 expression in the paw and cold nociception. Additionally, it seems to have a regulatory effect on neuropathic pain, and knock-out of α-Syn decreases this nociceptive subtype. $SNCA^{-/-}$ animals showed decreased nociceptive behavior in the SNI model of neuropathic pain. Western Blot analysis of the spinal cord revealed α-Syn upregulation 2 h after formalin injection and α-Syn downregulation 28 d after SNI induction. These are most likely nociceptive relevant regulatory mechanisms. IHC stainings of the spinal cord revealed α-Syn expression in laminae I-III of the dorsal horn, specifically in GABAergic interneurons. No expression of α-Syn in excitatory neurons was seen. The hypothesis is

that α-Syn is expressed in inhibitory interneurons of the descending nociceptive pathway. Activation of these neurons, which is supported by α-Syn expression, leads to a decreased activity of this antinociceptive pathway. The inhibition or knock-out of α-Syn leads to disinhibition and stronger antinociceptive effects of the descending pathway. Therefore, the results suggest that α-Syn has an impact on nociceptive transmission. The knock-out of α-Syn decreased the nociceptive behavior in different pain models without manipulation of the physiological functions of the animals.

Furthermore, α-Syn may promote the growth of murine melanoma. $SNCA^{-/-}$ mice exhibited a trend to a decreased tumor growth and significantly decreased tumor-associated nociception after the inoculation of murine B16 melanoma cells into the paw. The decreased nociception in this model is likely due to the effects of α-Syn on the nociceptive system, since there was no significant difference of tumor size between the genotypes. A variety of studies already described the influence of α-Syn on tumor growth. These results were not entirely confirmed by this work.

mRNA expression of nociceptive and inflammatory genes was performed in the spinal cord via qPCR after animals underwent the SNI model for neuropathic pain, the melanoma model for tumor-associated pain, and the formalin model for inflammatory pain. There were some changes in the baseline level of $SNCA^{-/-}$ animals compared to WT. Briefly, some pro-inflammatory and antinociceptive genes, e.g. COX-2, TNFA, and DOR were upregulated. After performing the nociceptive tests all these genes were downregulated at different time-points. This implies the regulation of different inflammatory and nociceptive pathways by α-Syn.

This work concludes that IKKε and TBK1 are upregulated in human malignant melanoma, the inhibition of these kinases by amlexanox inhibits melanoma progression, and that α-Syn has pro-nociceptive and possible oncogenic characteristics.

7. References

1. Markovic SN, Erickson LA, Rao RD, et al. Malignant Melanoma in the 21st Century, Part 1: Epidemiology, Risk Factors, Screening, Prevention, and Diagnosis. *Mayo Clinic Proceedings*. 2007;82(3):364-380.
2. Garbe C, Schadendorf D, Stolz W, et al. Short German guidelines: Malignant melanoma. *Journal der Deutschen Dermatologischen Gesellschaft*. 2008;6:S9-S14.
3. Mahendraraj K, Sidhu K, Lau CSM, McRoy GJ, Chamberlain RS, Smith FO. Malignant Melanoma in African-Americans: A Population-Based Clinical Outcomes Study Involving 1106 African-American Patients from the Surveillance, Epidemiology, and End Result (SEER) Database (1988-2011). *Medicine*. 2017;96(15):e6258.
4. Braun-Falco O, Burgdorf WHC, Landthaler M. *Dermatologie und Venerologie.* 5th ed. Dordrecht: Springer; 2005.
5. Garbe C, Leiter U. Melanoma epidemiology and trends. *Clinics in Dermatology*. 2009;27(1):3-9.
6. Nikolaou V, Stratigos AJ. Emerging trends in the epidemiology of melanoma. *Br J Dermatol*. 2014;170(1):11-19.
7. Guy GP, JR, Thomas CC, Thompson T, Watson M, Massetti GM, Richardson LC. Vital signs: Melanoma incidence and mortality trends and projections - United States, 1982-2030. *MMWR. Morbidity and mortality weekly report*. 2015;64(21):591-596.
8. Lens MB, Dawes M. Global perspectives of contemporary epidemiological trends of cutaneous malignant melanoma. *Br J Dermatol*. 2004;150(2):179-185.
9. Siegel RL, Miller KD, Jemal A. Cancer statistics, 2019. *CA: a cancer journal for clinicians*. 2019;69(1):7-34.
10. Erdmann F, Lortet-Tieulent J, Schüz J, et al. International trends in the incidence of malignant melanoma 1953-2008-are recent generations at higher or lower risk? *Int. J. Cancer*. 2013;132(2):385-400.
11. Cummins DL, Cummins JM, Pantle H, Silverman MA, Leonard AL, Chanmugam A. Cutaneous Malignant Melanoma. *Mayo Clinic Proceedings*. 2006;81(4):500-507.
12. Sandru A, Voinea S, Panaitescu E, Blidaru A. Survival rates of patients with metastatic malignant melanoma. *J Med Life*. 2014;7(4):572-576. https://pubmed.ncbi.nlm.nih.gov/25713625.

13. Moran B, Silva R, Perry AS, Gallagher WM. Epigenetics of malignant melanoma. *Seminars in cancer biology*. 2018;51:80-88.
14. Chin L, Merlino G, DePinho RA. Malignant melanoma: Modern black plague and genetic black box. *Genes & Development*. 1998;12(22):3467-3481.
15. Chang AE, Karnell LH, Menck HR. The National Cancer Data Base report on cutaneous and noncutaneous melanoma. *Cancer*. 1998;83(8):1664-1678.
16. Boer FL, Eikelder MLG ten, Kapiteijn EH, Creutzberg CL, Galaal K, van Poelgeest MIE. Vulvar malignant melanoma: Pathogenesis, clinical behaviour and management: Review of the literature. *Cancer treatment reviews*. 2019;73:91-103.
17. Watson M, Geller AC, Tucker MA, Guy GP, JR, Weinstock MA. Melanoma burden and recent trends among non-Hispanic whites aged 15-49years, United States. *Preventive medicine*. 2016;91:294-298.
18. Osterlind A, Hou-Jensen K, Møller Jensen O. Incidence of cutaneous malignant melanoma in Denmark 1978-1982. Anatomic site distribution, histologic types, and comparison with non-melanoma skin cancer. *British journal of cancer*. 1988;58(3):385-391.
19. Green A, MacLennan R, Youl P, Martin N. Site distribution of cutaneous melanoma in Queensland. *Int. J. Cancer*. 1993;53(2):232-236.
20. Breslow A. Thickness, Cross-Sectional Areas and Depth of Invasion in the Prognosis of Cutaneous Melanoma. *Annals of Surgery*. 1970;172(5):902-908.
21. Haass NK, Smalley KSM, Li L, Herlyn M. Adhesion, migration and communication in melanocytes and melanoma. *Pigment Cell Research*. 2005;18(3):150-159.
22. Sample A, He Y-Y. Mechanisms and prevention of UV-induced melanoma. *Photodermatology, photoimmunology & photomedicine*. 2018;34(1):13-24.
23. Marks R. Epidemiology of melanoma. Clinical dermatology Review article. *Clin Exp Dermatol*. 2000;25(6):459-463.
24. Obrador E, Liu-Smith F, Dellinger RW, Salvador R, Meyskens FL, Estrela JM. Oxidative stress and antioxidants in the pathophysiology of malignant melanoma. *Biological chemistry*. 2019;400(5):589-612.
25. Chen ST, Geller AC, Tsao H. Update on the Epidemiology of Melanoma. *Curr Derm Rep*. 2013;2(1):24-34.

26. Maldonado JL, Fridlyand J, Patel H, et al. Determinants of BRAF mutations in primary melanomas. *JNCI Journal of the National Cancer Institute*. 2003;95(24):1878-1890.
27. Gear H, Williams H, Kemp EG, Roberts F. BRAF mutations in conjunctival melanoma. *Investigative ophthalmology & visual science*. 2004;45(8):2484-2488.
28. Cheng L, Lopez-Beltran A, Massari F, MacLennan GT, Montironi R. Molecular testing for BRAF mutations to inform melanoma treatment decisions: A move toward precision medicine. *Modern pathology : an official journal of the United States and Canadian Academy of Pathology, Inc*. 2018;31(1):24-38.
29. Box NF, Vukmer TO, Terzian T. Targeting p53 in melanoma. *Pigment cell & melanoma research*. 2014;27(1):8-10.
30. Shi S-W, Li B, Dong Y, et al. In Vitro and Clinical Studies of Gene Therapy with Recombinant Human Adenovirus-p53 Injection for Malignant Melanoma. *Human gene therapy. Clinical development*. 2019;30(1):7-18.
31. Hayward NK, Wilmott JS, Waddell N, et al. Whole-genome landscapes of major melanoma subtypes. *Nature*. 2017;545(7653):175-180.
32. Goldstein AM, Chan M, Harland M, et al. Features associated with germline CDKN2A mutations: A GenoMEL study of melanoma-prone families from three continents. *Journal of medical genetics*. 2007;44(2):99-106.
33. Bishop DT, Demenais F, Iles MM, et al. Genome-wide association study identifies three loci associated with melanoma risk. *Nat Genet*. 2009;41(8):920-925.
34. Duffy DL, Iles MM, Glass D, et al. IRF4 Variants Have Age-Specific Effects on Nevus Count and Predispose to Melanoma. *The American Journal of Human Genetics*. 2010;87(1):6-16.
35. MacGregor S, Montgomery GW, Liu JZ, et al. Genome-wide association study identifies a new melanoma susceptibility locus at 1q21.3. *Nat Genet*. 2011;43(11):1114-1118.
36. Barrett JH, Iles MM, Harland M, et al. Genome-wide association study identifies three new melanoma susceptibility loci. *Nat Genet*. 2011;43(11):1108-1113.
37. Quesada V, Conde L, Villamor N, et al. Exome sequencing identifies recurrent mutations of the splicing factor SF3B1 gene in chronic lymphocytic leukemia. *Nat Genet*. 2011;44(1):47-52.

38. The Cancer Genome Atlas Network. Comprehensive molecular portraits of human breast tumours. *Nature*. 2012;490(7418):61-70.
39. Beroukhim K, Pourang A, Eisen DB. Risk of second primary cutaneous and noncutaneous melanoma after cutaneous melanoma diagnosis: A population-based study. *Journal of the American Academy of Dermatology*. 2020;82(3):683-689.
40. Paszkowska-Szczur K, Scott RJ, Serrano-Fernandez P, et al. Xeroderma pigmentosum genes and melanoma risk. *Int. J. Cancer*. 2013;133(5):1094-1100.
41. Dalvin LA, Damento GM, Yawn BP, Abbott BA, Hodge DO, Pulido JS. Parkinson Disease and Melanoma: Confirming and Reexamining an Association. *Mayo Clinic Proceedings*. 2017;92(7):1070-1079.
42. Olsen JH, Friis S, Frederiksen K, McLaughlin JK, Mellemkjaer L, Møller H. Atypical cancer pattern in patients with Parkinson's disease. *British journal of cancer*. 2005;92(1):201-205.
43. Kobayashi S. Choose Delicately and Reuse Adequately: The Newly Revealed Process of Autophagy. *Biological & pharmaceutical bulletin*. 2015;38(8):1098-1103.
44. Dökümcü K, Simonian M, Farahani RM. miR4673 improves fitness profile of neoplastic cells by induction of autophagy. *Cell death & disease*. 2018;9(11):1068.
45. Paglin S, Hollister T, Delohery T, et al. A novel response of cancer cells to radiation involves autophagy and formation of acidic vesicles. *Cancer research*. 2001;61(2):439-444.
46. Qu X, Yu J, Bhagat G, et al. Promotion of tumorigenesis by heterozygous disruption of the beclin 1 autophagy gene. *J. Clin. Invest.* 2003;112(12):1809-1820.
47. Ndoye A, Weeraratna AT. Autophagy- An emerging target for melanoma therapy. *F1000Res*. 2016;5:1888.
48. Lazova R, Klump V, Pawelek J. Autophagy in cutaneous malignant melanoma. *Journal of cutaneous pathology*. 2010;37(2):256-268.
49. Atkinson V. Recent advances in malignant melanoma. *Internal medicine journal*. 2017;47(10):1114-1121.
50. Karin M, Greten FR. NF-κB: Linking inflammation and immunity to cancer development and progression. *Nat Rev Immunol*. 2005;5(10):749-759.
51. Perkins ND. Integrating cell-signalling pathways with NF-κB and IKK function. *Nat Rev Mol Cell Biol*. 2007;8(1):49-62.

52. Karin M, Yamamoto Y, Wang QM. The IKK NF-kappa B system: A treasure trove for drug development. *Nature reviews. Drug discovery*. 2004;3(1):17-26.
53. Yamamoto Y, Gaynor RB. IkappaB kinases: Key regulators of the NF-kappaB pathway. *Trends in biochemical sciences*. 2004;29(2):72-79.
54. Karin M, Ben-Neriah Y. Phosphorylation meets ubiquitination: The control of NF-kappaB activity. *Annual review of immunology*. 2000;18:621-663.
55. Plaksin D, Baeuerle PA, Eisenbach L. KBF1 (p50 NF-kappa B homodimer) acts as a repressor of H-2Kb gene expression in metastatic tumor cells. *The Journal of experimental medicine*. 1993;177(6):1651-1662.
56. Xia L, Tan S, Zhou Y, et al. Role of the NFκB-signaling pathway in cancer. *OncoTargets and therapy*. 2018;11:2063-2073.
57. Shimada T, Kawai T, Kiyoshi T, et al. IKK-i, a novel lipopolysaccharide-inducible kinase that is related to IkB kinases. *International Immunology*. 1999;11(8):1357-1362.
58. Peters RT, Maniatis T. A new family of IKK-related kinases may function as IκB kinase kinases. *Biochimica et Biophysica Acta (BBA) - Reviews on Cancer*. 2001;1471(2):M57-M62.
59. Kravchenko VV, Mathison JC, Schwamborn K, Mercurio F, Ulevitch RJ. IKKi/IKKepsilon plays a key role in integrating signals induced by pro-inflammatory stimuli. *The Journal of biological chemistry*. 2003;278(29):26612-26619.
60. Niederberger E, Möser CV, Kynast KL, Geisslinger G. The Non-Canonical Ikb Kinases IKKe and TBK1 as Potential Targets for the Development of Novel Therapeutic Drugs. *Current molecular medicine*. 2013;13:1-9.
61. Chau T-L, Gioia R, Gatot J-S, et al. Are the IKKs and IKK-related kinases TBK1 and IKK-ε similarly activated? *Trends in biochemical sciences*. 2008;33(4):171-180.
62. Verhelst K, Verstrepen L, Carpentier I, Beyaert R. IκB kinase ε (IKKε): A therapeutic target in inflammation and cancer. *Biochemical pharmacology*. 2013;85(7):873-880.
63. Tojima Y, Fujimoto A, Delhase M, et al. NAK is an IkB kinase-activating kinase. *Nature*. 2000;404:778-782.
64. Fitzgerald KA, McWhirter SM, Faia KL, et al. IKKepsilon and TBK1 are essential components of the IRF3 signaling pathway. *Nature immunology*. 2003;4(5):491-496.
65. Peters RT, Liao S-M, Maniatis T. IKKe Is Part of a Novel PMA-Inducible IkB Kinase Complex. *Melcular Cell*. 2000;(5):513-522.

66. Souri Z, Wierenga APA, van Weeghel C, et al. Loss of BAP1 Is Associated with Upregulation of the NFkB Pathway and Increased HLA Class I Expression in Uveal Melanoma. *Cancers*. 2019;11(8).
67. Lugović-Mihić L, Ćesić D, Vuković P, Novak Bilić G, Šitum M, Špoljar S. Melanoma Development: Current Knowledge on Melanoma Pathogenesis. *Acta dermatovenerologica Croatica : ADC*. 2019;27(3):163-168.
68. Buss H, Dörrie A, Schmitz ML, Hoffmann E, Resch K, Kracht M. Constitutive and interleukin-1-inducible phosphorylation of p65 NF-{kappa}B at serine 536 is mediated by multiple protein kinases including IkB kinase (IKK)-a, IKKb, IKKe, TRAF family member-associated (TANK)-binding kinase 1 (TBK1), and an unknown kinase and couples p65 to TATA-binding protein-associated factor II31-mediated interleukin-8 transcription. *The Journal of biological chemistry*. 2004;279(53):55633-55643.
69. Adli M, Baldwin AS. IKK-i/IKKε Controls Constitutive, Cancer Cell-associated NF-κB Activity via Regulation of Ser-536 p65/RelA Phosphorylation. *The Journal of biological chemistry*. 2006;281(37):26976-26984.
70. Wortzel I, Seger R. The ERK Cascade: Distinct Functions within Various Subcellular Organelles. *Genes Cancer*. 2011;2(3):195-209. https://pubmed.ncbi.nlm.nih.gov/21779493.
71. Clément J-F, Meloche S, Servant MJ. The IKK-related kinases: From innate immunity to oncogenesis. *Cell Res*. 2008;18(9):889-899.
72. Roskoski R, JR. Targeting ERK1/2 protein-serine/threonine kinases in human cancers. *Pharmacological research*. 2019;142:151-168.
73. Péant B, Diallo J-S, Lessard L, et al. Regulation of IkappaB kinase epsilon expression by the androgen receptor and the nuclear factor-kappaB transcription factor in prostate cancer. *Molecular cancer research*. 2007;5(1):87-94.
74. Mattioli I, Geng H, Sebald A, et al. Inducible phosphorylation of NF-kappa B p65 at serine 468 by T cell costimulation is mediated by IKK epsilon. *The Journal of biological chemistry*. 2006;281(10):6175-6183.
75. Krayem M, Sabbah M, Najem A, et al. The Benefit of Reactivating p53 under MAPK Inhibition on the Efficacy of Radiotherapy in Melanoma. *Cancers*. 2019;11(8).
76. Harris J, Olière S, Sharma S, et al. Nuclear Accumulation of cRel following C-Terminal phosphorylation by TBK1/IKKε. *J Immunol*. 2006;177(4):2527-2535.

77. Sweeney SE, Mo L, Firestein GS. Antiviral gene expression in rheumatoid arthritis: Role of IKKε and interferon regulatory factor 3. *Arthritis Rheum*. 2007;56(3):743-752.
78. Wei C-Y, Wang L, Zhu M-X, et al. TRIM44 activates the AKT/mTOR signal pathway to induce melanoma progression by stabilizing TLR4. *Journal of experimental & clinical cancer research : CR*. 2019;38(1):137.
79. Liu Y, Kang X, Niu G, et al. Shikonin induces apoptosis and prosurvival autophagy in human melanoma A375 cells via ROS-mediated ER stress and p38 pathways. *Artificial cells, nanomedicine, and biotechnology*. 2019;47(1):626-635.
80. Wenzina J, Holzner S, Puujalka E, et al. Inhibition of p38/MK2 Signaling Prevents Vascular Invasion of Melanoma. *The Journal of investigative dermatology*. 2020;140(4):878-890.e5.
81. Pomerantz JL. NF-kappa B activation by a signaling complex containing TRAF2, TANK and TBK1, a novel IKK-related kinase. *The EMBO Journal*. 1999;18(23):6694-6704.
82. Takahashi-Yanaga F, Sasaguri T. GSK-3β regulates cyclin D1 expression: A new target for chemotherapy. *Cellular Signalling*. 2008;20(4):581-589.
83. Corr M, Boyle DL, Ronacher L, Flores N, Firestein GS. Synergistic benefit in inflammatory arthritis by targeting IκB kinase ϵ and interferon β. *Ann Rheum Dis*. 2009;68(2):257-263.
84. Chien Y, Kim S, Bumeister R, et al. RalB GTPase-Mediated Activation of the IκB Family Kinase TBK1 Couples Innate Immune Signaling to Tumor Cell Survival. *Cell*. 2006;127(1):157-170.
85. Yang J, Richmond A. Constitutive IkB Kinase Activity Correlates with Nuclear Factor-kB Activation in Human Melanoma Cells. *Cancer research*. 2001;61:4901-4909.
86. Cheng C, Ji Z, Sheng Y, et al. Aphthous ulcer drug inhibits prostate tumor metastasis by targeting IKKε/TBK1/NF-κB signaling. *Theranostics*. 2018;8(17):4633-4648.
87. Leonardi M, Perna E, Tronnolone S, Colecchia D, Chiariello M. Activated kinase screening identifies the IKBKE oncogene as a positive regulator of autophagy. *Autophagy*. 2019;15(2):312-326.
88. Yin M, Wang X, Lu J. Advances in IKBKE as a potential target for cancer therapy. *Cancer Med*. 2019;9(1):247-258.

89. Xie X, Zhang D, Zhao B, et al. IkappaB kinase epsilon and TANK-binding kinase 1 activate AKT by direct phosphorylation. *Proceedings of the National Academy of Sciences of the United States of America*. 2011;108(16):6474-6479.
90. Boehm JS, Zhao JJ, Yao J, et al. Integrative genomic approaches identify IKBKE as a breast cancer oncogene. *Cell*. 2007;129(6):1065-1079.
91. Cheng A, Guo J, Henderson-Jackson E, Kim D, Malafa M, Coppola D. IκB Kinase ε Expression in Pancreatic Ductal Adenocarcinoma. *Am J Clin Pathol*. 2011;136(1):60-66.
92. Qin B, Cheng K. Silencing of the IKKε gene by siRNA inhibits invasiveness and growth of breast cancer cells. *Breast cancer research*. 2010;12(5):1-15.
93. Rajurkar M, Jesus-Monge WE de, Driscoll DR, et al. The activity of Gli transcription factors is essential for Kras-induced pancreatic tumorigenesis. *Proceedings of the National Academy of Sciences*. 2012;109(17):E1038-E1047.
94. Göktuna Sİ. IKBKE inhibits TSC1 to activate the mTOR/S6K pathway for oncogenic transformation. *Turkish journal of biology = Turk biyoloji dergisi*. 2018;42(4):268-278.
95. Yang W, Qu Y, Tan B, et al. Prognostic significance of preoperative IKBKE expression in esophageal squamous cell carcinoma. *OncoTargets and therapy*. 2018;11:1305-1314.
96. Wang X, Teng F, Lu J, Mu D, Zhang J, Yu J. Expression and prognostic role of IKBKE and TBK1 in stage I non-small cell lung cancer. *Cancer management and research*. 2019;11:6593-6602.
97. Hutti JE, Shen RR, Abbott DW, et al. Phosphorylation of the Tumor Suppressor CYLD by the Breast Cancer Oncogene IKKε Promotes Cell Transformation. *Molecular cell*. 2009;34(4):461-472.
98. Servant MJ, Clément JF, Meloche S. The IKK-related kinases, unsuspected culprits in oncogenesis? *Atlas of Genetics and Cytogenetics in Oncology and Haematology*. 2011;(2).
99. Barbie DA, Tamayo P, Boehm JS, et al. Systematic RNA interference reveals that oncogenic KRAS-driven cancers require TBK1. *Nature*. 2009;462(7269):108-112.
100. Kumar S, Gu Y, Abudu YP, et al. Phosphorylation of Syntaxin 17 by TBK1 Controls Autophagy Initiation. *Developmental cell*. 2019;49(1):130-144.e6.

101. Ou Y-H, Torres M, Ram R, et al. TBK1 Directly Engages Akt/PKB Survival Signaling to Support Oncogenic Transformation. *Molecular cell*. 2011;41(4):458-470.

102. Korherr C, Gille H, Schafer R, et al. Identification of proangiogenic genes and pathways by high-throughput functional genomics: TBK1 and the IRF3 pathway. *Proceedings of the National Academy of Sciences*. 2006;103(11):4240-4245.

103. Zhang Z, Lu J, Guo G, et al. IKBKE promotes glioblastoma progression by establishing the regulatory feedback loop of IKBKE/YAP1/miR-Let-7b/i. *Tumour biology*. 2017;39(7):1-10.

104. Liu Y, Lu J, Zhang Z, et al. Amlexanox, a selective inhibitor of IKBKE, generates anti-tumoral effects by disrupting the Hippo pathway in human glioblastoma cell lines. *Cell death & disease*. 2017;8(8):1-12.

105. Vu HL, Aplin AE. Targeting TBK1 Inhibits Migration and Resistance to MEK Inhibitors in Mutant NRAS Melanoma. *Molecular cancer research : MCR*. 2014;12(10):1509-1519.

106. Möser CV, Meissner M, Laarmann K, et al. The protein kinase IKKepsilon contributes to tumour growth and tumour pain in a melanoma model. *Biochemical pharmacology*. 2016;103:64-73.

107. Zhang J, Feng H, Zhao J, et al. IκB Kinase ε Is an NFATc1 Kinase that Inhibits T Cell Immune Response. *Cell reports*. 2016;16(2):405-418.

108. Eskiocak B, McMillan EA, Mendiratta S, et al. Biomarker Accessible and Chemically Addressable Mechanistic Subtypes of BRAF Melanoma. *Cancer discovery*. 2017;7(8):832-851.

109. Reilly SM, Chiang S-H, Decker SJ, et al. An inhibitor of the protein kinases TBK1 and IKK-ε improves obesity-related metabolic dysfunctions in mice. *Nat Med*. 2013;19(3):313-321.

110. Makino H, Saijo T, Ashida Y, Kuriki H, Maki Y. Mechanism of Action of an Antiallergic Agent, Amlexanox (AA-673), in Inhibiting Histamine Release from Mast Cells. *Int Arch Allergy Immunol*. 2004;82(1):66-71.

111. Bell J. Amlexanox for the Treatment of Recurrent Aphthous Ulcers. *Clinical Drug Investigation*. 2005;25(9):555-566.

112. Atanasova VS, Jiang Q, Prisco M, et al. Amlexanox Enhances Premature Termination Codon Read-Through in COL7A1 and Expression of Full Length Type VII

Collagen: Potential Therapy for Recessive Dystrophic Epidermolysis Bullosa. *The Journal of investigative dermatology*. 2017;137(9):1842-1849.

113. Banning A, Schiff M, Tikkanen R. Amlexanox provides a potential therapy for nonsense mutations in the lysosomal storage disorder Aspartylglucosaminuria. *Biochimica et biophysica acta. Molecular basis of disease*. 2018;1864(3):668-675.
114. He Q, Xia X, Yao K, et al. Amlexanox reversed non-alcoholic fatty liver disease through IKKε inhibition of hepatic stellate cell. *Life sciences*. 2019;239:117010.
115. Tamai H, Yamaguchi H, Miyake K, et al. Amlexanox Downregulates S100A6 to Sensitize KMT2A/AFF1-Positive Acute Lymphoblastic Leukemia to TNFα Treatment. *Cancer research*. 2017;77(16):4426-4433.
116. Zhang Y, Guan H, Li J, Fang Z, Chen W, Li F. Amlexanox Suppresses Osteoclastogenesis and Prevents Ovariectomy-Induced Bone Loss. *Sci Rep*. 2015;5(1):337.
117. Möser CV, Kynast K, Baatz K, et al. The protein kinase IKKε is a potential target for the treatment of inflammatory hyperalgesia. *Journal of immunology*. 2011;187(5):2617-2625.
118. A Loudon J. Preventing and Correcting Communicable and Non-Communicable Chronic Disease via Amlexanox – Dual 'No-Nonsense' and Inflammatory Axis Targeting. *J Bioanal Biomed*. 2013;05(05).
119. Homan K, Wu E, Cannavo A, Koch W, Tesmer J. Identification and Characterization of Amlexanox as a G Protein-Coupled Receptor Kinase 5 Inhibitor. *Molecules*. 2014;19(10):16937-16949.
120. Balkwill F, Mantovani A. Cancer and Inflammation: Implications for Pharmacology and Therapeutics. *Clin Pharmacol Ther*. 2010;87(4):401-406.
121. Ben-Neriah Y, Karin M. Inflammation meets cancer, with NF-κB as the matchmaker. *Nature immunology*. 2011;12(8):715-723.
122. Tofaris GK, Spillantini MG. Physiological and pathological properties of alpha-synuclein. *Cellular and molecular life sciences*. 2007;64(17):2194-2201.
123. Jensen PH, Nielsen MS, Jakes R, Dotti CG, Goedert M. Binding of a-Synuclein to Brain Vesicles Is Abolished by Familial Parkinson's Disease Mutation. *The Journal of biological chemistry*. 1998;273(41):26292-26294.

124. Ye Y, Klenerman D, Finley D. N-Terminal Ubiquitination of Amyloidogenic Proteins Triggers Removal of Their Oligomers by the Proteasome Holoenzyme. *Journal of molecular biology*. 2020;432(2):585-596.

125. Giasson BI, Murray IVJ, Trojanowski JQ, Lee VM-Y. A hydrophobic stretch of 12 amino acid residues in the middle of alpha-synuclein is essential for filament assembly. *The Journal of biological chemistry*. 2001;276(4):2380-2386.

126. Ueda K, Fukushima H, Masliah E, et al. Molecular cloning of cDNA encoding an unrecognized component of amyloid in Alzheimer disease. *Proceedings of the National Academy of Sciences of the United States of America*. 1993;90:11282-11286.

127. Han H, Weinreb PH, Lansburry PT. The core Alzheimer's peptide NAC forms amyloid fibrils which seed and are seeded by b-amyloid: is NAC a common trigger or target in neurodegenerative disease? *Current Biology*. 1995;2(3):163-170.

128. Liu H, Chen L, Zhou F, et al. Anti-oligomerization sheet molecules: Design, synthesis and evaluation of inhibitory activities against α-synuclein aggregation. *Bioorganic & medicinal chemistry*. 2019;27(14):3089-3096.

129. Qu J, Yan H, Zheng Y, et al. The Molecular Mechanism of Alpha-Synuclein Dependent Regulation of Protein Phosphatase 2A Activity. *Cellular physiology and biochemistry : international journal of experimental cellular physiology, biochemistry, and pharmacology*. 2018;47(6):2613-2625.

130. Murray IVJ, Giasson BI, Quinn SM, et al. Role of alpha-synuclein carboxy-terminus on fibril formation in vitro. *Biochemistry*. 2003;42(28):8530-8540.

131. Crowther RA, Jakes R, Spillantini MG, Goedert M. Synthetic filaments assembled from C-terminally truncated α-synuclein. *FEBS Letters*. 1998;436:309-312.

132. Alderson TR, Markley JL. Biophysical characterization of α-synuclein and its controversial structure. *Intrinsically disordered proteins*. 2013;1:18-39.

133. van der Wateren IM, Knowles TPJ, Buell AK, Dobson CM, Galvagnion C. C-terminal truncation of α-synuclein promotes amyloid fibril amplification at physiological pH. *Chemical science*. 2018;9(25):5506-5516.

134. Nielsen MS, Vorum H, Lindersson E, Jensen PH. Ca2+ binding to alpha-synuclein regulates ligand binding and oligomerization. *The Journal of biological chemistry*. 2001;276(25):22680-22684.

135. Lautenschläger J, Stephens AD, Fusco G, et al. C-terminal calcium binding of α-synuclein modulates synaptic vesicle interaction. *Nat Commun*. 2018;9(1):712.

136. Park SM, Jung HY, Kim TD, Park JH, Yang C-H, Kim J. Distinct roles of the N-terminal-binding domain and the C-terminal-solubilizing domain of alpha-synuclein, a molecular chaperone. *The Journal of biological chemistry*. 2002;277(32):28512-28520.

137. Maroteaux L, Campanelli JT, Scheller RH. Synuclein: A neuron-specific protein localized to the nucleus and presynaptic nerve terminal. *The Journal of Neuroscience*. 1988;8(8):2804-2815.

138. Cookson MR. The biochemistry of Parkinson's disease. *Annual review of biochemistry*. 2005;74:29-52.

139. Uversky VN. Intrinsically disordered proteins from A to Z. *The international journal of biochemistry & cell biology*. 2011;43(8):1090-1103.

140. Bartels T, Choi JG, Selkoe DJ. α-Synuclein occurs physiologically as a helically folded tetramer that resists aggregation. *Nature*. 2011;477(7362):107-110.

141. Schildknecht S, Gerding HR, Karreman C, et al. Oxidative and nitrative alpha-synuclein modifications and proteostatic stress: Implications for disease mechanisms and interventions in synucleinopathies. *Journal of neurochemistry*. 2013;125(4):491-511.

142. Chandra S, Gallardo G, Fernández-Chacón R, Schlüter OM, Südhof TC. Alpha-synuclein cooperates with CSPalpha in preventing neurodegeneration. *Cell*. 2005;123(3):383-396.

143. Alim MA, Hossain MS, Arima K, et al. Tubulin seeds alpha-synuclein fibril formation. *The Journal of biological chemistry*. 2002;277(3):2112-2117.

144. Sidhu A, Wersinger C, Moussa CE-H, Vernier P. The role of alpha-synuclein in both neuroprotection and neurodegeneration. *Annals of the New York Academy of Sciences*. 2004;1035:250-270.

145. Lykkebo S, Jensen PH. Alpha-synuclein and presynaptic function. *NeuroMolecular Medicine*. 2002;2:115-130.

146. Abeliovich A, Schmitz Y, Farinas I, et al. Mice Lacking a-Synuclein Display Functional Deficits in the Nigrostriatal Dopamine System. *Neuron*. 2000;25:239-252.

147. Logan T, Bendor J, Toupin C, Thorn K, Edwards RH. α-Synuclein promotes dilation of the exocytotic fusion pore. *Nature neuroscience*. 2017;20(5):681-689.

148. Sulzer D, Edwards RH. The physiological role of α-synuclein and its relationship to Parkinson's Disease. *Journal of neurochemistry*. 2019;150(5):475-486.

149. Sharma SK, Chorell E, Wittung-Stafshede P. Insulin-degrading enzyme is activated by the C-terminus of α-synuclein. *Biochemical and biophysical research communications*. 2015;466(2):192-195.

150. Roberts HL, Brown DR. Seeking a mechanism for the toxicity of oligomeric α-synuclein. *Biomolecules*. 2015;5(2):282-305.

151. Ekstrand MI, Terzioglu M, Galter D, et al. Progressive parkinsonism in mice with respiratory-chain-deficient dopamine neurons. *PNAS*. 2007;104(4):1325-1330.

152. Cabin DE, Shimazu K, Murphy D, et al. Synaptic Vesicle Depletion Correlates with Attenuated Synaptic Responses to Prolonged Repetitive Stimulation in Mice Lacking a-Synuclein. *The Journal of Neuroscience*. 2002;(22):8797-8807.

153. Austin SA, Floden AM, Murphy EJ, Combs CK. Alpha-synuclein expression modulates microglial activation phenotype. *The Journal of Neuroscience*. 2006;26(41):10558-10563.

154. Spillantini MG, Schmidt ML, Lee VM-Y, Trojanowski JQ, Jakes R, Goedert M. a-Synuclein in Lewy bodies. *Nature*. 1997;(388):839-840.

155. Shults CW. Lewy bodies. *PNAS*. 2006;103(6):1661-1668.

156. Fanciulli A, Wenning GK. Multiple-system atrophy. *The New England journal of medicine*. 2015;372(3):249-263.

157. Rijk MC, Launer LJ, Berger K, et al. Prevalence of Parkinson's disease in Europe: A collaborative study of population-based cohorts. Neurologic Diseases in the Elderly Research Group. *Neurology*. 2000;54:S21-3.

158. Samii A, Nutt JG, Ransom BR. Parkinson's disease. *The Lancet*. 2004;363(9423):1783-1793.

159. Tysnes O-B, Storstein A. Epidemiology of Parkinson's disease. *Journal of neural transmission (Vienna, Austria : 1996)*. 2017;124(8):901-905.

160. Antonini A, Tinazzi M, Abbruzzese G, et al. Pain in Parkinson's disease: Facts and uncertainties. *European Journal of Neurology*. 2018;25(7):917-e69.

161. Goedert M, Compston A. Parkinson's disease — the story of an eponym. *Nature Reviews Neurology*. 2018;14(1):57-62.

162. Caballol N, Martí MJ, Tolosa E. Cognitive dysfunction and dementia in Parkinson disease. *Movement disorders*. 2007;22(17):358-366.

163. Jankovic J. Parkinson's disease: Clinical features and diagnosis. *Journal of neurology, neurosurgery, and psychiatry*. 2008;79(4):368-376.

164. Polymeropoulos MH, Lavedan C, Leroy E, et al. Mutation in the alpha-synuclein gene identified in families with Parkinson's disease. *Science*. 1997;276(5321):2045-2047.

165. Spillantini MG, Crowther RA, Jakes R, Hasegawa M, Goedert M. a-Synuclein in filamentous inclusions of Lewy bodies from Parkinson's disease and dementia with Lewy bodies. *Proceedings of the National Academy of Sciences of the United States of America*. 1998;95:6469-6473.

166. Marui W, Iseki E, Kato M, Akatsu H, Kosaka K. Pathological entity of dementia with Lewy bodies and its differentiation from Alzheimer's disease. *Acta neuropathologica*. 2004;108(2):121-128.

167. Li J, Uversky VN, Fink AL. Conformational behavior of human a-Synuclein is modulated by familial parkinson's disease point mutations A30P and A53T. *NeuroToxicology*. 2002;23:553-567.

168. Hirsch EC. Iron transport in Parkinson's disease. *Parkinsonism and Related Disorders*. 2009;1353(8020):209-211.

169. Obeso JA, Rodriguez-Oroz MC, Goetz CG, et al. Missing pieces in the Parkinson's disease puzzle. *Nature medicine*. 2010;16(6):653-661.

170. Cuenca L, Gil-Martinez AL, Cano-Fernandez L, et al. Parkinson's disease: A short story of 200 years. *Histology and histopathology*. 2019;34(6):573-591.

171. Pan T, Zhu J, Hwu W-J, Jankovic J. The role of alpha-synuclein in melanin synthesis in melanoma and dopaminergic neuronal cells. *PloS one*. 2012;7(9):e45183.

172. Rodriguez-Leyva I, Chi-Ahumada E, Mejía M, et al. The Presence of Alpha-Synuclein in Skin from Melanoma and Patients with Parkinson's Disease. *Movement disorders clinical practice*. 2017;4(5):724-732.

173. Stoker TB, Torsney KM, Barker RA. Emerging Treatment Approaches for Parkinson’s Disease. *Frontiers in neuroscience*. 2018;12:693. https://www.frontiersin.org/article/10.3389/fnins.2018.00693.

174. Leipold E, Liebmann L, Korenke GC, et al. A de novo gain-of-function mutation in SCN11A causes loss of pain perception. *Nat Genet*. 2013;45(11):1399-1404.

175. Mischkowski D, Palacios-Barrios EE, Banker L, Dildine TC, Atlas LY. Pain or nociception? Subjective experience mediates the effects of acute noxious heat on autonomic responses. *Pain*. 2018;159(4):699-711.

176. Chhabria A. Psychogenic Pain Disorder - Differential Diagnosis and Treatment. *Journal of the Association of Physicians of India*. 2015;(2):36-40.

177. Scholz J, Woolf CJ. Can we conquer pain? *Nature neuroscience*. 2002;5 Suppl:1062-1067.

178. Schady WJL, Torebjörk HE, Ochoa JL. Peripheral projections of nerve fibres in the human median nerve. *Brain research*. 1983;277:249-261.

179. Moore C, Gupta R, Jordt S-E, Chen Y, Liedtke WB. Regulation of Pain and Itch by TRP Channels. *Neuroscience bulletin*. 2018;34(1):120-142.

180. Nagi SS, Marshall AG, Makdani A, et al. An ultrafast system for signaling mechanical pain in human skin. *Science advances*. 2019;5(7):eaaw1297.

181. Djouhri L, Lawson SN. Abeta-fiber nociceptive primary afferent neurons: a review of incidence and properties in relation to other afferent A-fiber neurons in mammals. *Brain research reviews*. 2004;46(2):131-145.

182. Gangadharan V, Kuner R. Pain hypersensitivity mechanisms at a glance. *Disease Models & Mechanisms*. 2013;6(4):889-895.

183. Tobaldini G, Sardi NF, Guilhen VA, Fischer L. Pain Inhibits Pain: An Ascending-Descending Pain Modulation Pathway Linking Mesolimbic and Classical Descending Mechanisms. *Molecular neurobiology*. 2019;56(2):1000-1013.

184. Zhuo M. Ionotropic glutamate receptors contribute to pain transmission and chronic pain. *Neuropharmacology*. 2017;112(Pt A):228-234.

185. Dubin AE, Patapoutian A. Nociceptors: The sensors of the pain pathway. *J. Clin. Invest.* 2010;120(11):3760-3772.

186. Bingham B, Ajit SK, Blake DR, Samad TA. The molecular basis of pain and its clinical implications in rheumatology. *Nature clinical practice. Rheumatology*. 2009;5(1):28-37.

187. Cherny N, Fallon M, Kaasa S, Portenoy RK, Currow DC. *Oxford Textbook of Palliative Medicine:* Oxford University Press; 2015; 1.

188. Ververs JMMA, Roumen RMH, Vingerhoets AJJM, et al. Risk, severity and predictors of physical and psychological morbidity after axillary lymph node dissection for breast cancer. *European Journal of Cancer*. 2001;37(8):991-999.

189. Scarborough BM, Smith CB. Optimal pain management for patients with cancer in the modern era. *CA: a cancer journal for clinicians*. 2018;68(3):182-196.

190. Cipta A, Pietras C, Weiss T, Strouse T. Cancer-related pain management in clinical oncology. *J Community Support Oncol*. 2015;13(10):347-355.

191. Mantyh PW. Cancer pain and its impact on diagnosis, survival and quality of life. *Nat Rev Neurosci*. 2006;7(10):797-809.

192. Joyce JA, Pollard JW. Microenvironmental regulation of metastasis. *Nat Rev Cancer*. 2009;9(4):239-252.

193. Ossipov MH. The Perception and Endogenous Modulation of Pain. *Scientifica*. 2012;2012(4):1-25.

194. Mantyh PW. Bone cancer pain. *Current Opinion in Supportive and Palliative Care*. 2014;8(2):83-90.

195. Lam DK, Schmidt BL. Serine proteases and protease-activated receptor 2-dependent allodynia: A novel cancer pain pathway. *Pain*. 2010;149(2):263-272.

196. Yang Y, Li S, Jin Z-R, et al. Decreased abundance of TRESK two-pore domain potassium channels in sensory neurons underlies the pain associated with bone metastasis. *Science signaling*. 2018;11(552).

197. Soreide K, Janssen EA, Körner H, Baak JPA. Trypsin in colorectal cancer: Molecular biological mechanisms of proliferation, invasion, and metastasis. *J. Pathol.* 2006;209(2):147-156.

198. DeClerck YA, Mercurio AM, Stack MS, et al. Proteases, Extracellular Matrix, and Cancer. *The American journal of pathology*. 2004;164(4):1131-1139.

199. Ossovskaya VS, Bunnett NW. Protease-activated receptors: Contribution to physiology and disease. *Physiological reviews*. 2004;84(2):579-621.

200. Ohtori S, Inoue G, Koshi T, et al. Characteristics of sensory dorsal root ganglia neurons innervating the lumbar vertebral body in rats. *The journal of pain : official journal of the American Pain Society*. 2007;8(6):483-488.

201. Schaible H-G. Mechanisms of chronic pain in osteoarthritis. *Current rheumatology reports*. 2012;14(6):549-556.

202. Mantyh WG, Jimenez-Andrade JM, Stake JI, et al. Blockade of nerve sprouting and neuroma formation markedly attenuates the development of late stage cancer pain. *Neuroscience*. 2010;171(2):588-598.

203. Bloom AP, Jimenez-Andrade JM, Taylor RN, et al. Breast cancer-induced bone remodeling, skeletal pain, and sprouting of sensory nerve fibers. *The journal of pain : official journal of the American Pain Society*. 2011;12(6):698-711.

204. Li J, Sun Y, Ding G, Jiang F. Persistent pain accelerates xenograft tumor growth of breast cancer in rat. *Biochemical and biophysical research communications*. 2018;495(4):2432-2438.

205. Ferrero-Miliani L, Nielsen OH, Andersen PS, Girardin SE. Chronic inflammation: Importance of NOD2 and NALP3 in interleukin-1beta generation. *Clinical and experimental immunology*. 2007;147(2):227-235.

206. Li Y, Soendergaard C, Bergenheim FH, et al. COX-2-PGE(2) Signaling Impairs Intestinal Epithelial Regeneration and Associates with TNF Inhibitor Responsiveness in Ulcerative Colitis. *EBioMedicine*. 2018;36:497-507.

207. Kawabata A. Prostaglandin E2 and pain--an update. *Biological & pharmaceutical bulletin*. 2011;34(8):1170-1173.

208. Boyden SD, Hossain IN, Wohlfahrt A, Lee YC. Non-inflammatory Causes of Pain in Patients with Rheumatoid Arthritis. *Current rheumatology reports*. 2016;18(6):30.

209. Pahwa R, Goyal A, Bansal P. Chronic Inflammation. https://www.ncbi.nlm.nih.gov/books/NBK493173/. Accessed 2020 Mar 2.

210. Vasko MR. Inflammatory Pain. In: Binder MD, Hirokawa N, Windhorst U, eds. *Encyclopedia of Neuroscience*. Berlin, Heidelberg: Springer Berlin Heidelberg; 2009:1952-1955.

211. Reed GW, Nissen SE. NSAID choice: Lessons from PRECISION. *Aging*. 2019;11(8):2181-2182.

212. Iqbal Z, Azmi S, Yadav R, et al. Diabetic Peripheral Neuropathy: Epidemiology, Diagnosis, and Pharmacotherapy. *Clinical therapeutics*. 2018;40(6):828-849.

213. Foley PL, Vesterinen HM, Laird BJ, et al. *Prevalence and natural history of pain in adults with multiple sclerosis: Systematic review and meta-analysis*. United States; 2013 May.

214. Portenoy RK. Painful polyneuropathy. *Neurologic clinics*. 1989;7(2):265-288.

215. Vaillancourt PD, Langevin HM. Painful peripheral neuropathies. *The Medical clinics of North America*. 1999;83(3):627-42, vi.

216. Costigan M, Scholz J, Woolf CJ. Neuropathic Pain: A Maladaptive Response of the Nervous System to Damage. *Annu. Rev. Neurosci.* 2009;32(1):1-32.

217. Woolf CJ, Salter MW. Neuronal Plasticity: Increasing the gain in pain. *Science*. 2000;288:1765-1768.

218. Torrance N, Smith BH, Bennett MI, Lee AJ. The Epidemiology of Chronic Pain of Predominantly Neuropathic Origin. Results From a General Population Survey. *The Journal of Pain*. 2006;7(4):281-289.

219. del Rey A, Apkarian AV, Martina M, Besedovsky HO. Chronic neuropathic pain-like behavior and brain-borne IL-1β. *Annals of the New York Academy of Sciences*. 2012;1262(1):101-107.

220. Newton RA, Bingham S, Davey PD, et al. Identification of differentially expressed genes in dorsal root ganglia following partial sciatic nerve injury. *Neuroscience*. 2000;95(4):1111-1120.

221. Campbell JN, Meyer RA. Mechanisms of neuropathic pain. *Neuron*. 2006;52(1):77-92. https://pubmed.ncbi.nlm.nih.gov/17015228.

222. Barrell K, Smith AG. Peripheral Neuropathy. *The Medical clinics of North America*. 2019;103(2):383-397.

223. Xie R-G, Zheng D-W, Xing J-L, et al. Blockade of persistent sodium currents contributes to the riluzole-induced inhibition of spontaneous activity and oscillations in injured DRG neurons. *PloS one*. 2011;6(4):e18681.

224. Sheets PL, Heers C, Stoehr T, Cummins TR. Differential block of sensory neuronal voltage-gated sodium channels by lacosamide (2R)-2-(acetylamino)-N-benzyl-3-methoxypropanamide, lidocaine, and carbamazepine. *The Journal of pharmacology and experimental therapeutics*. 2008;326(1):89-99.

225. Nassar MA, Baker MD, Levato A, et al. Nerve injury induces robust allodynia and ectopic discharges in Nav1.3 null mutant mice. *Molecular pain*. 2006;2:33.

226. Jiang Y-Q, Xing G-G, Wang S-L, et al. Axonal accumulation of hyperpolarization-activated cyclic nucleotide-gated cation channels contributes to mechanical allodynia after peripheral nerve injury in rat. *Pain*. 2008;137(3):495-506.

227. Chaplan SR, Guo H-Q, Lee DH, et al. Neuronal hyperpolarization-activated pacemaker channels drive neuropathic pain. *The Journal of neuroscience : the official journal of the Society for Neuroscience*. 2003;23(4):1169-1178.

228. Lee DH, Chang L, Sorkin LS, Chaplan SR. Hyperpolarization-activated, cation-nonselective, cyclic nucleotide-modulated channel blockade alleviates mechanical allodynia and suppresses ectopic discharge in spinal nerve ligated rats. *The journal of pain : official journal of the American Pain Society*. 2005;6(7):417-424.

229. Meacham K, Shepherd A, Mohapatra DP, Haroutounian S. Neuropathic Pain: Central vs. Peripheral Mechanisms. *Current pain and headache reports*. 2017;21(6):28.

230. Wieseler-Frank J, Maier SF, Watkins LR. Central proinflammatory cytokines and pain enhancement. *Neuro-Signals*. 2005;14(4):166-174.

231. Ueda H. Systems Pathology of Neuropathic Pain and Fibromyalgia. *Biological & pharmaceutical bulletin*. 2019;42(11):1773-1782.

232. Gilron I. Neuropathic pain: A practical guide for the clinician. *Canadian Medical Association Journal*. 2006;175(3):265-275.

233. Gosselin R-D, Suter MR, Ji R-R, Decosterd I. Glial cells and chronic pain. *The Neuroscientist : a review journal bringing neurobiology, neurology and psychiatry*. 2010;16(5):519-531.

234. Gierthmühlen J, Baron R. Neuropathic Pain. *Seminars in neurology*. 2016;36(5):462-468.

235. Backonja M, Wallace MS, Blonsky ER, et al. NGX-4010, a high-concentration capsaicin patch, for the treatment of postherpetic neuralgia: A randomised, double-blind study. *The Lancet Neurology*. 2008;7(12):1106-1112.

236. Simpson DM, Brown S, Tobias J. Controlled trial of high-concentration capsaicin patch for treatment of painful HIV neuropathy. *Neurology*. 2008;70(24):2305-2313.

237. Attal N, Cruccu G, Baron R, et al. EFNS guidelines on the pharmacological treatment of neuropathic pain: 2010 revision. *European Journal of Neurology*. 2010;17(9):1113-e88.

238. Rahn EJ, Hohmann AG. Cannabinoids as pharmacotherapies for neuropathic pain: From the bench to the bedside. *Neurotherapeutics*. 2009;6(4):713-737.

239. Macone A, Otis JAD. Neuropathic Pain. *Seminars in neurology*. 2018;38(6):644-653.

240. Decosterd I, Woolf CJ. Spared nerve injury: An animal model of persistent peripheral neuropathic pain. *Pain*. 2000;87(2):149-158.

241. Möser CV, Möller M, Fleck SC, Thomas D, Geisslinger G, Niederberger E. Inhibition of the protein kinase IKKepsilon attenuates neuropathic pain in mice. *Neuropharmacology*. 2019;146:198-211.

242. Feldman JP, Goldwasser R, Mark S, Schwartz J, Orion I. A mathematical model for tumor volume evaluation using two-dimensions. *Journal of applied quantitative methods*. 2009;4(4):455-462.

243. Liu L, Duff K. A technique for serial collection of cerebrospinal fluid from the cisterna magna in mouse. *Journal of visualized experiments*. 2008;(21):1-3.

244. Möller M, Wasel J, Schmetzer J, et al. The Specific IKKε/TBK1 Inhibitor Amlexanox Suppresses Human Melanoma by the Inhibition of Autophagy, NF-κB and MAP Kinase Pathways. *International journal of molecular sciences*. 2020;21(13).

245. Terheyden P, Krackhardt A, Eigentler T. The Systemic Treatment of Melanoma. *Deutsches Arzteblatt international*. 2019;116(29-30):497-504.

246. Ge Y, Xu K. Alpha-synuclein contributes to malignant progression of human meningioma via the Akt/mTOR pathway. *Cancer Cell Int*. 2016;16(1):231.

247. Lee SE, Hong M, Cho J, Lee J, Kim K-M. IKKε and TBK1 expression in gastric cancer. *Oncotarget*. 2017;8(10):16233-16242.

248. Yu T, Yi Y-S, Yang Y, Oh J, Jeong D, Cho JY. The pivotal role of TBK1 in inflammatory responses mediated by macrophages. *Mediators of inflammation*. 2012;2012:979105.

249. Gridling M, Ficarro SB, Breitwieser FP, et al. Identification of kinase inhibitor targets in the lung cancer microenvironment by chemical and phosphoproteomics. *Molecular Cancer Therapeutics*. 2014;13(11):2751-2762.

250. Guan H, Zhang H, Cai J, et al. IKBKE is over-expressed in glioma and contributes to resistance of glioma cells to apoptosis via activating NF-κB. *J. Pathol.* 2011;223(3):436-445.

251. Li H, Chen L, Zhang A, et al. Silencing of IKKε using siRNA inhibits proliferation and invasion of glioma cells in vitro and in vivo. *Int J Oncol*. 2012;41(1):169-178.

252. Klionsky DJ, Abeliovich H, Agostinis P, et al. Guidelines for the use and interpretation of assays for monitoring autophagy in higher eukaryotes. *Autophagy*. 2008;4(2):151-175.

253. Pilli M, Arko-Mensah J, Ponpuak M, et al. TBK-1 promotes autophagy-mediated antimicrobial defense by controlling autophagosome maturation. *Immunity*. 2012;37(2):223-234.

254. Richter B, Sliter DA, Herhaus L, et al. Phosphorylation of OPTN by TBK1 enhances its binding to Ub chains and promotes selective autophagy of damaged mitochondria. *Proceedings of the National Academy of Sciences of the United States of America*. 2016;113(15):4039-4044.

255. Hara Y, Nakamura M. Overexpression of autophagy-related beclin-1 in advanced malignant melanoma and its low expression in melanoma-in-situ. *European Journal of Dermatology*. 2012;22(1):128-129.

256. Lazova R, Camp RL, Klump V, Siddiqui SF, Amaravadi RK, Pawelek JM. Punctate LC3B Expression Is a Common Feature of Solid Tumors and Associated with Proliferation, Metastasis, and Poor Outcome. *Clinical Cancer Research*. 2012;18(2):370-379.

257. Yun C, Lee S. The Roles of Autophagy in Cancer. *IJMS*. 2018;19(11):3466.

258. Bijnsdorp IV, Peters GJ, Temmink OH, Fukushima M, Kruyt FA. Differential activation of cell death and autophagy results in an increased cytotoxic potential for trifluorothymidine compared to 5-fluorouracil in colon cancer cells. *Int. J. Cancer*. 2010;6:NA-NA.

259. Selvakumaran M, Amaravadi RK, Vasilevskaya IA, O'Dwyer PJ. Autophagy Inhibition Sensitizes Colon Cancer Cells to Antiangiogenic and Cytotoxic Therapy. *Clinical cancer research : an official journal of the American Association for Cancer Research*. 2013;19(11).

260. Ueda Y, Richmond A. NF-kappaB activation in melanoma. *Pigment Cell Research*. 2006;19(2):112-124.

261. Amiri KI, Richmond A. Role of nuclear factor-kappa B in melanoma. *Cancer metastasis reviews*. 2005;24(2):301-313.

262. Roberts PJ, Der CJ. Targeting the Raf-MEK-ERK mitogen-activated protein kinase cascade for the treatment of cancer. *Oncogene*. 2007;26(22):3291-3310.

263. Vander Heiden MG, Plas DR, Rathmell JC, Fox CJ, Harris MH, Thompson CB. Growth factors can influence cell growth and survival through effects on glucose metabolism. *Molecular and cellular biology*. 2001;21(17):5899-5912.

264. Sarraf SA, Sideris DP, Giagtzoglou N, et al. PINK1/Parkin Influences Cell Cycle by Sequestering TBK1 at Damaged Mitochondria, Inhibiting Mitosis. *Cell reports*. 2019;29(1):225-235.e5.

265. Hoeflich KP, Gray DC, Eby MT, et al. Oncogenic BRAF Is Required for Tumor Growth and Maintenance in Melanoma Models. *Cancer research*. 2006;66(2):999-1006.

266. Boussemart L, Malka-Mahieu H, Girault I, et al. eIF4F is a nexus of resistance to anti-BRAF and anti-MEK cancer therapies. *Nature*. 2014;513(7516):105-109.

267. Truven Health Analytics I. Amlexanox mucuous membrane oral. https://www.drugs.com/cons/amlexanox-mucous-membrane-oral.html. Updated August 8, 2019.

268. RxList I. Aphtasol (amlexanox) Oral Paste. https://www.rxlist.com/aphthasol-drug.htm#description. Accessed October 7, 2019.

269. Oral EA, Reilly SM, Gomez AV, et al. Inhibition of IKKε and TBK1 Improves Glucose Control in a Subset of Patients with Type 2 Diabetes. *Cell metabolism*. 2017;26(1):157-170.e7.

270. Cruz VH, Brekken RA. Assessment of TANK-binding kinase 1 as a therapeutic target in cancer. *Journal of cell communication and signaling*. 2018;12(1):83-90.

271. Durand JK, Zhang Q, Baldwin AS. Roles for the IKK-Related Kinases TBK1 and IKKε in Cancer. *Cells*. 2018;7(9).

272. Baba H, Shimoji K, Yoshimura M. Norepinephrine Facilitates Inhibitory Transmission in Substantia Gelatinosa of Adult Rat Spinal Cord (Part 1). *Anesthesiology*. 2000;92(2):473.

273. Todd AJ. Neuronal circuitry for pain processing in the dorsal horn. *Nat Rev Neurosci*. 2010;11(12):823-836.

274. Taguchi K, Watanabe Y, Tsujimura A, Tanaka M. Expression of α-synuclein is regulated in a neuronal cell type-dependent manner. *Anatomical science international*. 2019;94(1):11-22.

275. Stevens LC. A new inbred subline of mice (129-terSv) with a high incidence of spontaneous congenital testicular teratomas. *JNCI Journal of the National Cancer Institute*. 1973;50(1):235-242.

276. Threadgill DW, Yee D, Matin A, Nadeau JH, Magnuson T. Genealogy of the 129 inbred strains: 129/SvJ is a contaminated inbred strain. *Mammalian genome : official journal of the International Mammalian Genome Society*. 1997;8(6):390-393.

277. Mogil JS, Wilson SG, Bon K, et al. Heritability of nociception I: Responses of 11 inbred mouse strains on 12 measures of nociception. *Pain*. 1999;80:67-82.

278. Almaraz L, Manenschijn J-A, La Peña E de, Viana F. TRPM8. *Handbook of experimental pharmacology*. 2014;222:547-579.

279. Dhaka A, Murray AN, Mathur J, Earley TJ, Petrus MJ, Patapoutian A. TRPM8 is required for cold sensation in mice. *Neuron*. 2007;54(3):371-378.

280. Gureviciene I, Gurevicius K, Tanila H. Role of a-synuclein in synaptic glutamate release. *Neurobiology of disease*. 2007;28:83-89.

281. Ito H, Nakayama K, Jin C, Suzuki Y, Yazawa I. α-Synuclein accumulation reduces GABAergic inhibitory transmission in a model of multiple system atrophy. *Biochemical and biophysical research communications*. 2012;428(3):348-353.

282. Zhang G, Gao Z, Guan S, Zhu Y, Wang J-H. Upregulation of excitatory neurons and downregulation of inhibitory neurons in barrel cortex are associated with loss of whisker inputs. *Molecular brain*. 2013;6(1):2. https://doi.org/10.1186/1756-6606-6-2.

283. Guerriero RM, Giza CC, Rotenberg A. Glutamate and GABA imbalance following traumatic brain injury. *Curr Neurol Neurosci Rep*. 2015;15(5):27. https://pubmed.ncbi.nlm.nih.gov/25796572.

284. Takazawa T, MacDermott AB. Synaptic pathways and inhibitory gates in the spinal cord dorsal horn. *Annals of the New York Academy of Sciences*. 2010;1198:153-158.

285. Koch SC, Acton D, Goulding M. Spinal Circuits for Touch, Pain, and Itch. *Annual review of physiology*. 2018;80:189-217.

286. Wood JN, Todd AJ, Wang F, eds. *The Oxford Handbook of the Neurobiology of Pain:* Oxford University Press; 2018.

287. Lema Tomé CM, Tyson T, Rey NL, Grathwohl S, Britschgi M, Brundin P. Inflammation and α-synuclein's prion-like behavior in Parkinson's disease--is there a link? *Molecular neurobiology*. 2013;47(2):561-574.

288. Allen Reish HE, Standaert DG. Role of α-synuclein in inducing innate and adaptive immunity in Parkinson disease. *Journal of Parkinson's disease*. 2015;5(1):1-19.

289. Valek L, Auburger G, Tegeder I. Sensory neuropathy and nociception in rodent models of Parkinson's disease. *Disease Models & Mechanisms*. 2019;12(6).

290. Eidson LN, Kannarkat GT, Barnum CJ, et al. Candidate inflammatory biomarkers display unique relationships with alpha-synuclein and correlate with measures of disease severity in subjects with Parkinson's disease. *J Neuroinflammation*. 2017;14(1):164. https://doi.org/10.1186/s12974-017-0935-1.

291. White AJ, Wijeyekoon RS, Scott KM, et al. The Peripheral Inflammatory Response to Alpha-Synuclein and Endotoxin in Parkinson's Disease. *Front Neurol*. 2018;9:946. https://pubmed.ncbi.nlm.nih.gov/30524354.

292. Benskey MJ, Sellnow RC, Sandoval IM, Sortwell CE, Lipton JW, Manfredsson FP. Silencing Alpha Synuclein in Mature Nigral Neurons Results in Rapid Neuroinflammation and Subsequent Toxicity. *Frontiers in molecular neuroscience*. 2018;11:36. https://www.frontiersin.org/article/10.3389/fnmol.2018.00036.

293. Faustini G, Marchesan E, Zonta L, et al. Alpha-Synuclein Preserves Mitochondrial Fusion and Function in Neuronal Cells. *Oxidative Medicine and Cellular Longevity*. 2019;2019:4246350. https://doi.org/10.1155/2019/4246350.

294. Martin F, Fletcher D, Chauvin M, Bouhassira D. Constitutive cyclooxygenase-2 is involved in central nociceptive processes in humans. *Anesthesiology*. 2007;106(5):1013-1018. https://pubmed.ncbi.nlm.nih.gov/17457134.

295. Takeda, Kenji, M.D., Sawamura, Shigehito, M.D., Ph.D., Tamai, Hisayoshi, M.D., Sekiyama, Hiroshi, M.D., Hanaoka, Kazuo, M.D., Ph.D. Role for Cyclooxygenase 2 in the Development and Maintenance of Neuropathic Pain and Spinal Glial Activation. *Anesthesiology*. 2005;103(4):837-844.

296. Israeli E, Yakunin E, Zarbiv Y, et al. α-Synuclein Expression Selectively Affects Tumorigenesis in Mice Modeling Parkinson's Disease. *PloS one*. 2011;6(5):e19622.

297. Shekoohi S, Rajasekaran S, Yang S, et al. Abstract 896: Knocking out the gene (SNCA) that codes for the Parkinson's disease-related protein alpha-synuclein in SK-Mel-28 melanoma cells significantly retards tumor growth in SCID mice. In: Molecular and Cellular Biology / Genetics: American Association for Cancer Research; 2019:896.

8. Danksagung

An diesem Punkt meiner Arbeit möchte ich allen Menschen danken, die mich und meine Arbeit unterstützt haben.

Zuallererst möchte ich Prof. Dr. Ellen Niederberger für ihre Unterstützung, Betreuung und ihre gut durchdachten Beiträge danken. Ohne Sie und den Direktor des Instituts, Prof. Dr. Dr. Gerd Geißlinger, wäre diese Arbeit nicht möglich gewesen.

Als nächstes möchte ich Prof. Dr. Stefan Eimer für seine Mitbetreuung und die äußerst hilfreichen Anregungen danken.

Mein Dank geht auch an meine Kolleginnen und Kollegen Ulrike W., Nina S., Sebastian B. und Khadija E.-H. Sie alle haben mir während meiner Zeit als Doktorand sehr geholfen und durch sie hat mir die Arbeit hier eine Menge Spaß gemacht.

Dann möchte ich allen, die an der Erzielung von Ergebnissen beteiligt waren, für diese Arbeit danken. Dr. Christine V. M., Julia W., Julia S. und unseren technischen Assistentinnen Julia H., Christine M. und Annett W.-S.

Ein weiteres Dankeschön geht speziell an Lucie V. und Lara F. für alle Memes und Gifs die hin- und hergeschickt wurden. Ohne euch wäre meine Arbeit wahrscheinlich Monate früher beendet worden.

Zum Schluss und am Meisten von allen möchte ich meiner Familie und meinen Freunden für all die Hilfe, Liebe, Unterstützung und Geduld danken, die sie mir entgegengebracht haben, und für die Zeit, die sie in mich investiert haben. Ganz speziell meiner Partnerin Rebecca E. dafür, dass sie mich in der Zeit des Schreibens ertragen hat und trotz allem noch für das Korrekturlesen zur Verfügung stand.

Ich bin Euch allen zutiefst dankbar.

9. Lebenslauf

Vorname: Moritz

Name: Möller

Geburtstag: 05.03.1993

Geburtsort: Marburg

07/2017 – 06/2020	**Goethe Universität, Frankfurt** Promotion: Klinische Pharmakologie Schwerpunkte: Schmerz- und onkologische Forschung Dissertation: The role of IKKε, TBK1, and alpha-Synuclein in the pathogenesis of melanoma and pain Betreuer: Prof Dr. E. Niederberger / Prof. Dr. S. Eimer Abschluss: Dr. rer. nat.
10/2015 – 06/2017	**Goethe Universität, Frankfurt** Masterstudium: Interdisciplinary Neuroscience Schwerpunkte: Molekularbiologische und elektrophysiologische Neurobiologie Masterarbeit: The role of alpha-Synuclein in inflammatory and neuropathic nociception in mice Betreuer: Prof. Dr. E. Niederberger Abschluss: Master of Science, 1,1

10/2012 – 07/2015 **Philipps Universität, Marburg**

Bachelorstudium: Humanbiologie

Schwerpunkte: Neuro- und Zellbiologie

Bachelorarbeit: Characterization and isolation of human B1-Lymphocytes, producing naturally occurring autoantibodies against alpha-Synuclein

Betreuer: Prof. Dr. R. Dodel

Abschluss: Bachelor of Science, 1,3

1999 – 2012 **Alfred-Wegener-Schule, Kirchhain**

Allgemeine Hochschulreife

Leistungskurse: Biologie und Chemie

Abschluss: 1,3

Publikationsliste

Möller M, Wasel J, Schmetzer J, et al. The Specific IKKε/TBK1 Inhibitor Amlexanox Suppresses Human Melanoma by the Inhibition of Autophagy, NF-κB and MAP Kinase Pathways.

International journal of molecular sciences. 2020;21(13)

King-Himmelreich TS, Möser CV, Wolters MC, et al. AMP-activated kinase and the endogenous endocannabinoid system might contribute to antinociceptive effects of prolonged moderate caloric restriction in mice.

Mol Pain. 2017;13:1744806917703111. doi:10.1177/1744806917703111

Möser CV, Möller M, Fleck SC, Thomas D, Geisslinger G, Niederberger E. Inhibition of the protein kinase IKKepsilon attenuates neuropathic pain in mice.

Neuropharmacology. 2019;146:198–211. doi:10.1016/j.neuropharm.2018.12.004

Martin LM, Möller M, Weiss U, et al. 5-Amino-1-β-D-Ribofuranosyl-Imidazole-4-Carboxamide (AICAR) Reduces Peripheral Inflammation by Macrophage Phenotype Shift.

Int J Mol Sci. 2019;20(13):3255. Published 2019 Jul 2. doi:10.3390/ijms20133255

Albus A, Jördens M, Möller M, Dodel R. Encoding the Sequence of Specific Autoantibodies Against beta-Amyloid and alpha-Synuclein in Neurodegenerative Diseases.

Front Immunol. 2019;10:2033. Published 2019 Aug 27. doi:10.3389/fimmu.2019.02033

10. Glossar

AMPA	α-amino-3-hydroxy-5-methyl-4-isoxazolepropionic acid
ANOVA	Analysis of variance
APS	Ammonium persulfate
Bcl-2	B-cell-lymphoma-2
b-Raf	Rapidly accelerated fibrosarcoma
BafA	Bafilomycin A1
BSA	Bovine serum albumin
CDK4	Cyclin dependent kinase 4
CDKN2A	Cyclin dependent kinase inhibitor 2A
cDNA	Complementary DNA
CGRP	Calcitonin gene-related peptide
$CHCl_3$	Chloroform
CNS	Central nervous system
COX	Cyclooxygenase
CSF	Cerebrospinal fluid
DAPI	4’,6-diamidino-2-phenylindole
DAPI	4’,6-diamidino-2-phenylindole
DLB	Dementia with Lewy bodies
DMEM	Dulbecco's Modified Eagle's Medium
DMSO	Dimethyl sulfoxide
DNA	Deoxyribonucleic acid
DPBS	Dulbecco’s Phosphate Buffered Saline
DRG	Dorsal Root Ganglion
EGF	Epidermal growth factor
EMEM	Eagle’s Minimum Essential Medium
Erk	Extracellular signal-regulating kinase
FACS	Fluorescence-activated cell sorting
FCS	Fetal calf serum
GPCR	G-protein coupled receptor

GSK-3	Glycogen synthase kinase-3
HCN	hyperpolarization-activated cyclic nucleotide-gated cation channels
IDP	Intrinsically-disordered protein
IFN	Interferon
IHC	Immunohistochemistry
IKK	Inhibitor of NF-κB kinase
IKKε	Inhibitor of NF-κB kinase subunit epsilon
IL	Interleukin
IRF	Interferon regulatory factor
IκB	Inhibitor of kappa B
KCl	Potassium chloride
L	Length
LPS	Lipopolysaccharide
MAPK	Mitogen activated protein kinase
MDM2	Mouse double minute 2
mGluR	metabotropic glutamate receptor
MKK	MAP kinases kinases
mRNA	Messenger RNA
MSA	Multiple system atrophie
mTOR	Mammalian target of rapamycin
NAC	Non-amyloid-β component
NAP1	NAK-associated protein 1
NEMO	NF-κB-Essential-Modulator
NF-κB	nuclear factor kappa-light-chain-enhancer of activated B cells
NGF	Nerve growth factor
NGS	Normal goat serum
NIK	NF-κB inducing kinase
NMDA	N-methyl-D-aspartate
NSAID	Non-steroidal anti-inflammatory drug
PAG	Periaqueductal grey matter

PAR	Protease activated receptor
PBS	Phosphate-buffered saline
PCR	Polymerase chain reaction
PD	Parkinson’s disease
PDTC	Pyrrolidinedithiocarbamate ammonium
PI	Propidium iodide
PI3K	Phosphoinositide-3-kinase
PKC	Protein kinase C
PMA	Phorbol 12-myristate 13-acetate
PWL	Paw withdrawal latency
qPCR	Quantitative real-time polymerase chain reaction
r.t.u.	Ready to use
RalB	Ras-like GTPase B
RANKL	Receptor activator of the NF-κB ligand
Ras	GTPase rat sarcoma
RNA	Ribonucleic acid
rpm	Rounds per minute
RT	Room temperature
SC	Spinal Cord
SDS	Sodium dodecyl sulfate
SDS-PAGE	SDS polyacrylamide gel electrophoresis
SEM	Standard error of the mean
SINTBAD	NAP1 and TBK1 adaptor
SNI	Spared nerve injury
T2K	TRAF2-associated kinase
TAK1	TGF-β activated kinase-1
TANK	TRAF-associated NF-κB activator
TBK1/NAK	TANK-binding kinase 1
TBST	Tris-buffered saline with Tween20
TLR	Toll-like-receptor
TNF	Tumor necrosis factor

TRAF2	TNF receptor-associated factor 2
TRP	Transient receptor potential channel
UCT	University Cancer Center
W	Width
WB	Western Blot
WST-1	4-[3-(4-Iodophenyl)-2-(4-nitrophenyl)-2H-5-tetrazolio]-1,3-benzene disulfonate
α-Syn	Alpha Synuclein